THE ROLE OF GLYCOGEN SYNTHASE KINASE-3β

IN THE REGULATION OF MITOCHONDRIAL

MEMBRANE PERMEABILITY

DISSERTATION

Presented to the Faculty of

The Graduate School of Biomedical Sciences at

The University of North Texas Health Science Center

In Partial Fulfillment of the Requirements

For the Degree of

DOCTOR OF PHILOSOPHY

By

Morgan Madison Brooks B.A.

Fort Worth, Texas

November, 2014

TABLE OF CONTENTS

LIST OF FIGURES

Chapter V

LIST OF ABBREVIATIONS

OFZ – Organelle Free Zone
PCO – Posterior Capsule Opacification
EMT – Epithelial to Mesenchymal Transition
GSK-3β – Glycogen Synthase Kinase-3β
HLE-B3 – Human Lens Epithelial cell
ROS – Reactive Oxygenated Species
ΔΨ – Mitochondrial Membrane Potential
mMPT – Mitochondrial Membrane Permeability Transition
ANT – Adenine Nucleotide Translocator
GS – Glycogen Synthase
Mitoprotection – The prevention of mitochondrial depolarization
ERK – Extracellular Signal-Regulated Kinase
SB216763 – 3-(2,4-dichlorophenyl)-4-(1-methyl-1H-indol-3-yl)-1H-pyrrole-2,5-dione
DMSO – Dimethyl Sulfoxide
JC-1 – 1H-benzimidazolium-5,6-dichloro-2-[3-(5,6-dichloro-1,3-diethyl-1,3-dihydro-2H-benz-imidazol-2-ylidene)-1-propenyl]-1,3-diethyl-iodide
MEM – Minimal Essential Media
BLEC – Bovine Lens Epithelial Cell
BAX – Bcl-2 Associated X
MEK – Mitogen-Activated Protein Kinase Kinase
UO126 – 1,4-diamino-2,3-dicyano-1,4-bis[2-aminophenylthio] butadiene
JNK – c-Jun N-terminal Kinase
ELISA – Enzyme-Linked Immunosorbent Assay
VEGF – Vascular Endothelial Growth Factor
α-SMA – α-Smooth Muscle Actin
TGF-β – Transformin Growth Factor-β
HIF – Hypoxia Inducible Factor
MET – Mesenchymal to Epithelial Transition

CHAPTER I

Introduction

The Human Lens

The human lens can grossly be described as an asymmetrical (the anterior semi-minor axis < the posterior semi-minor axis), oblate (flattened toward poles), spheroids (approaching in shape to a sphere) [1]. The lens itself is composed of two cell types: epithelial cells that constitute a single layer positioned on the anterior surface of the capsule and fiber cells which make up the bulk of the lens tissue [2]. These two cell types develop during embryogenesis from the lens vesicle; and, as development continues epithelial cells near the equator will differentiate into fiber cells [2]. Fiber cells are characterized as long ribbon like cells that are arranged end to end around a polar axis (parallel to the visual axis) to form a series of concentric shells (Figure 1.1 A & B) [3].

The formation of lens fiber cells occurs throughout life with new layers of cells being continuously overlaid onto older cells, in register, creating age-related concentric growth shells [1]. According to Kusak et. al. 2004 "… it has been proposed that the highly ordered arrangement of lens fibers contributes to lens transparency by transforming the individual fibers into a series of coaxial refractive surfaces [4]. As a result, a large amount of light scattering is minimized as light is transmitted through the membranes of hundreds of thousands of fibers." [3] Furthermore, the fiber cells synthesize and order the short range packing of the crystalline proteins which provide the transparent refractive medium that light passes through in the lens [5]. In order to maintain transparency lens fiber cells degrade all of their organelles (nucleus, mitochondria, endoplasmic reticulum, Golgi apparatus, etc.) creating essentially organelle free zones (OFZ) that act as age related refractive index gradients in which the central indices are

greater than the peripheral indices [5]. With the formation of this refractive medium and OFZ much of the small light scattering that would exist if the lens were composed of a homogenous index is neutralized [6]. Overall, the primary reason for lens clarity is the minimal amount of light scattering produced as light is transmitted through the lens.

Cataractogenesis

Juxtaposed to this clarity, cataractous lenses are more opaque or have regions of increased opacity due to excessive light scattering as light passes through areas of compromised lens tissue [3]. The World Health Organization estimates that of the 39 million people worldwide that are blind almost 18 million suffer from cataracts; making it the second leading cause of blindness in the world [7]. During cataract formation the lens shifts from being fully transparent to more opaque/cloudy as seen in Figure 1.2.

If left untreated cataracts can cause complete blindness. There are several causes of cataracts including trauma, age, genetics, and environmental dangers (toxins, radiation, UV light, etc.); all of which lead to a break down in lens transparency [8]. In the majority of cataracts the loss of transparency is attributed to a breakdown in lens fiber cell homeostasis brought on by nonfunctioning crystalline proteins [8]. Crystallines (primarily α-crystalline) are chaperone proteins used to prevent proteins from aggregating into nonfunctional structures as well as prevent the precipitation of denatured proteins [9]. If the crystallines were to become nonfunctioning there would be increased denaturation/aggregation of these crystalline proteins along with a buildup of high molecular weight protein aggregates [9, 10]. The increase in crystalline and other proteins would lead to increased light scattering ultimately causing opacity [10]. Eventually, this opacity will encompass the whole lens leading to blindness which requires immediate treatment to correct.

The most effective way to treat cataracts is to have a surgeon remove the cataractous lens by phacoemulsification and place an artificial intraocular lens inside the capsular bag. During the surgery the normally hypoxic lens is exposed to atmospheric oxygen. According to Petrash et. al. 2013 "although cataract surgery is considered a safe and effective surgical procedure, it can be conservatively estimated that up to 20% of cataract cases develop posterior capsular opacification (PCO), which results in a loss of clear vision following a period of weeks to months after surgery." [11] PCO occurs when those epithelial cells that remained after cataract surgery begin to migrate onto the posterior side of the intraocular lens (Figure 1.3) [12]. Eventually PCO can block light from passing through the intraocular lens causing blindness [12]. One of the characteristics of PCO is the transformation of the epithelial cells from an epithelial phenotype to a mesenchymal stem cell like phenotype in a process known as epithelial to mesenchymal transition (EMT) [11]. It is theorized that the initiation of EMT is caused by damage to glycogen synthase kinase-3β (GSK-3β) during the brief exposure to atmospheric oxygen that occurs while undergoing cataract surgery. It is further theorized that this damage to GSK-3β can make the newly formed mesenchymal cells more resistant to mitochondrial depolarization.

GSK-3β, Mitoprotection, and EMT

In the presence of atmospheric oxygen human lens epithelial cells (HLE-B3) demonstrated an increase in the formation of reactive oxygenated species (ROS) [13]. A sufficient increase of ROS can cause a collapse of mitochondrial membrane potential ($\Delta\Psi$) in a process termed mitochondrial membrane permeability transition (mMPT) [14, 15]. Dissipation of $\Delta\Psi$ prompts further disruption of the electron transport chain, decreasing the production of ATP, additionally increasing the formation of ROS in a harmful cycle [16, 17]. The loss of $\Delta\Psi$ can

lead to swelling and eventual rupturing of the mitochondria that could ultimately cause cellular dysfunction and possible cell death [18]. Upon rupturing of the mitochondria, Cytochrome c is released into the cytosol where it promotes the formation of the apoptosome (a complex of Apaf-1, Cytochrome c, and caspase-9) [18]. Once formed, the apoptosome will cleave pro-caspase-3 and transform it into activated caspase-3 [18]. Activated caspase-3 then executes cellular apoptosis which can be phenotypically characterized by DNA fragmentation, chromatin condensation, membrane blebbing, and cell shrinkage [18-20]. To prevent the initiation of apoptosis caused by the rupturing of the mitochondria several mechanisms have been developed by cells to maintain $\Delta\Psi$.

In particular HLE-B3 cells have developed protective mechanisms to prevent the loss of $\Delta\Psi$ during oxidative stress by focusing on blocking mMPT. mMPT is mediated via the opening of the mitochondrial permeability transition pore; a pore permeable to solutes of less than 1.5 kDa and sensitive to an accumulation of ROS [21-23]. While the exact composition of the mitochondrial permeability transition pore is unknown, the current view is that the pore is created by the coupling of adenine nucleotide translocator (ANT) on the inner mitochondrial membrane and voltage dependent anion channel on the outer mitochondrial membrane with cyclophilin D, benzodiazepine receptors, hexokinases, and creatine kinases; with the last one serving regulatory but not structural functions [24, 25]. It has been suggested that GSK-3β modulates the function of these proteins through direct interaction based on studies demonstrating that GSK-3β exists in the mitochondria and its concentration in the mitochondria increases during ischemia [26-28]. The proposed model states that "phosphorylated GSK-3β interacts with ANT and reduces the affinity of ANT to cyclophilin D, which theoretically suppresses the opening of mitochondrial permeability transition pore." [26] Thus, GSK-3β is

considered to be immediately proximal to the mitochondrial permeability transition pore and acts as a point of integration for a multiplicity of protective signals [29].

GSK-3β is a 47 kDa enzyme that is expressed in all eukaryotes as one of two isoforms of GSK-3; a serine/threonine kinase that was first identified to phosphorylate and down-regulate glycogen synthase (GS) [30, 31]. The role of GSK-3β has been shown in the regulation of many cellular functions such as cell survival, apoptosis, adhesion, motility, and differentiation [32-34]. Juxtaposed to these beneficial functions, GSK-3β has been connected to several human disorders including neurodegenerative diseases, psychiatric disorders, parenchymal renal disease, and cancer [30]. As opposed to most kinases, GSK-3β is highly active in its basal state and has a chronic (usually negative) inhibitory effect on its downstream substrates until it is serine-phosphorylated (inactivated) by stimulation of its upstream regulators [30]. One of the main phosphorylation sites of GSK-3β lies within the amino-terminal domain at Ser9. Phosphorylation at this site inhibits GSK-β's chronic (negative) activity resulting in the activation of its downstream substrates [35]. The active form of GSK-3β has a priming phosphate site and a catalytic site that are both available for substrate binding. When Ser9 is phosphorylated it acts as a pseudo-substrate inhibitor by having the phosphorylated Serine bind to the priming phosphate site causing the amino terminus to block the catalytic site [35]. This blocking of the catalytic site prevents GSK-3β from activating its downstream substrates including components of the mitochondrial transition pore thereby preventing mitochondrial depolarization (here to fore being termed mitoprotection).

The concept of mitoprotection dictates that delaying the opening of the mitochondrial permeability transition pore prevents mitochondrial depolarization, thereby averting entry into the cell death pathway. Recent studies involving pre/post-conditioning ischemic reperfusion in

mouse and rat cardiac myocytes have shown that under conditions of oxidative stress, inhibition of GSK-3β activity prevents the loss of ΔΨ [36, 37]. One such study, Forster et al 2010 [37] demonstrated that inhibition of GSK-3β by SB216763 prevented the oxidant induced depolarization of ΔΨ in rat ventricular myocytes. This result occurred presumably through inactive GSK-3β blocking the opening of the mitochondrial permeability transition pore whereas active GSK-3β would allow for dynamic opening and closing of the pore. Thus, GSK-3β is a crucial enzyme involved in the prevention of mMPT through its dynamic regulation of the opening and closing of the mitochondrial permeability transition pore [38, 39].

One of the multiple protective proteins that converge on GSK-3β is the phosphorylated form of extracellular signal-regulated kinase1/2 (ERK1/2) [40]. ERK1/2 exists as two highly conserved serine/threonine kinase isoforms (ERK1 and ERK2) that are activated via phosphorylation on both threonine and tyrosine residues [41]. Phosphorylated ERK1/2 is the main downstream target of the Ras/Raf signaling pathway and its activation has been associated with several functions including cell proliferation, mitochondrial depolarization and apoptosis [14, 42, 43]. Studies conducted on metastatic carcinoma cells have shown ERK1/2 activation can cause GSK-3β to become phosphorylated at Ser9, thus inactivating the enzyme [40]. To carry out this phosphorylation, activated ERK1/2 serves as a scaffold that holds GSK-3β next to p90RSK in order to facilitate the inhibitory phosphorylation of GSK-3β at Ser9 by p90RSK [44]. Additionally, Flynn et. al. [14], demonstrated that upon RNA suppression of ERK1/2 there is a collapse of ΔΨ during oxidative stress in HLE-B3 cells. Note: in this study it was also demonstrated that the RNA suppression of BAD had no influence over ΔΨ indicating that ERK1/2 is a protein responsible for regulating mitoprotection in HLE-B3 cells. Combined, these

studies suggest that ERK1/2 can prevent the disruption of ΔΨ by inactivating GSK-3β thereby presumably blocking the opening of the mitochondrial transition pore.

Hypothesis

The role GSK-3β and ERK1/2 play in mitoprotection has yet to be established in an ocular system and warrants further study. The information that could be gleaned from studying these enzymes has implications in understanding the mitoprotective mechanisms possibly utilized by mesenchymal cells during PCO. My *long-term goal* is to identify potential enzymes that can be pharmacologically manipulated to prevent cellular damage caused by oxidative stress while possibly influencing the initiation/persistence of EMT. The *objective here* is to use HLE-B3 cells to characterize GSK-3β as an essential enzyme needed to prevent the depolarization of the mitochondria and to understand the role this enzyme plays in EMT. My *central hypothesis* is that GSK-3β is a crucial enzyme involved in the intiation/persistence of EMT as well as being involved in the mitoprotective mechanisms that prevent the dysfunction of human lens epithelial cells. I plan to accomplish the objectives of this research project and prove my hypothesis by performing the following three *specific aims:*

Aim I: To test the hypothesis that GSK-3β is a crucial enzyme regulating mitoprotection, and determine whether its activity can be influenced by affecting the signal transduction pathway further upstream.

Aim II: To determine how the regulatory protein ERK regulates mitoprotection by influencing the levels of apoptotic proteins.

Aim III: Provide a possible mechanism for the persistence of EMT in an ocular system under hypoxic conditions.

The following three chapters will address the studies carried out to test our aims and ultimately prove our hypothesis. Chapter II will serve as an in depth analysis of the emission spectroscopy technique that was developed to observe the functional impact of GSK-3β inactivation on $\Delta\Psi$. Chapter III will demonstrate the studies utilized to complete Specific Aims 1 and 2. Chapter IV will take the data from Aims 1 and 2 combined with previous studies from our lab to provide a possible mechanism for the persistence of EMT under hypoxic conditions that can potentially be manipulated in such a way as to prevent EMT without causing any harm to both diseased and non-diseased tissue.

Figures

Figure 1.1

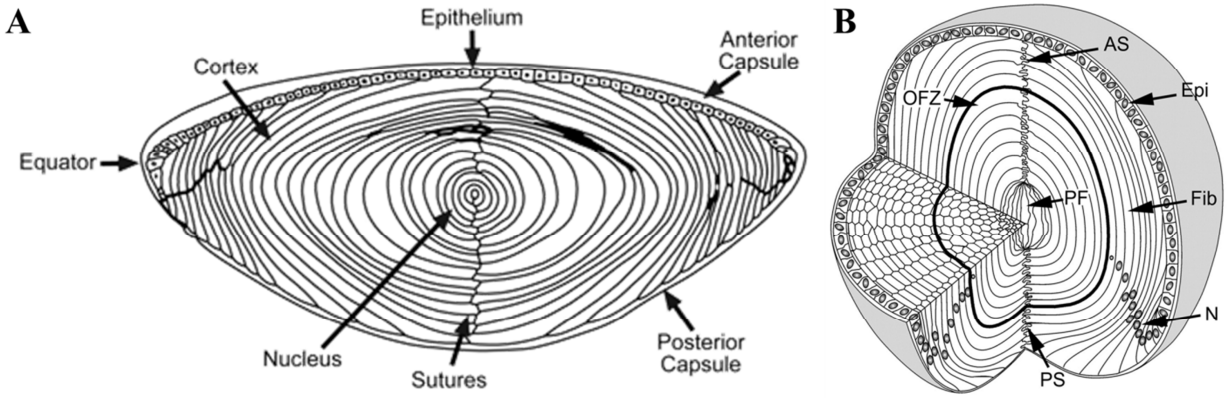

Figure 1.1. Diagram of lens structure. A: Human lens cross section taken from http://www.photobiology.info/Roberts.html. **B:** Mouse lens cross section. The abbreviations are defined as follows: epithelial cells (Epi), fiber cells (Fib), anterior lens sutures (AS), posterior lens sutures (PS), nuclei (N), organelle-free zone (OFZ), and primary fiber cells (PF). Taken from Shi et al 2009 [45].

Figure 1.2

Figure 1.2 Comparison of a normal lens (left) and a cataract in the lens (right). Cataracts make the lens appear cloudy and can cause full opacity of the lens, leading to complete blindness. Taken from http://www.mrdavidcheung.com/cataracts.html.

Figure 1.3

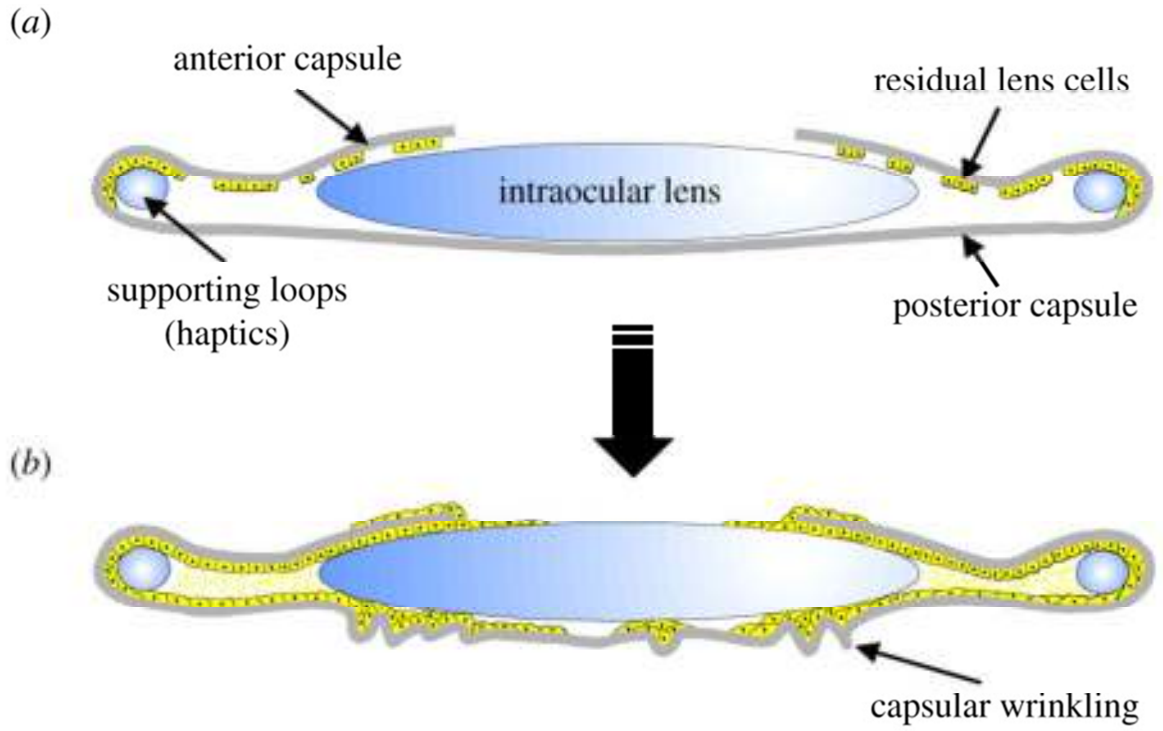

Figure 1.3 Schematic representation of the post-surgical capsular bag (a) and the extensive growth and modification that gives rise to PCO (b). Taken from Wormstone et al 2002 [12].

Introduction to Chapter II

Chapter II is a journal article published in Molecular Vision in June of 2013. This portion of the project focused on developing a novel technique to analyze the JC-1 dye in the presence of the drug SB216763; and, occurred concurrently with the experiments from the following Chapter III. Additionally, this Chapter provided insights into understanding if the inactivation of GSK-3β can influence mitochondrial depolarization.

Inactivation of GSK-3β is thought to cause increased mitoprotection (see Chapter I). Because of this observation, our lab inactivated GSK-3β via the drug SB216763 in HLE-B3 cells and measured the amount of mitochondrial depolarization under oxidative stress. To carry out these experiments a JC-1 dye was utilized. Ideally, this dye works by giving the user a green fluorescence and a red fluorescence which can be used to calculate a green to red ratio and subsequently determine the extent of mitochondrial depolarization. However, the drug SB216763 auto-fluoresces providing a broad contribution to the green fluorescence which interferes with the JC-1 analysis. This Chapter outlines a technique that serves as a viable means to analyze the JC-1 dye by suppressing the green contribution provided by SB216763; thus, allowing for an accurate measure of mitochondrial depolarization to be made. Overall, this study provided a way to overcome a significant hurdle and led to the development of a novel technique that became very useful later on in this project.

CHAPTER II

Lenticular mitoprotection. Part A: Monitoring mitochondrial depolarization with JC-1 and artifactual fluorescence by the GSK-3β inhibitor, SB216763.

Modified from Brooks et al. *Molecular Vision.* 2013; 19:1406-1412

Abstract

Purpose: Dissipation of the electrochemical gradient across the inner mitochondrial membrane results in mMPT, a potential early marker for the onset of apoptosis. In this study, we demonstrate a role for GSK-3β in regulating mMPT. Using direct inhibition of GSK-3β with the GSK-3β inhibitor SB216763, mitochondria may be prevented from depolarizing thereby increasing mitoprotection. Cells treated with SB216763 showed an artifact of fluorescence similar to the green emission spectrum of the JC-1 dye. We demonstrate the novel use of spectral de-convolution to negate the interfering contributing fluorescence by SB216763, thus allowing an unfettered analysis of the JC-1 dye to determine the $\Delta\Psi$.

Methods: Secondary cultures of HLE-B3 cells were exposed to acute hypoxic conditions (~1% O_2) followed by exposure to atmospheric oxygen (~21% O_2). The fluorescent dye JC-1 was used to monitor the extent of mitochondrial depolarization upon exposure of inhibitor treatment relative to the control cells (mock inhibition) in atmospheric oxygen. Annexin V-fluorescein isothiocyanate/propidium iodide staining was implemented to determine cell viability.

Results: Treatment of HLE-B3 cells with SB216763 (12 μM), when challenged by oxidative stress, suppressed mitochondrial depolarization relative to control cells as demonstrated with JC-1 fluorescent dye analysis. Neither the control nor the SB216763 treated HLE-B3 cells tested positive with annexin V-fluorescein isothiocyanate/propidium iodide staining under the conditions of the experiment.

Conclusions: Inhibition of GSK-3β activity by SB216763 blocked mMPT relative to the slow but consistent depolarization observed with the control cells. We conclude that inhibition of

GSK-3β activity by the GSK-3β inhibitor SB216763 provides positive protection against mitochondrial depolarization.

Introduction

Any outside stress such as oxidative stress from exposure to atmospheric oxygen or the loss of cellular respiration can increase the levels of ROS in HLE-B3 cells [13]. A sufficient buildup of ROS may cause a collapse of ΔΨ by mMPT [14, 15]. Should a collapse of ΔΨ occur it could prompt a harmful cycle in which the loss of ΔΨ disrupts the electron transport chain leading to increased formation of ROS which in turn causes further collapse of the ΔΨ [16, 17]. Loss of ΔΨ can have serious effects on the cell causing cellular dysfunction and possibly cell death via the release of apoptotic factors from the mitochondria [18].

Due to mMPT being mediated mainly via the opening of the mitochondrial permeability transition pore, HLE-B3 cells have developed protective mechanisms that target this pore in order to prevent the loss of ΔΨ [21-23]. Studies in the cardioprotection literature have shown that GSK-3β is a crucial enzyme involved in preventing the collapse of ΔΨ through dynamic regulation of the opening and closing of the mitochondrial permeability transition pore [38, 39]. Active GSK-3β allows the pore to open whereas the enzyme's inactivation blocks the pore from opening. The concept of mitoprotection states that blocking the opening of the permeability transition pore prevents mitochondrial depolarization; subsequently preventing cellular dysfunction and possible cell death [30]. Recent studies involving pre-/post-conditioning ischemic reperfusion in mouse and rat cardiac myocytes have shown that under conditions of oxidative stress, inhibition of GSK-3β activity prevents the loss of ΔΨ [30, 36, 37]. These studies suggest that inhibition GSK-3β may increase mitoprotection in cells by impeding mMPT. To date, no such studies linking GSK-3β with mMPT have been reported in an ocular system.

Currently, there have been no reported studies involving the use of SB216763 (a GSK-3β inhibitor) as it influences ΔΨ as analyzed with the potentiometric dye JC-1. In this report, we show that SB216763 contributes to the green emission spectrum thus contributing to a false result of depolarization. Our study describes the use of a technique that will enable the precise re-convolution of the proper contributions from JC-1 green and red emissions. The data demonstrate that preventing mitochondrial depolarization, via the use of SB216763, presumably due to blocking the opening of the mitochondrial membrane permeability transition pore, positively correlates with inhibiting GSK-3β enzymatic activity.

The influence of SB216763 on the pore as analyzed with JC-1 analysis has not previously been reported due to the emission spectrum of cells treated with SB216763 in the absence of JC-1 revealing a broad-spectrum over the range of 500–650 nm. In this study, we make novel use of spectral deconvolution based on experimental measurements, fluorophore reference spectra, and an algorithm for least-squares minimization to produce corresponding unmixed spectra. After deconvolution the green/red intensity ratios (540/595 nm) provided by the JC-1 dye were used to calculate the extent of mitochondrial depolarization.

Methods

Materials: Glycogen synthase kinase inhibitor 3-(2,4-dichlorophenyl)-4-(1-methyl-1H-indol-3-yl)-1H-pyrrole-2,5-dione (SB216763) was purchased from Sigma-Aldrich (St. Louis, MO). The stock inhibitor was prepared by adding dimethyl sulfoxide (DMSO) to make 16 mM of SB216763. The mitochondrial dye 1H-benzimidazolium-5,6-dichloro-2-[3-(5,6-dichloro-1,3-diethyl-1,3-dihydro-2H-benzimidazol-2-ylidene)-1-propenyl]-1,3-diethyl-iodide (JC-1) was obtained from Life Technologies (Grand Island, NY). All other reagents were acquired from other commercially available sources as previously reported [14].

Cell cultures: HLE-B3 cells, a human lens epithelial cell line immortalized by the SV-40 virus [46], were obtained from U. Andley (Washington University School of Medicine, Department of Ophthalmology, St. Louis, MO). The cells were maintained in minimal essential media (MEM) containing 5.5 mM glucose supplemented with 20% fetal bovine serum (Gemini Bio-Products, Sacramento, CA), 2 mM L-glutamine, nonessential amino acids, and 0.02 g/L gentamycin solution (Sigma-Aldrich) and cultured at 37 °C and 5% CO_2 to 95% O_2 [14]. All experiments were performed using monolayers of HLE-B3 cells that did not exceed passage 25. Cells were sub-cultured 4 to 5 days before the experiment and placed in MEM containing 20% fetal bovine serum. On the day of the planned experiment, cells were washed in serum-free MEM and then switched to serum-free MEM.

JC-1 fluorescence analysis and confocal microscopy: After the HLE-B3 cells were subjected to inhibitor treatment; the cells were stained with JC-1 to determine $\Delta\Psi$. JC-1 is a membrane-permeable lipophilic dye that exists as J-aggregates in the mitochondrial matrix (red fluorescence) and as monomers in the cytoplasm (green fluorescence). During mitochondrial depolarization, the red J-aggregates form green monomers due to a change in $\Delta\Psi$ [47]. Thus, depolarization can be measured as an increasing green fluorescent/red fluorescent intensity ratio.

The JC-1 assay was performed as follows. HLE-B3 cell monolayers were maintained in serum-free MEM with or without inhibitor treatment, brought through atmospheric oxygen (~21% O_2) exposure (90 min) into hypoxic (~1% O_2) exposure (3 h), and then later switched back to ambient oxygen as described above. At the end of the hypoxic exposure, the hypoxic media (oxygen depleted) was poured off, and fresh (oxygen rich) serum-free MEM with or without an inhibitor containing 5 μg/ml of the JC-1 dye was added for 30 min in a tissue culture incubator. The stained HLE-B3 cells were then rinsed twice using serum-free MEM, and fresh

oxygenated serum-free MEM (with or without inhibitor, but no JC-1 dye) was added. After the fresh media was added, the cells were analyzed with a Cary Eclipse spectrofluorometer (Varian Inc., Belrose, Australia).

Emission spectrum analysis: Fluorescence emission spectra were collected in 15 min intervals using a Cary Eclipse spectrofluorometer. Measurements were performed in front-face mode using secondary cultures of HLE-B3 cells on coverslips in the presence of an inhibitor or DMSO. The JC-1 emission spectrum was measured with the excitation at 470 nm. To analyze the ratiometric changes of the JC-1 spectrum, we performed spectral deconvolution with Mathcad software (Parametric Technology Corp., Needham, MA). The deconvolution was based on experimental measurements, fluorophore reference spectra, and an algorithm for least-squares minimization to produce corresponding unmixed spectra in graph form with error provided in minimal least-squares values for flexibility in analysis. After deconvolution, the green/red fluorescent intensity ratios (540/595 nm) were calculated to determine mitochondrial depolarization.

Annexin V-fluorescein isothiocyanate/propidium iodide apoptosis detection assay: To evaluate cell viability, a Clontech Apoalert annexin V apoptosis assay (Mountain View, CA) was used in conjunction with confocal microscope imaging to monitor apoptosis and necrosis. HLE-B3 cells were incubated for 90 min with serum-free MEM containing SB216763 (12 μM) or 0.05% DMSO vehicle in atmospheric oxygen (~21% O_2). After the incubation period, the cells were switched to hypoxia (~1% O_2) for 3 h. At the end of the hypoxic exposure, the oxygen-depleted media was removed, and fresh, oxygenated serum-free MEM containing either SB216763 or DMSO control was added for 60 min in atmospheric oxygen. At the end of this 60 min period, half the cell samples were stained with annexin V-fluorescein isothi-

cyanate/propidium iodide by removing the culture media, and washed one time with the blocking buffer provided in the Apoalert annexin V apoptosis detection kit (Clontech). After the wash, the samples had blocking buffer containing 50 ng/ml annexin V-fluorescein isothiocyanate and 125 ng/ml propidium iodide added to the dishes for 15 min in the dark at room temperature. The blocking buffer was subsequently removed, and fresh serum-free MEM containing SB216763 or DMSO was added. The samples not stained with annexin V-fluorescein isothicyanate/propidium iodide remained in serum-free MEM containing either SB216763 or DMSO throughout the washing and 15 min staining period. Random samples were imaged on a Zeiss LSM 410 confocal microscope (Peabody, MA). Red propidium iodide fluorescence, indicates the staining of DNA, in combination with green annexin V fluorescence, indicates a loss of plasma membrane integrity, is observed in necrotic cell death whereas green annexin V fluorescence alone is observed in apoptotic cell death [48].

Results

SB216763 inhibits the enzymatic activity of glycogen synthase kinase-3β and prevents mitochondrial depolarization during oxidative stress. The SB216763-treated and DMSO mock-treated cells were monitored for mMPT using the JC-1 dye. The basis of the JC-1 depolarization assay is to monitor the shift from red fluorescence to green fluorescence caused by the conversion of J-aggregates in the mitochondrial matrix (red) to J-monomers dispersing in the cytosol (green) upon opening of the membrane permeability transition pore. The emission spectrum of the cells treated with SB216763 in the absence of JC-1 revealed a broad-spectrum over the range of 500–650 nm (Figure 2.1A). The emission spectra of the JC-1 stained cells treated with DMSO consisted of two, well-separated spectra: green with a maximum at 540 nm and red with the maximum at 595 nm (Figure 2.1B). Cells stained with JC-1 and jointly treated

with SB216763 displayed a broad-spectrum fluorescence because the green fluorescence contributed by the inhibitor overlapped with the green and red fluorescence of the JC-1 dye, distorting the green peak that skewed the green/red ratio (Figure 2.1C). The distortion caused by the SB216763 fluorescence was subtracted from the total spectrum using spectral deconvolution. As stated in the Methods section, deconvolution was achieved by using the fluorophore reference spectra in Figure 2.1A and an algorithm for least-squares minimization. The deconvolution produced corresponding spectra with clear green (540 nm) and red (595 nm) maximums that were used to calculate the green/red ratio (Figure 2.1D). Analysis of the green/red ratio revealed that SB216763-treated cells had substantially suppressed mitochondrial depolarization relative to the controls (Figure 2.1E).

SB216763 does not affect cell viability. To determine the effect of inhibition of GSK-3β activity by treatment with SB216763 on cell viability, an annexin V-fluorescein isothi-cyanate/propidium iodide assay was implemented under similar conditions as the JC-1 analysis. Mock treated control cells (DMSO) not stained with annexin V-fluorescein isothicyanate/propidium iodide are shown in Figure 2.2A. The SB216763 treated cells stained with annexin V-fluorescein isothicyanate/propidium iodide (Figure 2.2B) showed a lack of red cells with green halo, indicating no apoptosis/necrosis. (Fluorescent green staining of the plasma membrane indicates apoptosis by the release of annexin V to the outer leaflet of the plasma membrane. Red staining of DNA with propidium iodide, in conjunction with green annexin V staining, indicates a loss of plasma membrane integrity typical of necrotic cells) [48]. However, artifactual SB216763 fluorescence resulting from undissolved particulate matter was noted. Cells treated with annexin V-fluorescein isothicyanate/propidium iodide alone confirmed the lack of red and green fluorescence (Figure 2.2C). The SB216763 treated cells in the absence of annexin

V-fluorescein isothicyanate/propidium iodide corroborated the fact that SB216763 displays artifactual fluorescence (Figure 2.2D).

Discussion

The dynamics of the mitochondrial membrane permeability transition pore and its regulation regarding the opening and closing of the pore are tightly controlled by GSK-3β [29, 30, 38, 39]. SB216763 is a potent and highly selective inhibitor of GSK-3β activity [49]. A role for GSK-3β in mitoprotection has been supported by the work of Juhaszova et al [30], who concluded that "this enzyme, located proximally (in the sense of a signaling cascade) to the mitochondrial transition pore complex, acts as a master switch to convey a multiplicity of protective signals to their final point, the mitochondrial permeability transition pore." Forster et al [37] demonstrated that inhibition of GSK-3β by SB216763 prevented the oxidant-induced depolarization of $\Delta\Psi$ (presumably caused by the inhibition of the opening of the transition pore) in rat ventricular myocytes. The reintroduction of atmospheric oxygen after acute hypoxia led to a slow but inevitable loss of $\Delta\Psi$ (Figure 2.1E). SB216763 was used to demonstrate that inactivation of GSK-3β prevents the loss of $\Delta\Psi$ (Figure 2.1E).

Interpretations other than inhibiting GSK-3β results in preventing the opening of the mitochondrial permeability transition pore are equally plausible as an explanation for our data. JC-1 is a novel membrane-permeable cationic carbocyanine dye that accumulates to a high concentration in the mitochondria as J-aggregates and exhibits an emission maximum at about 590 nm. JC-1 may diffuse across the outer and inner mitochondrial membrane in response to the changes in the $\Delta\Psi$. Diffusion to the cytoplasm from the mitochondria results in a lower concentration, where the dye exists as a monomer and yields green fluorescence with an emission maximum about 540 nm. Loss of JC-1 from the mitochondria is not inevitably a

measure of opening of the membrane permeability transition pore. Rather, the loss is a measure of the decrease in the inner mitochondrial membrane potential, possibly due to the loss of integrity of the inner and outer mitochondrial membranes. That is, JC-1 is permeable to the mitochondrial membrane, independent of the transition pore, and the dye's accumulation or loss does not necessarily depend on the state of the transition pore. Therefore, treatment with SB216763 might alternatively be explained as the drug's ability to maintain the transmembrane potential of the inner mitochondrial membrane. Regardless of how one chooses to interpret the data, the fact remains that SB216763 elicited lenticular mitoprotection.

Past studies have suggested that the phosphorylation of GSK-3β indicates inactivation of the enzyme [35]. Therefore, a key question that we wished to address in our study was whether the presumed inhibition of GSK-3β activity would positively correlate with the prevention of opening the mitochondrial membrane transition pore. To evaluate whether SB216763 blocked mitochondrial depolarization, we performed a JC-1 assay. The fluorescence of the SB216763 inhibitor was broad and overlapped with the green (540 nm) and red (595 nm) peaks of JC-1 emission (Figure 2.1A). This significantly affected the signals detected from the cells, as seen in Figure 2.1C. The microscopy images were corrupted by the fluorescence of the SB216763 inhibitor, and we were not able to conclude about the eventual changes of green/red intensities of JC-1. Fortunately, the JC-1 emission consisted of two well-separated peaks (Figure 2.1B). Each measured spectrum presented in Figure 2.1C is composed of these two JC-1 peaks and the SB216763 broad spectrum. The spectral deconvolution described in the Methods section enables reconstruction of the JC-1 spectrum without SB216763 interference, as presented in Figure 2.1D. With this heightened sensitive technique, the changes in the JC-1 spectra of the control, mock treated cells indicated a gradual but measured depolarization over 75 min of analysis, in the

absence of SB216763 (Figure 2.1E). In the presence of SB216763, depolarization was effectively inhibited (Figure 2.1E). These results suggest that GSK-3β activity is a prerequisite for the normal functioning of the mitochondrial permeability transition pore to open and close. Furthermore, we suggest inhibiting GSK-3β activity can influence the dynamics of the mitochondrial permeability transition pore and subsequently prevent the loss of $\Delta\Psi$ (Figure 2.1E).

Others have previously reported that SB216763 displays artifactual fluorescence [50]. The emission spectrum of SB216763 treated cells illustrates a broad spectrum over the range of 500–650 nm (Figure 2.1A). Furthermore, Figure 2.2 explicitly demonstrates the green fluorescence of undissolved SB216763 particulate matter with cells treated with SB216763 in the absence of annexin V-fluorescein isothicyanate/propidium iodide. The particulates stick to the cell surface of the cells and are not incorporated within cells. Moreover, the lack of red cells with a green halo in either the SB + annexin V-fluorescein isothicyanate/propidium iodide–treated cells (Figure 2.2B) or annexin V-fluorescein isothicyanate/propidium iodide–treated cells in the absence of SB216763 (Figure 2.2C) indicates that apoptosis/necrosis is not occurring under the conditions of the experiment with either the control or SB216763 treated cells. The latter point is not trivial as it confirms that the technical manipulation of switching the cells from hypoxia to oxygen exposure (refer to Methods) is not, of itself, sufficient oxidative stress to elicit entry into the cell death pathway.

The noted green fluorescent aggregates (Figure 2.2D) were likely due to the poor solubility of the inhibitor, and therefore, the inhibitor may not have been effective at inhibiting GSK-3β activity. To confirm that SB216763 did, indeed, inactivate GSK-3β activity, we treated the HLE-B3 cells with SB216763 and verified the enzymes' inability to phosphorylate its

downstream substrate, GS. The failure to adequately phosphorylate GS indicated the inactivation of the active site of GSK-3β [51]. The inhibition of GSK-3β activity (as monitored by the failure to phosphorylate GS) positively associated with preventing mMPT; a result that will be discussed in greater detail in Chapter III. We further examined the influence of the inactivation of GSK-3β activity on another substrate, β-catenin. β-catenin is a prominent nuclear transcription factor whose activity is regulated by GSK-3β. When GSK-3β is active, it inactivates β-catenin by phosphorylation. Treatment of HLE-B3 cells with SB216763 in atmospheric oxygen resulted in decreased phosphorylated β-catenin, the consequence of which was the increased translocation of β-catenin (active form) to the nucleus (data not shown). This increased translocation of β-catenin plays an important role in understanding EMT which will be discussed further in Chapter IV.

In conclusion, the studies herein demonstrated that GSK-3β plays a pivotal role in regulating the mitochondrial membrane permeability transition pore under conditions of cell culture in atmospheric oxygen. Additionally, these studies have shown a novel technique that can be used to monitor changes in JC-1 fluorescence while in the presence of the drug SB216763.

Figures

Figure 2.1

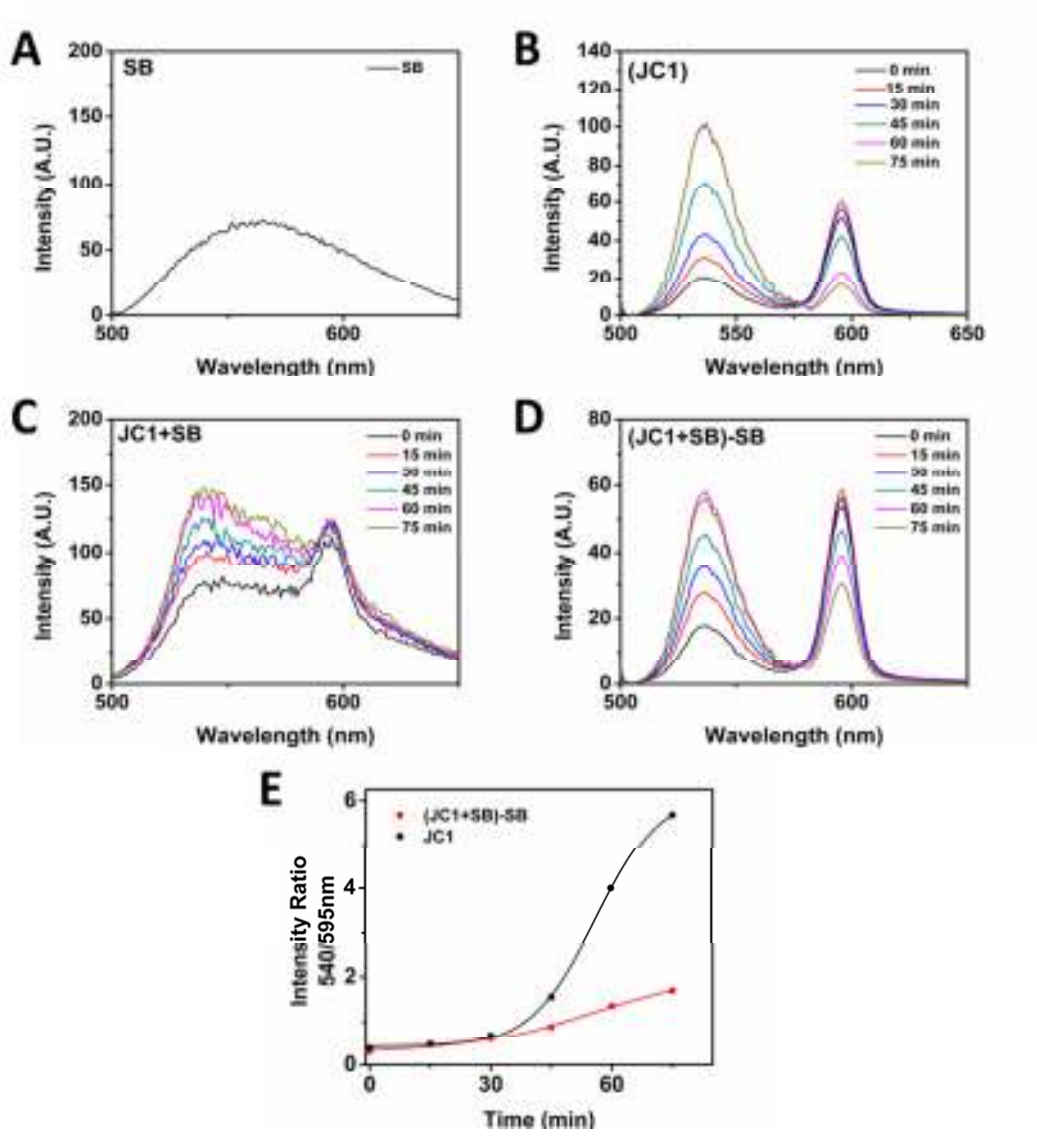

Figure 2.1. Emission spectrum analysis of mitochondrial depolarization in HLE-B3 cells treated with SB216763. HLE-B3 cells were incubated for 90 min with serum-free MEM containing SB216763 (12 μM) or 0.05% DMSO vehicle in atmospheric oxygen (~21% O_2). After the incubation period, the cells were switched to hypoxia (~1% O_2) for 3 h. At the end of the hypoxic exposure the oxygen depleted media was removed and fresh, oxygenated serum-free MEM containing 5μg/ml JC-1 with either SB216763 or DMSO was added for 30 min in atmo-

spheric oxygen. At the end of the 30 min period, the culture media was again removed and fresh serum-free MEM containing SB216763 or DMSO added. A random field of cells was scanned for emission spectrum analysis every 150 sec for 75 min but only the data points for every 15 min interval is shown. **A**: The analysis of the serial emission spectrum for HLE-B3 cells treated with SB216763. **B**: The analysis of the serial emission spectrum for HLE-B3 cells treated with DMSO in the presence of the potentiometric dye (JC-1). **C**: The analysis of the serial emission spectrum of HLE-B3 cells treated with SB216763 and JC-1. **D**: The analysis of the serial emission spectrum from the SB216763 treated cells (refer to **C**) after deconvolution was used to suppress the contribution from the inhibitor (refer to **A**). **E**: The graph of green emission (540 nm) over red emission (595 nm) of SB216763 treated cells with JC-1 after deconvolution (red dots) versus DMSO with JC-1control cells (black dots). The experiment was performed on three independent populations of lens epithelial cells. The data is not a composite of the three runs but rather the best of the three is shown.

Figure 2.2

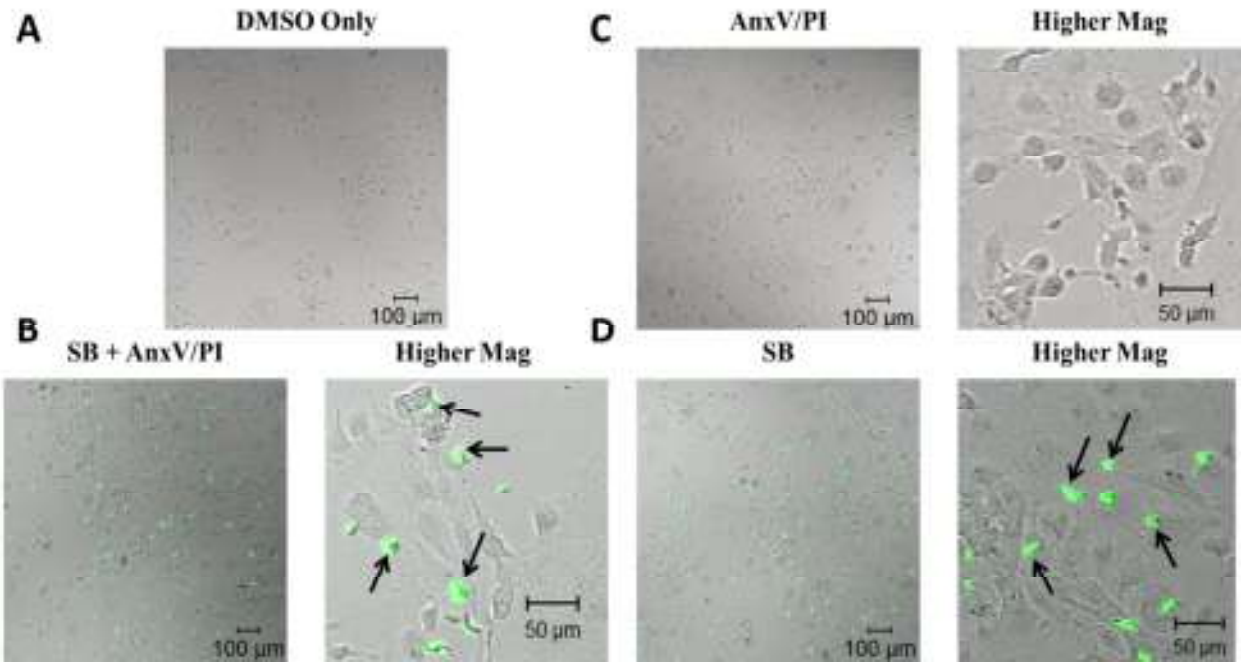

Figure 2.2. Annexin V-fluorescein isothicyanate/propidium iodide analysis of apoptosis in HLE-B3 cells treated with SB216763. Cells were treated with annexin V-fluorescein isothicyanate/propidium iodide either in the presence or absence of SB216763. **A:** Image of DMSO control cells without annexin V-fluorescein isothicyanate/propidium iodide. **B:** (left panel) Image of SB216763 treated cells additionally stained with annexin V-fluorescein isothicyanate/propidium iodide; (right panel) higher magnification. **C:** (left panel) Image of cells stained with annexin V-fluorescein isothicyanate/propidium iodide only; (right panel) higher magnification. **D:** (left panel) Image of SB216763 treated cells; (right panel) higher magnification. Black arrows indicate false fluorescence from undissolved SB216763 particulate.

Introduction to Chapter III

Chapter III contains a journal article that was published in Molecular Vision in November 2013. This portion of the project focused on understanding the mechanisms that influence mitoprotection via GSK-3β and one of its upstream regulators ERK1/2. To investigate these mechanisms in greater detail several enzymatic inhibitors were employed to inactivate key components of the mitoprotective pathway. One result from the use of these inhibitors of particular interest is the similarity in western blots between SB216763 and UO126 treated cells that yielded two opposite JC-1 profiles. Looking further into this discrepancy between the two inhibitors provided profound insights about ERK1/2 and its influence over apoptosis. Additionally, the studies presented within this chapter were able to show a similarity between the virally transformed HLE-B3 cells and the normal bovine lens epithelial cells (BLECs) when it came to ERK1/2 inactivation via treatment with UO126. Overall, these studies were able to define a mitoproctective mechanism utilized by lens epithelial cells during oxidative stress that encompasses a signaling pathway from ERK1/2 activation down to phosphorylated Bcl-2.

CHAPTER III

Lenticular mitoprotection. Part B: GSK-3β and regulation of mitochondrial permeability transition for lens epithelial cells in atmospheric oxygen.

Modified from Brooks et al. *Molecular Vision.* 2013; 19:2451-2467

Abstract

Purpose: Loss of integrity of either the inner or outer mitochondrial membrane results in the dissipation of the mitochondrial electrochemical gradient that leads to mMPT. This study emphasizes the role of GSK-3β in maintaining ΔΨ, thus increasing mitoprotection by preventing mitochondrial depolarization. Using SB216763, an inhibitor of GSK-3β, and drawing a distinction between it and UO126, an inhibitor of ERK1/2 phosphorylation, the means by which GSK-3β influences mitoprotection in cultured HLE-B3 cells and normal, secondary cultures of BLECs, maintained in atmospheric oxygen, was investigated.

Methods: Virally transfected HLE-B3 cells and normal BLEC cultures were exposed to acute hypoxic conditions (~1% O_2) followed by exposure to atmospheric oxygen (~21% O_2). Specific antisera and western blot analysis was used to examine the state of phosphorylation of ERK1/2 and GSK-3β, as well as the phosphorylation of a downstream substrate of GSK-3β, GS (useful in monitoring GSK-3β activity). The potentiometric dye JC-1 was used to monitor mitochondrial depolarization upon exposure of inhibitor treatment relative to the control cells (mock treated with DMSO vehicle) in atmospheric oxygen. Caspase-3 activation was scrutinized to determine whether mitochondrial depolarization inevitably leads to apoptosis.

Results: Treatment of HLE-B3 cells with SB216763 (12 μM) inactivated GSK-3β activity as verified by the enzyme's inability to phosphorylate its substrate, GS. SB216763 treated cells were not depolarized relative to the control cells as demonstrated with JC-1 fluorescent dye analysis. The HLE-B3 cells treated with UO126, which similarly blocked phosphorylation of GS, were nevertheless prone to mMPT relative to the control cells. Western blot analysis determined that Bcl-2-associated X (BAX) protein levels were unchanged for SB216763 treated and UO126 treated HLE-B3 cells when compared to their respective control

cells. However, unlike the SB216763 treated cells, the UO126 treated cells showed a marked absence of Bcl-2, as well as phosphorylated Bcl-2 relative to the controls. UO126 treatment of BLECs showed similar results with pBcl-2 levels, while the Bcl-2 content appeared unchanged relative to the control cells. HLE-B3 and normal BLEC cultures showed susceptibility to mMPT associated with the loss of pBcl-2 by UO126 treatment.

Conclusions: Mitochondrial depolarization may occur by one of two key occurrences: interruption of the electrochemical gradient across the inner mitochondrial membrane resulting in mMPT or by disruption of the integrity of the inner or outer mitochondrial membrane. The latter scenario is generally tightly regulated by members of the Bcl-2 family of proteins. Inhibition of GSK-3β activity by SB216763 blocks mMPT by preventing the opening of the mitochondrial permeability transition pore. UO126, likewise, inhibits GSK-3β activity, but unlike SB216763, inhibition of ERK1/2 phosphorylation induces the loss of intracellular pBcl-2 levels under conditions where intracellular BAX levels remain constant. These results suggest that the lenticular mitoprotection normally afforded by the inactivation of GSK-3β may, however, be bypassed by a loss of pBcl-2, an anti-apoptotic member of the Bcl-2 family. Bcl-2 prevents the translocation of BAX to the outer mitochondrial membrane inhibiting depolarization by disrupting the normal electrochemical gradient leading to mMPT.

Introduction

As stated previously in Chapter I, the dissipation of $\Delta\Psi$ occurs due to mMPT [14]. Lens epithelial cells represent an ideal model for studying mMPT because the lens thrives in a naturally hypoxic environment, and introducing atmospheric oxygen increases the formation of ROS, which, in turn, may cause a loss of $\Delta\Psi$ [14, 15]. The current literature suggests that mMPT is mediated via the opening of the mitochondrial permeability transition pore [21-23]. Studies

have shown that GSK-3β is immediately proximal to the mitochondrial permeability transition pore and acts as a point of integration for many protective signals [29]. Thus, GSK-3β is a crucial enzyme involved in preventing mMPT through regulating the opening and closing of the mitochondrial permeability transition pore [38, 39]. Additional studies involving ischemic reperfusion of cardiac myocytes have demonstrated that inhibiting GSK-3β can prevent the dissipation of ΔΨ during oxidative stress [30, 36, 37].

One of the multiple protective proteins that converge on GSK-3β is the phosphorylated form of ERK1/2 [40]. Flynn et al [14] has previously demonstrated that after RNA suppresses ERK, ΔΨ collapses during oxidative stress in HLE-B3 cells. Furthermore, studies conducted on metastatic carcinoma cells have shown that phosphorylated ERK1/2 can cause GSK-3β to become phosphorylated at its inhibitory serine, thus inactivating the enzyme [40]. Combined, these studies suggest that ERK1/2 can prevent the disruption of ΔΨ by inactivating GSK-3β, presumably blocking the opening of the mitochondrial transition pore. However, as will be demonstrated in this study, inhibiting ERK1/2 phosphorylation can, itself, cause mitochondrial depolarization regardless of the activity of GSK-3β.

To date, the role that GSK-3β plays regarding preventing mitochondrial depolarization has not been established in an ocular system. In the current study, we demonstrate that inactivating GSK-3β (as monitored by its failure to phosphorylate GS) using the pharmacological inhibitor SB216763 has a regulatory function in preventing mitochondrial depolarization. Furthermore, this study will reveal that the mitoprotection normally afforded by GSK-3β inactivation may be circumvented by inhibiting ERK1/2 phosphorylation, which culminates in inhibition of Bcl-2 phosphorylation, an anti-apoptotic member of the Bcl-2 family.

Methods

Materials: The mitogen activated protein kinase kinase 1/2 (MEK1/2) inhibitor 1,4-diamino-2,3-dicyano-1,4-bis[2-aminophenylthio] butadiene (UO126) was purchased from Cell Signaling Technology (Danvers, MA). The glycogen synthase kinase inhibitor SB216763 was purchased from Sigma-Aldrich (St. Louis, MO). The c-Jun N-terminal kinase (JNK) inhibitors SP600125 (JNK Inhibitor II) and AS601245 (JNK Inhibitor V) were purchased from EMD Millipore Chemicals (Billerica, MA). Stock inhibitors were prepared by adding to DMSO as follows: 20 mM for UO126, 16 mM for SB216763, 40 mM for SP600125, and 40 mM for AS601245. The mitochondrial dye JC-1 was obtained from Life Technologies (Grand Island, NY). All other reagents were acquired from other commercially available sources as previously reported [14].

Cell cultures: HLE-B3 cells, a human lens epithelial cell line immortalized by the SV-40 virus [46], were obtained from U. Andley (Washington University School of Medicine, Department of Ophthalmology, St. Louis, MO). Authentication of the HLE-B3 cell line was verified with STR profile analysis (American Type Culture Collection, Manassas, VA), which confirmed that the cell line was human and of female origin, as originally reported by Andley et al. [46]. A copy of the STR profile is available upon request. All studies with HLE-B3 cells were performed with pre-frozen stock cells (maintained in liquid nitrogen) between passages 14 and 17. No experiments exceeded five passages beyond the initial stock cell passage. The cells were maintained in MEM containing 5.5 mM glucose supplemented with 20% fetal bovine serum (Gemini Bio-Products, Sacramento, CA), 2 mM L-glutamine, nonessential amino acids, and 0.02 g/l gentamycin solution (Sigma-Aldrich) and cultured at 37 °C and 5% CO_2 to 95% O_2 [14]. Cells were sub-cultured 4 to 5 days before the experiment and placed in MEM containing 20%

fetal bovine serum. Twenty-four hours before the day of the experiment, the cells were switched to serum-free MEM. Unless otherwise specified, all experiments followed a common protocol: Cells were maintained in atmospheric oxygen (~21% O_2) for 90 min, and then switched to hypoxic conditions (~1% O_2) for 3 h, followed by reintroduction to atmospheric oxygen. Each experiment was executed with control DMSO only cells (mock inhibitor treatment) and cells treated with inhibitors. The DMSO concentration per experiment never exceeded 0.05%.

Bovine eyes obtained from a local abattoir were transported on ice to the laboratory, where the lenses were removed aseptically. BLECs were isolated and cultured in MEM containing 20% fetal bovine serum. All studies with BLECs were performed on cells of passage 2.

Western blot analysis: Whole cell lysates were collected from HLE-B3 cultures using the hot protein extraction method as described by Henrich et al. [52]. The cell cultures were rinsed at room temperature with phosphate buffered saline in final concentration: 150 mM sodium chloride, 10 mM sodium phosphate monobasic, 40 mM sodium phosphate dibasic, pH 7.4, before the monolayers were lysed with hot lysis buffer (~100 °C), subsequently scraped into 1.7 ml micro centrifuge tubes, and immediately sonicated. The lysis buffer consisted of 0.12 M Tris-HCl (pH 6.8), 4% sodium dodecyl sulfate, and 20% glycerol [14]. Part of the lysate samples were removed and used to determine the protein concentration. The protein concentration was calculated using a DC protein assay kit from Bio-Rad (Hercules, CA). The lysate samples contained 25 μg of protein, 1X sodium dodecyl sulfate laemmli buffer, and 1.5 μl 2-mercapto-ethanol (Sigma-Aldrich). The lysate samples were then boiled for 5 min and the proteins resolved on 12% sodium dodecyl sulfate-polyacrylamide gels. The proteins were then transferred

to a nitrocellulose membrane (Bio-Rad). The electrophoresis and western blot apparatus were from Hoefer Scientific (Holliston, MA).

For western blot analysis, nitrocellulose membranes were blocked with 0.1% bovine serum albumin in Tris-buffered saline for 60 min. These membranes were probed overnight at 4 °C with primary antibodies at a 1:1,000 dilution. The blots were then rinsed with 0.02% Tween-20 in Tris-buffered saline for 5 min 4X and then incubated in either goat anti-rabbit horseradish peroxidase conjugate or goat anti-mouse horseradish peroxidase conjugate at 1:10,000 dilution (Santa Cruz Biotechnology, Santa Cruz, CA) for 60 min at room temperature. Blots were again rinsed with 0.02% Tween-20 in Tris-buffered saline (4X 5 min washes), and proteins were detected using a SuperSignal West Pico chemiluminescent kit from Pierce (Rockford, IL) [14]. Probed membranes were visualized on a Fluoro Chem TM 8900 imager (Alpha Innotech, San Leandro, CA).

Primary antibodies were purchased from Cell Signaling Technology (Danvers, MA). The antibodies used in this study included rabbit anti-Bcl-2-associated X (BAX), rabbit anti-glycogen synthase, rabbit anti-phospho-glycogen synthase (Ser641), rabbit anti-phospho-GSK-3β (Ser9), rabbit anti-GSK-3β, mouse anti-phospho-p44/42 mitogen-activated protein kinase (Thr202/Tyr204), rabbit anti-p44/42 mitogen-activated protein kinase, rabbit anti-phospho-Bcl-2 (Ser70), rabbit anti-Bcl-2, and rabbit anti-phospho-c-Jun (Ser63). Rabbit anti-actin was provided by Santa Cruz Biotechnology (Santa Cruz, CA).

JC-1 fluorescence analysis and confocal microscopy: After the HLE-B3 cells were subjected to inhibitor treatment; the cells were stained with JC-1 to determine the $\Delta\Psi$. JC-1 is a membrane permeant lipophilic dye that exists as J-aggregates in the mitochondrial matrix (red fluorescence) and as monomers in the cytoplasm (green fluorescence). During mitochondrial

depolarization, the red J-aggregates flow out of the mitochondria and accumulate in the cytosol as green monomers [47]. Thus, depolarization can be measured as an increasing green/red fluorescent intensity ratio.

The JC-1 assay was performed as follows. HLE-B3 cell monolayers were maintained in serum-free MEM with or without inhibitor treatment, brought through 90 min of atmospheric oxygen (~21% O_2) exposure into 3 h of hypoxic (~1% O_2) exposure, and then later switched back to atmospheric oxygen. At the end of the hypoxic exposure, the hypoxic media on (oxygen depleted) was poured off, and fresh (oxygen rich) serum-free MEM with or without an inhibitor containing 5 μg/ml of the JC-1 dye was added for 30 min in a tissue culture incubator. The stained HLE-B3 cells were then rinsed twice using serum-free MEM, and fresh oxygenated serum-free MEM (with or without inhibitor, but no JC-1 dye) was added. A random field of cells was imaged every 150 sec for 60 min using an X10 objective on a confocal microscope (Ziess LSM410, LSM410, Thornwood, NY). The excitation wavelength was 488 nm, and the microscope was set to simultaneously detect green emission (540 nm) and red emission (595 nm) channels using a dual bandpass filter [14].

Caspase-3 apoptosis detection assay: A caspase-3 enzyme-linked immunosorbent assay (ELISA) (Invitrogen, Camarillo, CA) was used to determine apoptosis. HLE-B3 cell monolayers were maintained in serum-free MEM with or without treatment and brought through our experimental protocol, which included 90 min of atmospheric oxygen (~21% O_2) exposure followed by 3 h of hypoxic (~1% O_2) exposure, and then being subsequently switched back into atmospheric oxygen. Treatment included SB216763 (12 μM), UO126 (10 μM), staurosporine (100 nM), or 0.05% DMSO vehicle maintained throughout the course of the experiment. Sixty minutes after atmospheric oxygen was reintroduced, all samples were then lysed using our

previously described lysis buffer. Part of the lysate samples was removed and used to determine the protein concentration. The protein concentration was calculated by using a DC protein assay kit (Bio-Rad). Apoptotic activity was determined following the manufacturer's protocol using 10 μg of protein.

Statistical analysis: Images from JC-1 confocal microscopy were analyzed as individual red and green channels using Image J (Baltimore, MD). The background fluorescence was removed from each image before the intensity was measured. The fluorescence intensity signal from each image was quantified for the entire image and expressed as the ratio of green fluorescent intensity over red fluorescent intensity. Western blot densitometry was determined using Image J analysis. A student's t-test was performed by collecting the densitometry from the Western blot profiles of three individual cell cultures stemming from an initial single cell population using the software from Graphpad Prism, version 5.00 (La Jolla, CA). Statistical significance was determined based upon a P value < 0.05. Error bars represent SEM. For bar graphs representing the density of Western blot bands, a student's t-test was likewise applied.

Results

Switching HLE-B3 cell cultures from hypoxia to atmospheric oxygen or, conversely, from atmospheric oxygen to hypoxia, does not induce mitochondrial depolarization. JC-1 analysis of the DMSO mock-treated cells exposed to various cell culture conditions was implemented to determine whether environmental stress (i.e., hypoxia (~1% O_2), atmospheric oxygen (~21% O_2), or reversal from one condition to the other) elicited mitochondrial depolarization. Four conditions were tested: cells grown in constant atmospheric oxygen, cells switched from atmospheric oxygen to hypoxia, cells switched from hypoxia to atmospheric oxygen, and cells maintained in continuous hypoxia. Under all tested conditions the cells did not depolarize

indicating that either continuous hypoxic exposure, continuous exposure to atmospheric oxygen or switching cell culture environments does not induce depolarization (Figure 3.1).

SB216763 inhibits the enzymatic activity of GSK-3β and prevents mitochondrial depolarization during oxidative stress. To investigate the role GSK-3β plays in regulating cellular mitoprotection with cells maintained in hypoxia and subsequently exposed to atmospheric oxygen, HLE-B3 cells were treated with the GSK-3β inhibitor, SB216763. Non-phosphorylated GSK-3β is the active form of the enzyme, and in this form, the enzyme is capable of phosphorylating numerous downstream substrates including GS [35]. The phosphorylation of GS is thus a useful parameter for monitoring GSK-3β activity. Cultures of HLE-B3 cells were grown on 100 mm dishes until >85% confluence. Cells were treated with 12 μM SB216763 or mock-treated with DMSO vehicle. After 90 min in atmospheric oxygen (~21% O_2), the cells were placed under hypoxic (~1% O_2) conditions for 3 h and then switched back to atmospheric oxygen for 3 h. Samples were collected from cells consistently maintained in atmospheric oxygen (control), immediately after hypoxic exposure and 1 h, 2 h, and 3 h of reexposure to atmospheric oxygen. Western blot analysis showed that the HLE-B3 cells subjected to SB216763 treatment had levels of GSK-3β and pGSK-3β similar to those of the controls (Figure 3.2). However, treatment with SB216763 resulted in inhibition of phosphorylation of GS. The failure to phosphorylate GS indicates the active site of GSK-3β was inactivated. The continued presence of pGSK-3β in the treated cells was because the autophos-phorylation site of GSK-β was unaffected by SB216763 [53]. A key question that we wished to address in this study was whether inhibiting GSK-3β activity positively correlated with preventing mitochondrial depolarization. In Chapter II it was observed that SB216763 treated

cells monitored for mMPT using emission spectroscopy displayed suppressed mitochondrial depolarization relative to the control DMSO mock treated cells (Figure 2.1).

ERK1/2 inhibition prompts depolarization without affecting pGSK-3β under oxidative stress conditions. A parallel experiment, using the MEK1/2 inhibitor UO126, was also conducted on HLE-B3 cells to determine whether inhibiting ERK1/2 phosphorylation had any impact on the phosphorylation of GSK-3β and GS. Lens cells were treated with 10 μM UO126 or 0.05% DMSO in atmospheric oxygen (~21% O_2) for 90 min before being subsequently placed in hypoxic (~1% O_2) conditions for 3 h. Following the hypoxic exposure, new media was added to the culture dishes, and the cells were reexposed to atmospheric oxygen for up to 3 h in the continued presence or absence of UO126. Lysates of these cells were collected from cells maintained consistently in atmospheric oxygen, after the hypoxic exposure and 1 h, 2 h, and 3 h after atmospheric oxygen was reintroduced. Analysis of the western blot membranes showed marked inhibition of p42 ERK1/2 and p44 ERK1/2 (Figure 3.3, upper panel, left) relative to the control cells. The loss of ERK1/2 phosphorylation did not affect the relative levels of GSK-3β or pGSK-3β compared with the DMSO controls (Figure 3.3, upper panel, right), whereas inhibiting ERK1/2 phosphorylation prevented the downstream phosphorylation of GS. Therefore, the configuration of the ratio of pGSK-3β/GSK-3β and pGS/GS appeared identical irrespective of whether SB216763 or UO126 was used (compare the bar graphs of Figure 3.2 and Figure 3.3). Given the similarity in the profile of the ratio of pGSK-3β/GSK-3β and pGS/GS, a critical question was whether UO126 treated cells, similar to SB216763 treated cells, likewise prevented mitochondrial depolarization relative to the control DMSO mock treated cells or whether UO126 treated cells were prone to mMPT.

Parallel studies were conducted using JC-1 analysis. HLE-B3 cells were treated with 10 μM UO126 or 0.05% DMSO in atmospheric oxygen (~21% O_2) for 90 min and were then placed in hypoxic (~1% O_2) conditions for 3 h. The cells were exposed to the JC-1 dye for 30 min in atmospheric oxygen. Following the JC-1 application, fresh media with UO126 or DMSO was added to the culture plates. The cells were subsequently observed with confocal microscopy and the green and red intensities recorded every 150 sec for 60 min. The green to red ratio of the UO126 treated cells markedly increased over the time course relative to the control cells, indicating the loss of $\Delta\Psi$ (Figure 3.3, bottom panel).

There is a difference in SB216763 treatment versus UO126 treatment when observing BAX, Bcl-2, and Bcl-2 phosphorylation levels. As discussed above, comparison of the western blots for pGSK-3β/GSK-3β and pGS/GS between the two inhibitor treatments generated profiles that were similar, if not, identical (Figures 3.2 & 3.3). However, whereas treatment with the GSK-3β inhibitor, SB216763, likely blocked opening of the mitochondrial membrane permeability transition pores, effectively suppressing depolarization [54], treatment with UO126 elicited profound depolarization relative to the control cells (Figure 3.3, bottom panel). We therefore examined in greater detail the outcome of each inhibitor on the BAX, Bcl-2, and pBcl-2 levels.

Lysates from all experimental treatments were evaluated to determine the levels of Bcl-2, pBcl-2, and BAX. Western blot membranes from the SB216763 treated and UO126 treated cells, relative to their respective controls, indicated no alteration in the levels of BAX for the treated and control cells (Figure 3.4, upper panel and Figure 3.5, upper panel). The relative levels of pBcl-2 and Bcl-2 were not altered for the SB216763 treated cells compared with the control cells (Figure 3.4, middle panel). In contrast, the UO126 treated cells displayed significantly

diminished levels of pBcl-2 under all culture conditions, including normoxic control, hypoxic exposure, and the reintroduction of atmospheric oxygen (Figure 3.5, middle panel); a significant loss of Bcl-2 was also observed but, interestingly, only during the reintroduction of atmospheric oxygen phase (Figure 3.5, middle panel).

Of particular note, treatment with UO126 (Figure 3.5, upper left panel & bottom panels) but not with SB216763 (Figure 3.4, upper left panel & bottom panels) prevented the phosphorylation of c-Jun, through all culture conditions. The phosphorylation of c-Jun is a useful parameter for monitoring JNK activity. That is, UO126, while effectively inhibiting ERK1/2 phosphorylation (Figure 3.3, upper left panel), was nonetheless equally effective in inactivating JNK activity. This observation imposed a burden of proof upon us to determine whether the ERK1/2 pathway or the JNK pathway negatively impacted the pBcl-2 levels.

JNK inhibition does not affect Bcl-2 phosphorylation. HLE-B3 cells were treated with JNK inhibitors, SP600125 (5 μM, 10 μM, or 20 μM), AS601245 (5 μM, 10 μM, or 20 μM), or DMSO vehicle (control). These two inhibitors are potent adenosine triphosphate-competitive inhibitors that prevent JNK from transferring a phosphate group to its substrates [55, 56]. Phosphorylated JNK is the active form of the enzyme, and in this form, the enzyme is capable of phosphorylating numerous downstream substrates, including c-Jun. The phosphorylation of c-Jun is thus a useful parameter for monitoring JNK activity. Treated and control cells were brought through 90 min of atmospheric oxygen (~21% O_2) and placed in hypoxia (~1% O_2) for 3 h. At the end of the hypoxic exposure the treated and untreated cells were switched back into atmospheric oxygen for 3 h. During the switch to atmospheric oxygen, the hypoxic media was removed from the cultures, and fresh oxygenated media containing either inhibitor or vehicle was added. Lysates of all the cells were collected after 3 h of exposure to atmospheric oxygen.

SP600125 and AP601245 markedly reduced phospho-c-Jun at all concentrations relative to the control cells (Figure 3.6). Further analysis indicated no change in the levels of BAX, Bcl-2, or pBcl-2 for cells treated with SP600125 or AS601245 versus cells treated with DMSO vehicle (Figure 3.6). A slight increase in the levels of pERK1/2 was observed in cells with either inhibitor treatment relative to the control cells, the meaning of which is not immediately evident to us. However, whereas UO126 negatively impacted JNK activity (Figure 3.5), the JNK inhibitors did not cross-inactivate ERK1/2 phosphorylation (Figure 3.6). We therefore concluded that inhibition of the ERK1/2 pathway, not the JNK pathway, elicited the inhibition of phosphorylation of Bcl-2 (Figure 3.5).

Increased mitochondrial depolarization does not necessarily affect cell viability. To determine if the inhibition of ERK1/2 or GSK-3β activity influence the onset of apoptosis, an active caspase-3 ELISA was implemented. HLE-B3 cells were treated with either 12 μM SB216763, 10 μM UO126, 0.05% DMSO vehicle or 100 nM staurosporine. The 100 nM staurosporine concentration was used as a positive activator of caspase-3. Cells were incubated in atmospheric oxygen (~21% O_2) for 90 min and then placed in hypoxia (~1% O_2) for 3h. At the end of the hypoxic exposure, the media was removed from the treated and untreated cells, and fresh media was added. The cells were then placed in atmospheric oxygen for 60 min. All treatments were administered throughout the duration of the experiment. At the end of this 60 min period, all the samples were lysed with lysis buffer. The DMSO mock treated cells displayed minimal capase-3 activation relative to the cells treated with staurosporine (positive control), which showed a significant increase in caspase-3 activity (Figure 3.7). The UO126 treated and SB216763 treated cells demonstrated levels of capase-3 activity similar to the DMSO mock treated cells (Figure 3.7). The lack of caspase-3 activity in the UO126 treated and SB216763

treated cells indicates that apoptosis did not occur in the presence of either inhibitor, even though the UO126 treatment did elicit mMPT (Figure 3.3, bottom panel).

Bovine lens epithelium portrays similar responses to UO126 treatment as compared with HLE-B3 cells. To determine that our results (and consequent interpretations) had not been compromised by the viral transformation of the HLE-B3 cells, we repeated the UO126 treatment with secondary cultures of normal BLECs using the same conditions that were used for the HLE-B3 experiments, as described above. Inhibition of p42 ERK1/2 and p44 ERK1/2 relative to the control cells was noted (Figure 3.8, upper panel). As with the HLE-B3 cells (Figure 3.3, upper right panel), neither GSK-3β nor pGSK-3β were diminished (Figure 3.8, middle panel) when compared to the DMSO controls. Likewise, inhibition of ERK1/2 phosphorylation prevented the downstream phosphorylation of GS (Figure 3.3, upper right panel; & Figure 3.8, middle panel).

We further investigated the effect of UO126 treatment on BAX, Bcl-2, and pBcl-2 levels using secondary cultures of BLECs. Lysates were evaluated with western blot analysis to determine the levels of BAX, Bcl-2, and pBcl-2. Western blot membranes from the UO126 treated cells relative to their respective controls indicated some lane loading variability, but no obvious loss, in the levels of BAX (Figure 3.8, bottom panel), similar to that of the HLE-B3 cells (Figure 3.5, upper left panel). As with the HLE-B3 cells (Figure 3.5, upper left panel), the UO126 treated cells displayed a significant reduction in pBcl-2 under all culture conditions: normoxic control, hypoxic exposure, and the reintroduction of atmospheric oxygen (Figure 3.8, bottom panel). Of interest, unlike the HLE-B3 cells (Figure 3.5, middle panel) where a significant loss of Bcl-2 was noted only during the reintroduction of atmospheric oxygen phase; the BLECs demonstrated no dramatic reduction in the levels of Bcl-2 between the treated and untreated cells under any condition (Figure 3.8, bottom panel). Finally, as first observed with

HLE-B3 cells (Figure 3.5, upper left panel), UO126 inhibited the phosphorylation of c-Jun, through all culture conditions (Figure 3.8, bottom panel).

Bovine lens epithelium depolarize in the absence of pBcl-2. Parallel studies with UO126 were conducted using JC-1 analysis. Normal BLECs were treated with 10 μM UO126 or 0.05% DMSO in atmospheric oxygen (~21% O_2) for 90 min and then placed under hypoxic (~1% O_2) conditions for 3 h. The cells were exposed to the JC-1 dye for 30 min in atmospheric oxygen. Following the JC-1 application, fresh media with UO126 or DMSO was added to the culture plates. The cells were subsequently observed with confocal microscopy and the green and red intensities recorded every 150 sec for 60 min. As with the UO126 treated HLE-B3 cells (Figure 3.3, bottom panel) the green to red ratio of the UO126 treated BLECs markedly increased over the time course relative to the control cells, indicating the loss of $\Delta\Psi$ (Figure 3.9).

Discussion

To establish our reference baseline, it was first necessary to demonstrate that the experimental manipulation of switching cells from hypoxia to atmospheric oxygen or vice versa, from atmospheric oxygen to hypoxia, was not, of itself, sufficient oxidative stress to elicit mitochondrial depolarization (Figure 3.1). Once established that the physical manipulation of switching cell cultures from one oxygen pressure to another did not impose mitochondrial depolarization, we investigated the regulatory function of GSK-3β insofar as its ability to convey mitochondrial resistance to depolarization (i.e. increase mitoprotection).

First, we sought to clarify whether blocking GSK-3β's auto-phosphorylation site or inactivating its catalytic site conferred prevention of mitochondrial depolarization. To monitor the enzyme's active, catalytic site, we scrutinized the phosphorylation of a downstream substrate of GSK-3β, GS. Our data revealed that SB216763 did not block the auto-phosphorylation of

GSK-3β relative to control cells, but successfully eliminated the phosphorylation of GS, indicating that the catalytic site of GSK-3β was inactivated (Figure 3.2). Stated another way, the failure to phosphorylate GS, but not the auto-phosphorylation site of GSK-3β, appears to be a better predictor of whether inhibiting GSK-3β's enzymatic activity positively correlates with blocking mMPT. In Chapter II it was demonstrated that "inhibition of GSK-3β activity by SB216763 blocked mMPT relative to the slow but consistent depolarization observed with the control cells." [54]. It was concluded from these studies that inhibiting GSK-3β activity with the GSK-3β inhibitor SB216763 provides positive protection against mitochondrial depolarization [54].

The role of GSK-3β and how it may be influenced by upstream signaling mechanisms has been the focus of numerous studies. "There is evidence in different cell types that anti-apoptotic responses can be mediated by phosphatidylinositol 3-kinase (PI3K) and the Akt/PKB serine-threonine protein kinase, p42/p44 mitogen-activated protein kinases or extracellular response kinases (ERKs), Raf, and cyclic AMP-dependent protein kinase (PKA)." [57] To further delve into this issue, using the lens cell model, we compared and contrasted the pGSK-3β/GSK-3β, as well as the pGS/GS western blot profiles of cells treated with an inhibitor of ERK1/2 activity, UO126, against a known catalytic site inhibitor of GSK-3β, SB216763 (refer to above). We followed up with a JC-1 evaluation to monitor whether ERK1/2 inhibitor treatment prompted mitochondrial depolarization or whether, like SB216763, inhibiting ERK1/2 phosphorylation imposed resistance to mitochondrial depolarization [54].

Similar to the treatment with SB216763 (Figure 3.2), treatment with UO126 had no effect on auto-phosphorylation of GSK-3β relative to the control cells, but successfully eliminated the phosphorylation of GS (Figure 3.3, upper right panel). However, whereas treatment with

SB216763 resulted in suppression of mitochondrial depolarization (Figure 2.1E), unexpectedly, the UO126 treated cells displayed profound depolarization (Figure 3.3, bottom panel). We therefore sought to explain the apparent discrepancy between the similarity of the SB216763 and UO126 profiles of pGSK-3β/GSK-3β and pGS/GS and the observation that the former but not the latter conferred resistance to mitochondrial depolarization.

Western blot analysis of HLE-B3 cells treated with SB216763 or UO126 showed that the BAX levels were unchanged relative to mock treated control cells (Figure 3.4 vs 3.5). Moreover, the BAX content of the UO126 treated normal BLECs was similar relative to the control cells (Figure 3.8, bottom panel). This data supports the notion that BAX does not play a direct role in lens epithelial cell resistance to mitochondrial depolarization. We therefore directed our attention to answering the question, "Is it the continuous expression of Bcl-2 or the phosphorylation of Bcl-2 that confers resistance to mitochondrial depolarization?" The UO126 treated virally transformed HLE-B3 cells, and the normal BLECs demonstrated a propensity to depolarize (Figure 3.3, bottom panel; & Figure 3.9). Additionally, it was observed that UO126 treatment with HLE-B3 cells instigated a loss of Bcl-2 only under the condition of reintroduction of atmospheric oxygen (Figure 3.5) whereas UO126 treatment with normal BLECs did not diminish the levels of Bcl-2 (Figure 3.8, bottom panel), although with both types of cells a profound loss of pBcl-2 was apparent under all conditions (Figure 3.5, top left panel; & Figure 3.8, bottom panel). Therefore, since the bovine cells depolarized without the loss of Bcl-2, we conclude that pBcl-2 confers anti-depolarization resistance in lens epithelial cells.

Lei et al. 2002 [58-62] stated that, ". . . this phosphorylation has been reported to inhibit the pro-survival function of Bcl-2. This conclusion, however, is controversial as other studies have indicated that phosphorylation may enhance the anti-apoptotic actions of Bcl-2" [63-65].

The data from our studies lends support to the latter statement in that the depolarization observed with UO126 treatment is caused by a lack of pBcl-2 (Figures 3.3, 3.5, 3.8, & 3.9). The lack of pBcl-2 likely results in a loss of Bcl-2's anti-apoptotic functions as reported by others. Cellular apoptosis is regulated, in part, by maintaining a balance between the levels of the pro-survival protein, Bcl-2, and the pro-apoptotic protein, BAX. BAX is a pro-apoptotic member of the Bcl-2 family. Activation of BAX causes its translocation to the mitochondrial outer membrane and induces mitochondrial depolarization. However, before BAX can initiate this process, the protein must first translocate from the cytoplasm to the mitochondria. Bcl-2 influences apoptosis by regulating the translocation of BAX to the mitochondria [66, 67]. Any decrease in the levels of Bcl-2 (or in our case, pBcl-2) is likely to permit the translocation of BAX from the cytosol to the mitochondria and induce mitochondrial depolarization. Disruption of the integrity of the outer mitochondrial membrane would then be the cause of the initiation of the loss of $\Delta\Psi$, often cited as an early predictor of the onset of apoptosis.

Previous studies in our laboratory have shown that UO126 inhibits not only ERK1/2 phosphorylation but also JNK activity (unpublished observation). Studies have shown that phosphorylated JNK mediates the phosphorylation of the anti-apoptotic protein Bcl-2 [58-63]. Thus, as this relates to the studies described here, one possible explanation for the loss of $\Delta\Psi$ could have been attributed to the loss of JNK activity. To determine whether this was the case, we analyzed JNK activity with UO126 treatment. A common measure of JNK activity is to monitor the phosphorylation of one of its downstream substrates, c-Jun, where inhibition of the phosphorylation of c-Jun indicates inactivation of JNK. The level of phospho-c-Jun was similar with SB216763 treatment relative to control cells (Figure 3.4). UO126 inhibited c-Jun phosphorylation (Figure 3.5). Moreover, the resulting inhibition of c-Jun phosphorylation with

treatment by UO126 was accompanied by an apparent loss of pBcl-2, thus suggesting a potential connection between the JNK pathway and mitoprotection (Figure 3.5). UO126 treatment, since it inhibited JNK activity, complicated our ability to definitively interpret the data, in that our results would not permit us to immediately distinguish whether the inhibition of phosphorylation of ERK1/2 or JNK influenced the downstream reduction in pBcl-2 levels.

It therefore became necessary to determine which of the two pathways, ERK1/2 or JNK, was influencing the phosphorylation of Bcl-2. HLE-B3 cells were treated with two specific inhibitors of JNK activation. Analysis of the levels of phospho-c-Jun revealed that SP600125 and AS601245 effectively reduced the levels of phospho-c-Jun relative to that of the controls without affecting the pBcl-2 levels (Figure 3.6). Collectively, the data reported in Figure 3.5 and Figure 3.6 allowed us to assert that inactivating JNK does not influence Bcl-2 phosphorylation. Instead, inhibiting ERK1/2 phosphorylation causes the loss of Bcl-2 phosphorylation. We therefore conclude that inhibiting ERK1/2 phosphorylation circumvents the mitoprotection otherwise afforded by the inactivation of GSK-3β presumably because of the loss of pBcl-2 (Figures 3.5 & 3.8).

Mitochondrial depolarization is often cited as an early indicator of the onset of apoptosis. However, our studies establish that despite the mitochondrial depolarization initiated by UO126 treatment for HLE-B3 cells (Figure 3.3, bottom panel) in conjunction with the loss of pBcl-2 (Figure 3.5), the degree of mMPT was at an insufficient level to induce apoptosis in human lens epithelial cells, as indicated by the lack of active caspase-3 (Figure 3.7). Our result is not all that unexpected because it has previously been shown that there is considerable intracellular heterogeneity in the $\Delta\Psi$ of mitochondria [68]. In effect, the degree of mitochondrial depolarization as indicated by the JC-1 dye represents the collective states of depolarization from a

heterogeneous population of mitochondria. We conclude that one must exercise caution when equating mitochondrial depolarization with the onset of apoptosis. Cellular apoptosis/necrosis should be determined only after examination with annexin V/propidium iodide, DNA fragmentation, or caspase-3 or 9 cleavage, or some combination thereof.

In conclusion, the studies presented here further support our previous assertion from Chapter II that GSK-3β is a critical upstream regulator of mMPT for human lens epithelial cells cultured in atmospheric oxygen. In this study, we have established a direct relationship between the active catalytic site of GSK-3β and the normal functioning of the mitochondrial permeability transition pore to open and close. However, inhibiting ERK1/2 phosphorylation indirectly overrides the otherwise protective influence of GSK-3β to resist mMPT through a concomitant loss of pBcl-2 levels leading to mitochondrial depolarization. Restated, the fact that SB216763 and UO126 prevent the phosphorylation of GS suggests that GS phosphorylation, itself, may be regulated by one of the many signaling pathways activated by ERK1/2 independent of GSK-3β. At the same time, the ERK1/2 pathway also likely independently influences Bcl-2 phosphorylation. The mechanism by which UO126 administration leads to preventing phosphorylation of Bcl-2 is currently not understood and warrants further investigation.

Previous studies in our laboratory have shown that UO126 treatment elicits a significant decrease in the expression of vascular endothelial growth factor (VEGF) but only upon reintroduction from hypoxia to atmospheric oxygen (unpublished observation). However, UO126 does not have an effect on VEGF expression in hypoxia maintained cells [69]. VEGF acts as a pro-survival factor in hypoxic lens epithelial cells by maintaining consistent expression of the pro-survival protein Bcl-2, which likely prevents the translocation of cytosolic BAX to the outer mitochondrial membrane, thus preventing the initiation of mitochondrial depolarization

[69]. Because of the pro-survival role of VEGF in hypoxia, the last part of this project shifted toward elucidating the potential role GSK-3β might have in managing the sustained expression of VEGF and understanding how that role relates to GSK-3β's influence in the initiation/persistence of EMT under hypoxic conditions.

Figures

Figure 3.1

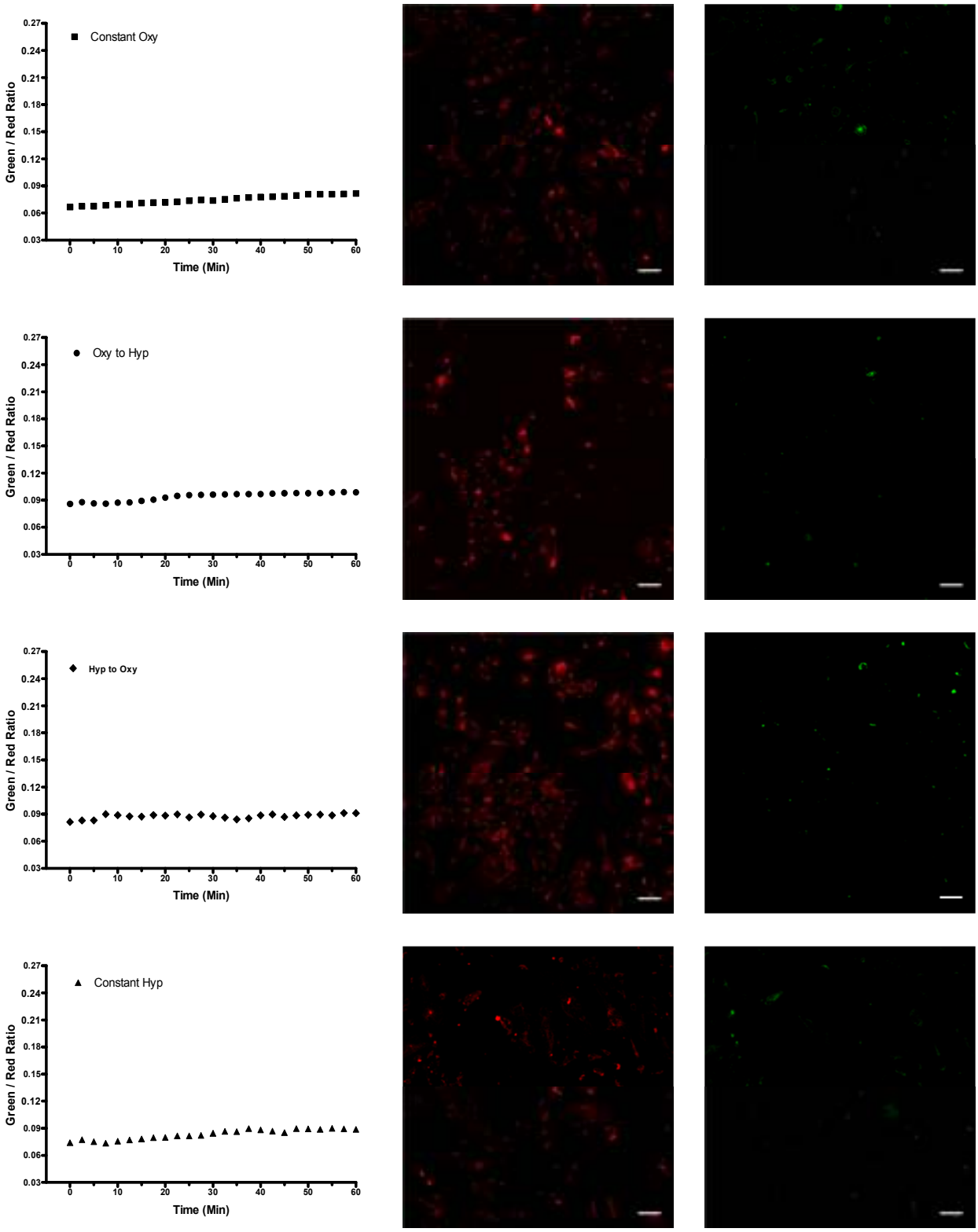

Figure 3.1. JC-1 stained mock treated (DMSO) HLE-B3 cells under several adaptations of hypoxic and atmospheric oxygen exposure. HLE-B3 cells were stained with JC-1 and observed with confocal microscopy with images captured every 150 sec over a 60 min period, under the following conditions: continuous hypoxia (~1%), continuous atmospheric O_2 (~21%), switching from hypoxia to atmospheric O_2, or switching from atmospheric O_2 to hypoxia. Top row: (continuous atmospheric O_2) Cells were maintained in atmospheric O_2 and stained for 30 min in atmospheric O_2. At the end of the 30 min staining period, fresh oxygenated media was added to the dishes. A random field of cells was then imaged. Note: The term "random field of cells" with all JC-1 analyses means an arbitrary field of cells is selected; and, the same field of cells is photographed throughout the 60 min image capture. Second row: (atmospheric O_2 to hypoxia) Cells were maintained in atmospheric O_2 and stained for 30 min in atmospheric O_2. At the end of the 30 min staining period, the cells were switched to hypoxic media (media preincubated at ~1% O_2). A random field of cells was immediately imaged. Third row: (hypoxia to atmospheric O_2) Cells were placed in hypoxic conditions for 3 h. At the end of the hypoxic exposure, the media was removed and replaced with fresh oxygenated media containing JC-1. The cells were stained for 30 min in atmospheric O_2. After this 30 min period, the media was removed and fresh oxygenated media was added. A random field of cells was then imaged. Fourth row: (continuous hypoxia) Cells were stained with media containing JC-1 for 30 min in atmospheric O_2. At the end of this 30 min period, the media was removed and fresh hypoxic media was added. The cells were then switched into hypoxic conditions for 3 h. The cells were then imaged following the 3 h hypoxic exposure. Under all experimental conditions, there was no evidence of loss of $\Delta\Psi$ throughout the 60 min image capture.

Figure 3.2

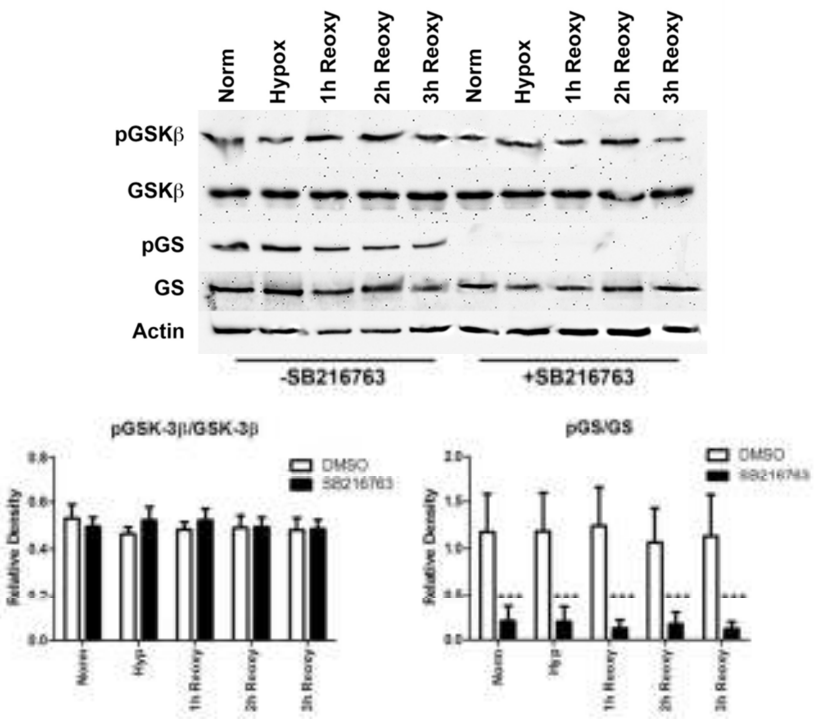

Figure 3.2. Western blot analysis of GSK-3β and GS phosphorylation in HLE-B3 cells in the presence or absence of SB216763. Total cell lysates were collected from >85% confluent HLE-B3 cell cultures that were incubated for 90 min in serum-free MEM, under conditions of atmospheric oxygen (~21% O_2), containing either 12 μM SB216763 or 0.05% DMSO vehicle. Cells were then exposed to hypoxia (~1% O_2) for 3 h in the continued presence of SB216763. At the end of the hypoxic incubation period, the hypoxic media was removed, and fresh, oxygenated serum-free MEM with SB216763 or DMSO vehicle was added to the cultures. Cells were then placed in atmospheric oxygen for up to 3 h. Cultures were collected after (1) continuous normoxic exposure, (2) after the 3 h hypoxic exposure, or (3) after reintroduction of atmospheric oxygen for 1, 2, or 3 h subsequent to the 3 h hypoxic exposure. Total cell lysates were analyzed with immunoblots using 25 μg of protein per lane. Anti-actin was used to normalize the bands to

ensure equivalent lane loading. Three experiments, using independent cell populations, were quantified using GraphPad Prism 5 and the relative densities plotted for pGSK-3β/GSK-3β and pGS/GS. No change was evident in the ratio of pGSK-3β/GSK-3β while significant inhibition of the phosphorylation of GS by SB216763 was noted. Error bars represent standard error. The asterisks (***) indicate $p<0.001$, Student *t* test.

Figure 3.3

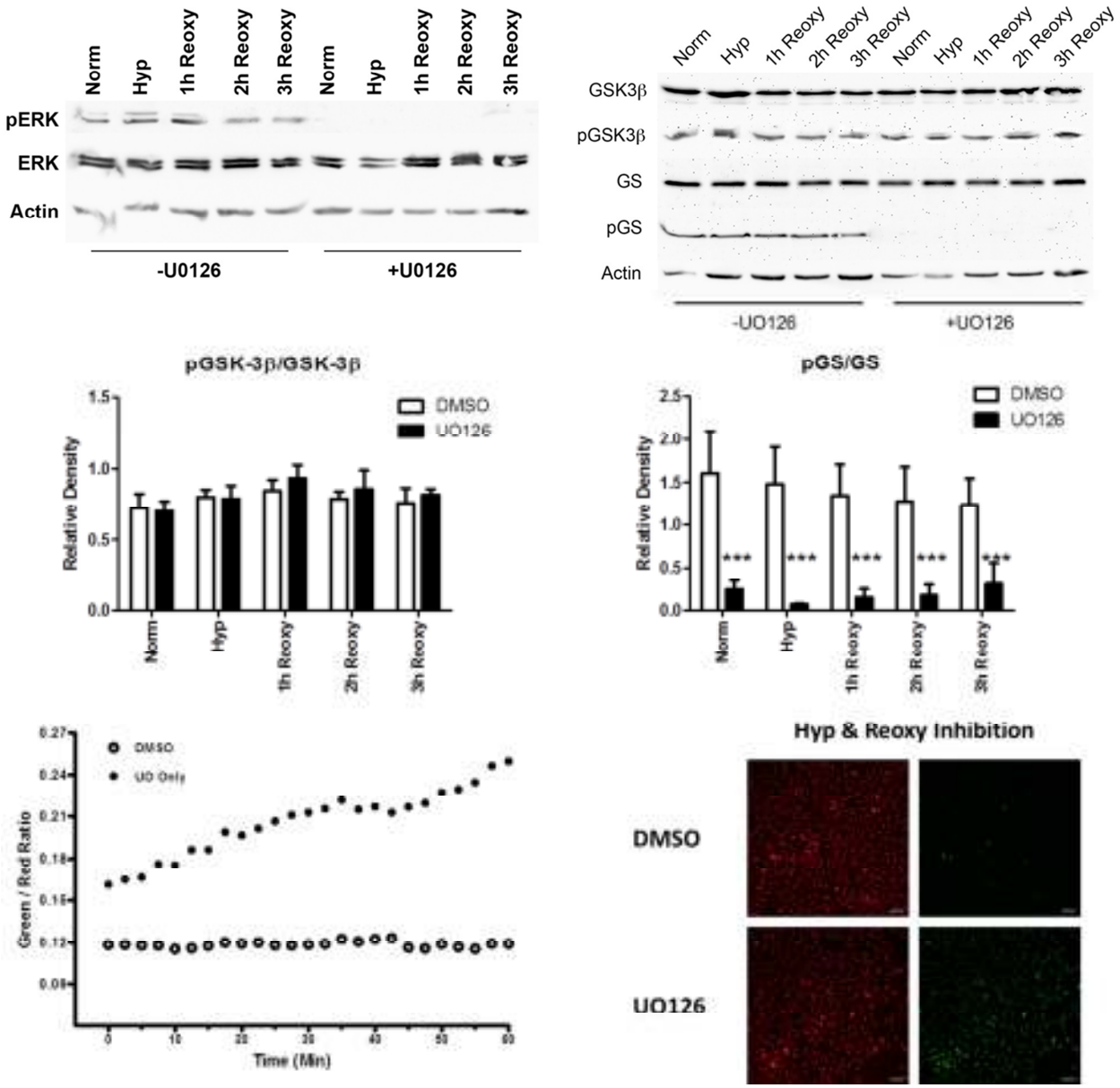

Figure 3.3. Western blot analysis of GSK-3β and GS phosphorylation along with JC-1 analysis of HLE-B3 cells treated with UO126 inhibitor. HLE-B3 cell cultures were incubated for 90 min in serum-free MEM, under conditions of atmospheric oxygen (~21% O_2), containing either 10 μM UO126 or 0.05% DMSO vehicle. Cells were then exposed to hypoxia (~1% O_2) for 3 h. At the end of the hypoxic incubation period, the hypoxic media was removed, and fresh, oxygenated serum-free MEM with UO126 or DMSO vehicle was added to the cultures. Cells

were then placed in atmospheric oxygen for up to 3 h. Cultures were collected after continuous normoxic exposure, after the 3 h hypoxic exposure, or after reintroduction of atmospheric oxygen for 1, 2, or 3 h subsequent to the 3 h hypoxic exposure. Total cell lysates were analyzed with immunoblots using 25 μg of protein per lane. Anti-actin was used to normalize the bands to ensure equivalent lane loading. The loss of phosphorylation of ERK1/2 by UO126 treatment was noted (top, left panel), as was the loss of phosphorylated GS (top, right panel). The relative densities of three experiments, using independent cell populations, were plotted for pGSK-3β/GSK-3β and pGS/GS. No change was evident in the ratio of pGSK-3β/GSK-3β while significant inhibition of the phosphorylation of GS by UO126 was indicated (middle panel). Error bars represent standard error. The asterisks (***) indicate $p<0.001$, Student *t* test. (Bottom left panel) HLE-B3 cells were incubated for 90 min with serum-free MEM, under atmospheric oxygen conditions, containing 10 μM UO126 or 0.05% DMSO vehicle. Cells were switched to hypoxia for 3 h in the continued presence of UO126 or DMSO vehicle. At the end of the hypoxic exposure the cells had their media removed; and, fresh oxygenated serum-free MEM containing 5 μg/ml JC-1 plus either UO126 or DMSO was added for 30 min in atmospheric oxygen. At the end of the 30 min incubation period, the media was again switched with fresh serum-free MEM containing UO126 or DMSO in the absence of the JC-1 dye. The same field of cells was imaged every 150 sec for 60 min. Serial confocal imaging of mitochondrial depolarization in HLE-B3 cells in the presence of UO126 demonstrated significant depolarization compared to control cells. (Bottom left panel) Images of the red and green intensity for the UO126 treated and DMSO treated cells at t=60 min (bar=20 μm). Note the marked intensity of the green channel with UO126 treated cells relative to DMSO mock treatment at the completion of the 60 min analysis (bottom right panel) indicating mitochondrial depolarization.

Figure 3.4

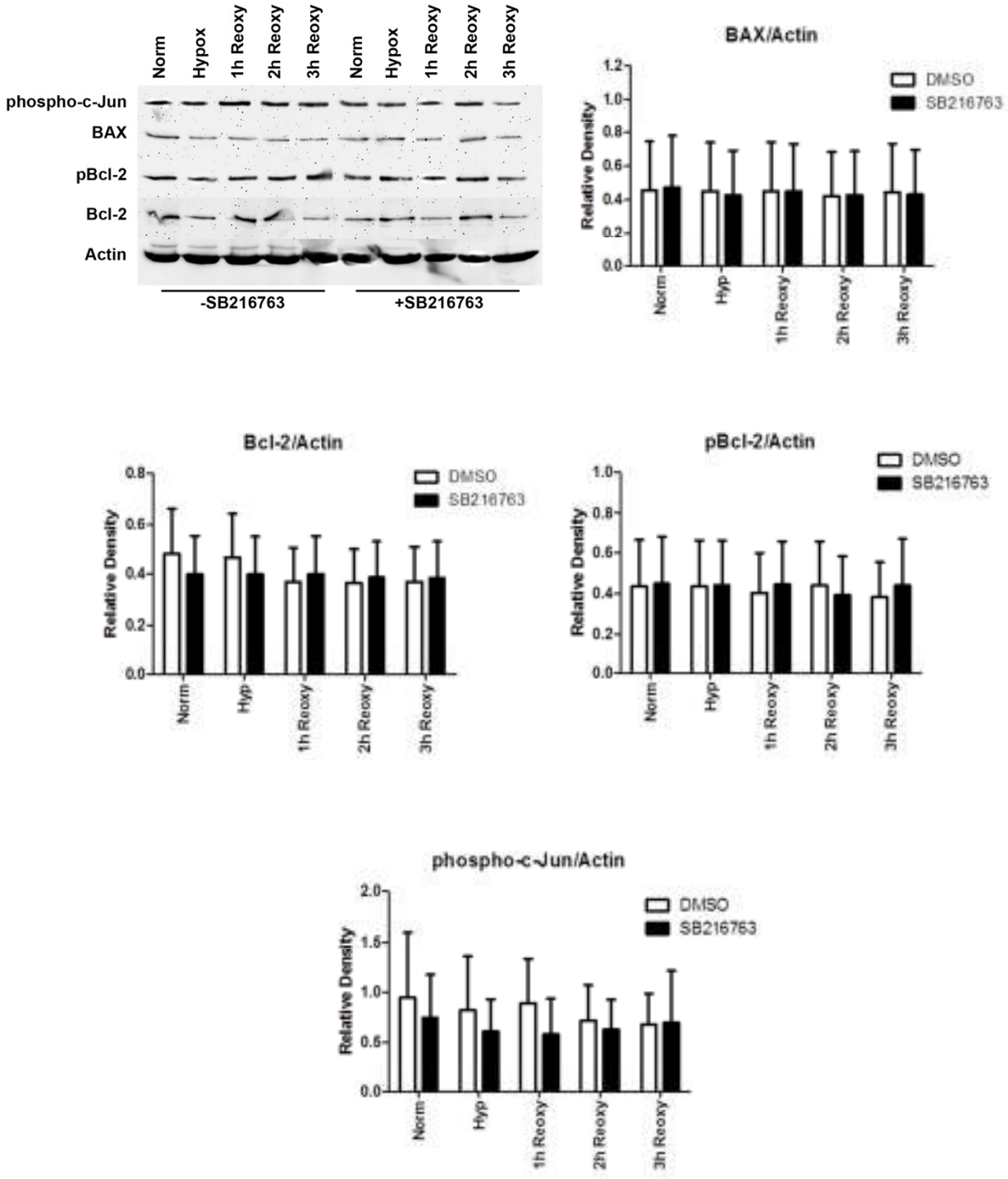
Norm
Hypox
1h Reoxy
2h Reoxy
3h Reoxy
Norm
Hypox
1h Reoxy
2h Reoxy
3h Reoxy
phospho-c-Jun
BAX
pBcl-2
Bcl-2
Actin
-SB216763
+SB216763
BAX/Actin
DMSO
SB216763
Relative Density
1.2
1.0
0.8
0.6
0.4
0.2
0.0
Norm
Hyp
1h Reoxy
2h Reoxy
3h Reoxy
Bcl-2/Actin
DMSO
SB216763
Relative Density
0.8
0.6
0.4
0.2
0.0
Norm
Hyp
1h Reoxy
2h Reoxy
3h Reoxy
pBcl-2/Actin
DMSO
SB216763
Relative Density
1.0
0.8
0.6
0.4
0.2
0.0
Norm
Hyp
1h Reoxy
2h Reoxy
3h Reoxy
phospho-c-Jun/Actin
DMSO
SB216763
Relative Density
2.0
1.5
1.0
0.5
0.0
Norm
Hyp
1h Reoxy
2h Reoxy
3h Reoxy

Figure 3.4. Western blot analysis of BAX, Bcl-2, pBcl-2, and phospho-c-Jun in HLE-B3 cells in the presence or absence of SB216763. Total cell lysates were collected from >85% confluent HLE-B3 cell cultures that were incubated for 90 min in serum-free MEM, under conditions of atmospheric oxygen (~21% O_2), containing either 12 μM SB216763 or 0.05% DMSO vehicle. Cells were then exposed to hypoxia (~1% O_2) for 3 h in the continued presence of SB216763 or DMSO vehicle. At the end of the hypoxic incubation period, the hypoxic media was removed, and fresh, oxygenated serum-free MEM with SB216763 or DMSO was added to the cultures. Cells were then placed in atmospheric oxygen for up to 3 h. Cultures were collected after (1) continuous normoxic exposure, (2) after the 3 h hypoxic exposure, or (3) after reintroduction of atmospheric oxygen for 1, 2, or 3 h subsequent to the 3 h hypoxic exposure. Total cell lysates were analyzed with immunoblots using 25 μg of protein per lane. Anti-actin was used to normalize the bands to ensure equivalent lane loading. Three experiments, using independent cell populations, were quantified using GraphPad Prism 5 and the relative densities plotted for BAX/actin, Bcl-2/actin, pBcl-2/actin, and phospho-c-Jun/Actin. No change was evident in the ratio of BAX/actin, Bcl-2/actin, pBcl-2/actin, or phospho-c-Jun/actin by treatment with SB216763. Error bars represent standard error, Student *t* test.

Figure 3.5

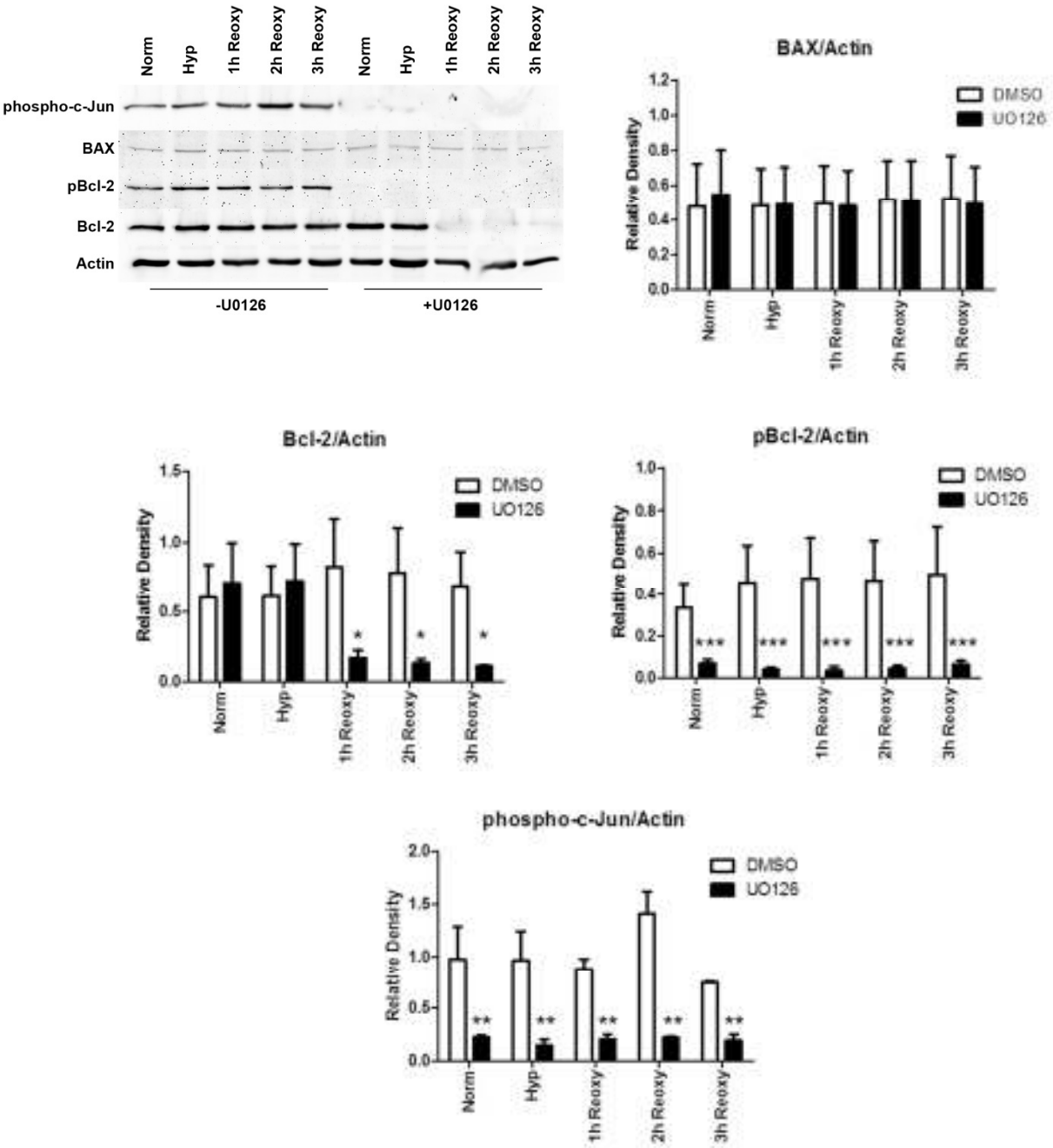

Figure 3.5. Western blot analysis of BAX, Bcl-2, pBcl-2, and phospho-c-Jun in HLE-B3 cells in the presence or absence of UO126. Total cell lysates were collected from >85% confluent HLE-B3 cell cultures that were incubated for 90 min in serum-free MEM, under conditions of atmospheric oxygen (~21% O_2), containing either 10 μM UO126 or 0.05% DMSO

vehicle. Cells were then exposed to hypoxia (~1% O_2) for 3 h in the continuous presence of UO126 or DMSO vehicle. At the end of the hypoxic incubation period, the hypoxic media was removed, and fresh, oxygenated serum-free MEM with UO126 or DMSO was added to the cultures. Cells were then placed in atmospheric oxygen for up to 3 h in the presence or absence of UO126. Cultures were collected after (1) continuous normoxic exposure, (2) after the 3 h hypoxic exposure, or (3) after reintroduction of atmospheric oxygen for 1, 2, or 3 h subsequent to the 3 h hypoxic exposure. Total cell lysates were analyzed with immunoblots using 25 μg of protein per lane. Anti-actin was used to normalize the bands to ensure equivalent lane loading. Three experiments, using independent cell populations, were quantified using GraphPad Prism 5. (Top left panel) The phosphorylation of c-Jun, as well as that of Bcl-2, was blocked by treatment with UO126 under all conditions as determined with western blot analysis. Interestingly, Bcl-2 levels were significantly diminished with treatment by UO126 but only upon reintroduction to atmospheric oxygen. (Top right panel) No change in relative density of the ratio of BAX/actin was evident by treatment with UO126 under any condition. Error bars represent standard error. (Middle left panel) A significant drop in Bcl-2 levels was noted but only upon reintroduction of atmospheric oxygen for the 1, 2, and 3 h incubation periods. The asterisk (*) indicates $p<0.05$, Student *t* test. (Middle right panel) A significant loss of pBcl-2 was noted under all conditions. The asterisks (***) indicate $p<0.001$, Student *t* test. (Bottom panel) Unlike with SB216763 (Figure 3.4), treatment with UO126 resulted in a marked decrease in the phosphorylation of c-Jun, indicating that UO126 adversely affects JNK activity. The asterisks (**) indicate $p<0.01$, Student *t* test.

Figure 3.6

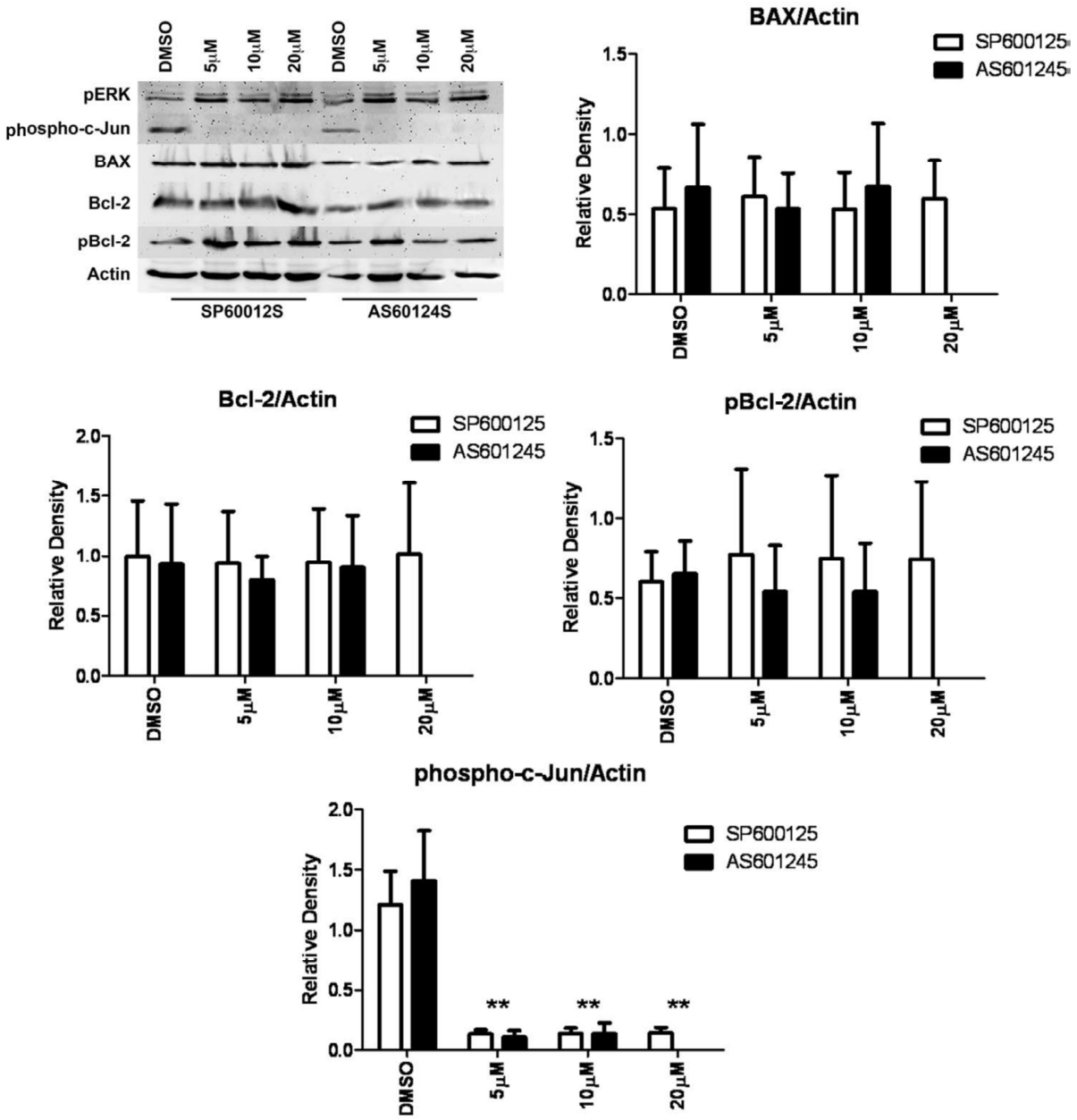

Figure 3.6. Western blot analysis of phospho-c-Jun in the presence of SP600125 or AS601245. HLE-B3 cell cultures were incubated for 90 min in serum-free MEM, under conditions of atmospheric oxygen (~21% O_2), containing either SP600125 (5 μM, 10 μM, or 20 μM), AS601245 (5 μM, 10 μM, or 20 μM), or DMSO (0.05%) vehicle. Cells were then exposed to hypoxia (~1% O_2) for 3 h in the continued presence of inhibitors. At the end of the hypoxic

exposure, the media was removed, and fresh, oxygenated serum-free MEM with either inhibitor or DMSO was added to the cultures. Cells were subsequently placed in atmospheric oxygen for 3 h. Whole cell lysates were collected at the end of the 3 h reintroduction of atmospheric oxygen. Lysates were analyzed with western blot for phospho-c-Jun, pERK1/2, BAX, Bcl-2, and pBcl-2 using 25 μg of protein per lane. Anti-actin was used to normalize the bands to ensure equivalent lane loading. The inhibition of the phosphorylation of c-Jun by either JNK inhibitor indicates the inactivation of JNK activity, while no loss of BAX, Bcl-2, or pBcl-2 was noted. Under this condition, the phosphorylation of ERK1/2 was unimpeded. This experiment was performed twice with two independent cell populations with identical results. Treatment with either JNK inhibitor, SP600125 or AS601245, resulted in a marked decrease in the phosphorylation of c-Jun, indicating that both inhibitors inhibited JNK activation. The asterisks (**) indicate $p<0.01$, Student *t* test. BAX, Bcl-2, and pBcl-2 were not significantly diminished relative to the DMSO control, indicating that the ERK1/2 pathway, but not the JNK pathway, is involved in the loss of Bcl-2 and pBcl-2 (Figure 3.5). Two experiments, using independent cell populations, were quantified using GraphPad Prism 5. Reader note: The 20 μM AS601245 was run only once as reflected in the western blot but not in the densitometry plots because we cannot generate statistics on one run.

Figure 3.7

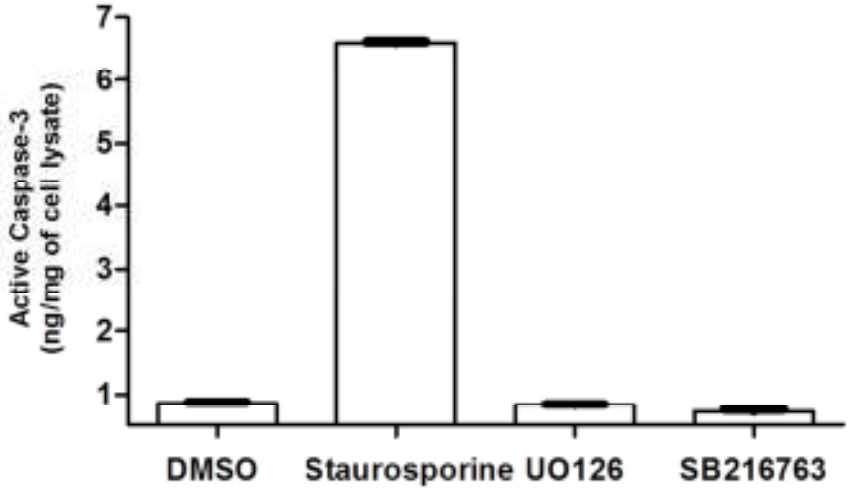

Figure 3.7. Active caspase-3 ELISA analysis of possible apoptosis in HLE-B3 cells treated with SB216763, UO126, staurosporine, or DMSO. The possibility of the onset of apoptosis was determined using an active capase-3 ELISA with HLE-B3 cells treated with SB216763 (12 μM), UO126 (10 μM), staurosporine (100 nM), or 0.05% DMSO vehicle. Treated and mock-treated HLE-B3 cells were incubated with serum-free MEM for 90 min in atmospheric oxygen (~21% O_2). The cells were then switched to hypoxia (~1% O_2) for 180 min in the continued presence of each individual treatment. At the end of the hypoxic exposure, the media was removed and replaced with fresh, oxygenated media still containing SB216763, UO126, staurosporine, or DMSO vehicle. The cells were placed in atmospheric oxygen for 60 min and subsequently lysed, and the quantity of protein determined per treatment. Caspase-3 activity was determined using 10 μg of protein following the manufacturer's instructions. Data are based upon results from three independent cell populations and were analyzed using GraphPad Prism 5. The error bars represent the standard error. Only treatment with staurosporine indicated a marked increase in activation of caspase-3.

Figure 3.8

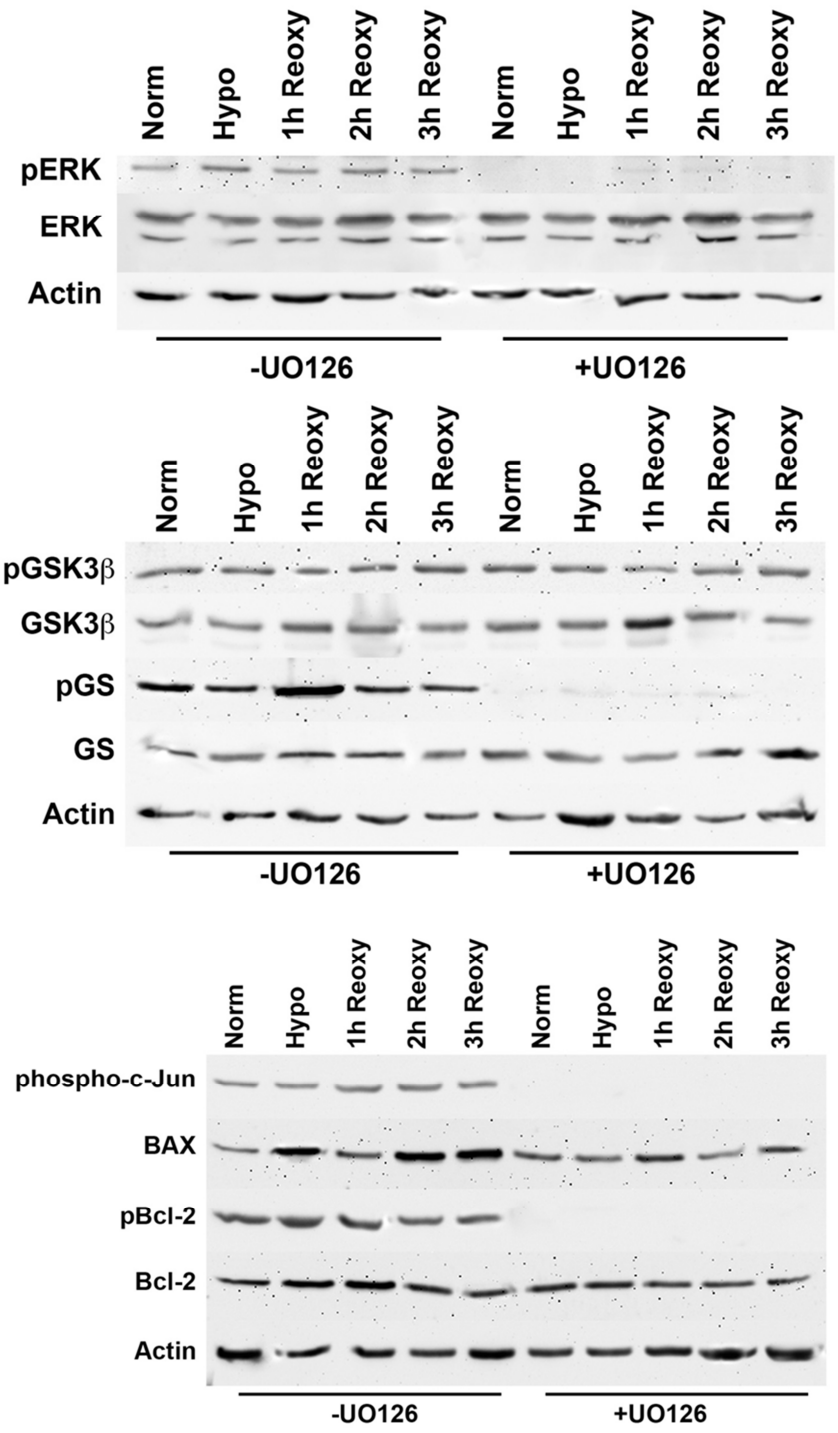
Norm
Hypo
1h Reoxy
2h Reoxy
3h Reoxy
Norm
Hypo
1h Reoxy
2h Reoxy
3h Reoxy
pERK
ERK
Actin
-UO126
+UO126
Norm
Hypo
1h Reoxy
2h Reoxy
3h Reoxy
Norm
Hypo
1h Reoxy
2h Reoxy
3h Reoxy
pGSK3β
GSK3β
pGS
GS
Actin
-UO126
+UO126
Norm
Hypo
1h Reoxy
2h Reoxy
3h Reoxy
Norm
Hypo
1h Reoxy
2h Reoxy
3h Reoxy
phospho-c-Jun
BAX
pBcl-2
Bcl-2
Actin
-UO126
+UO126

Figure 3.8. Western blot analysis of GSK-3β and GS phosphorylation along with analysis of BAX, Bcl-2, pBcl-2, and phospho-c-Jun levels in secondary cultures of normal BLECs treated with UO126. BLEC cultures were incubated for 90 min in serum-free MEM, under conditions of atmospheric oxygen (~21% O_2), containing either 10 μM UO126 or 0.05% DMSO vehicle. Cells were then exposed to hypoxia (~1% O_2) for 3 h in the presence of either UO126 or DMSO vehicle. At the end of the hypoxic incubation period, the hypoxic media was removed, and fresh, oxygenated serum-free MEM with UO126 or DMSO was added to the cultures. Cells were then placed in atmospheric oxygen for up to 3 h. Cultures were collected after (1) continuous normoxic exposure, (2) after the 3 h hypoxic exposure, or (3) after reintroduction of atmospheric oxygen for 1, 2, or 3 h subsequent to the 3 h hypoxic exposure. Total cell lysates were analyzed with immunoblots using 25 μg of protein per lane. Anti-actin was used to normalize the bands to ensure equivalent lane loading. Prevention of phosphorylation of ERK1/2 with UO126 treatment was noted (top panel), as was the inhibition of phosphorylated GS with western blot analysis (middle panel). The levels of GSK-3β and pGSK-3β were consistent in the presence and absence of UO126. The phosphorylation of c-Jun, as well as that of Bcl-2, was blocked by treatment with UO126 under all conditions as determined by western blot analysis (bottom panel). Of particular note, Bcl-2 levels were unaffected by UO126 treatment compared to HLE-B3 cells (Figure 3.5) where a significant diminution of Bcl-2 was observed but only upon reintroduction to atmospheric oxygen. No change in the relative levels of BAX was evident by treatment with UO126 under any condition. This experiment was run only once, to confirm that a similar pattern of biochemical modifications by treatment with UO126 was reproducible with secondary cultures of normal BLECs as was observed with HLE-B3 cells, affirming that the former results were not influenced by viral transformation.

Figure 3.9

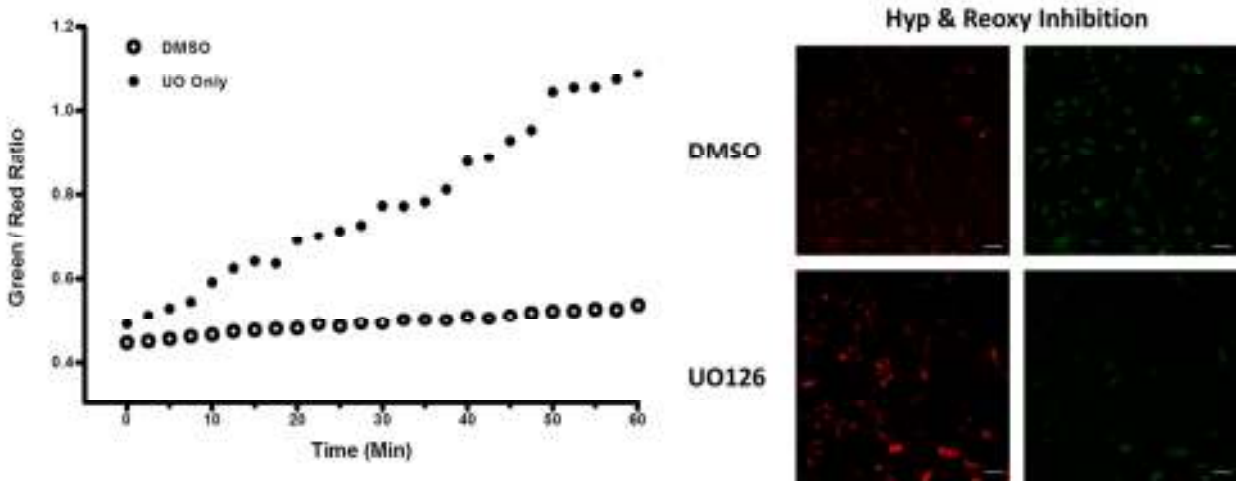

Figure 3.9. JC-1 analysis of normal BLECs treated with UO126. Secondary cultures of normal BLECs were incubated for 90 min in atmospheric oxygen (~21% O_2) with serum-free MEM containing 10 μM UO126 or 0.05% DMSO vehicle. Cells were switched to hypoxia (~1% O_2) for 3h in the continued presence or absence of UO126. At the end of the hypoxic exposure, the cell media was removed, and fresh oxygenated serum-free MEM containing 5 μg/ml JC-1 plus either UO126 or DMSO was added for 30 min in atmospheric oxygen. At the end of the 30 min incubation period, the media was again switched to fresh serum-free MEM containing UO126 or DMSO in the absence of the JC-1 dye. A random field of cells was chosen, and that field of cells was imaged every 150 sec for 60 min. Serial confocal imaging of mitochondrial depolarization of the secondary cultures of normal BLECs in the presence of UO126 demonstrated significant depolarization compared to control cells (left panel). Images of the red and green intensity for the UO126 treated and DMSO treated cells at t=60 min (bar=20 μm) are shown (right panel). Note the marked intensity of the green channel with the UO126 treated cells relative to DMSO mock treatment at the completion of the 60 min analysis, which indicates a propensity toward a significant degree of mitochondrial depolarization.

Introduction to Chapter IV

Chapter IV is a collection of studies that try to address a few key points in the persistence model of EMT, such as the role of the hypoxia inducible factor (HIF) proteins in regulating the expression of the EMT marker proteins; fibronectin and α–smooth muscle actin (α-SMA). The results of these studies also reconfirm the compensatory role of the HIF proteins in maintaining VEGF levels under hypoxic conditions. Overall, these studies suggest a possible target protein that could be manipulated to prevent EMT without harming the cell via mitochondrial depolarization.

Chapter IV

The role of GSK-3β and HIF-1α in the pathophysiology of epithelial to mesenchymal transition.

Abstract

Purpose: PCO is a debilitating disease that can develop after cataract surgery and ultimately lead to blindness. PCO is characterized by the occurrence of EMT wherein the epithelial cells that remained after cataract surgery transform from an epithelial phenotype to a mesenchymal phenotype. This EMT exists in two phases, initiation and persistence. The initiation phase utilizes β-catenin solely under conditions of atmospheric oxygen (~21% O_2) whereas the persistence phase utilizes HIF proteins in addition to β-catenin under hypoxic (~1% O_2) conditions. Through the use of pharmacological inhibitors of the HIF proteins, the studies herein demonstrate a novel way to prevent EMT from persisting while maintaining $\Delta\Psi$ under hypoxic conditions.

Method: Virally-transformed HLE-B3 cells were treated with 12 μM SB216763 (a specific GSK-3β inhibitor) alone or in combination with 50 μM HIF-1α or 50 μM HIF-2α translation inhibitor. Western blot analysis was employed to detect the levels of pBcl-2, Bcl-2 and the EMT marker proteins, α-SMA and fibronectin. Additional immunoblots were utilized to detect the levels of nuclear and cytoplasmic β-catenin. ELISA was used to measure the levels of VEGF in cell culture supernatants. JC-1 analysis was performed to analyze the influence of SB216763 in combination with a HIF-1α translation inhibitor on mitochondrial depolarization.

Results: Cultured HLE-B3 epithelial cells maintained in hypoxia (~1% O_2) for 3 h and treated with SB216763, SB216763 + a HIF-1α translation inhibitor, or SB216763 + a HIF-2α translation inhibitor showed increased levels of nuclear β-catenin. All treatments enhanced nuclear β-catenin activity which in turn elicited increased VEGF expression relative to mock treated controls. Additionally, EMT marker proteins were increased upon treatment with SB216763 or SB216763 + a HIF-2α translation inhibitor. Cells treated with SB216763 + a HIF-

1α translation inhibitor demonstrated a marked decrease in EMT marker proteins as compared to SB216763 treated cells. JC-1 analysis reconfirmed that treatment with SB216763 prevented mitochondrial depolarization an effect similarly seen in cells treated with SB216763 + a HIF-1α translation inhibitor. Normal BLECs showed similar results to HLE-B3 cells in that SB216763 or SB216763 + a HIF-2α translation inhibitor treatment increased EMT marker proteins where as SB216763 + a HIF-1α translation inhibitor treatment decreased these proteins.

Conclusion: EMT during hypoxic conditions utilizes both HIF proteins and β-catenin to increase EMT marker proteins while maintaining ΔΨ through increased levels of VEGF. Our data suggests that EMT can be prevented, as measured by the loss of fibronectin and α-SMA, without causing the mitochondria to depolarize by inhibiting the translation of HIF-1α. The loss of HIF-1α with an associated loss of EMT marker proteins is due to the possible binding of HIF-1α to β-catenin. As demonstrated in other cell lines the loss of binding between HIF-1α and β-catenin prevents the expression of the EMT marker proteins that would otherwise be produced under hypoxic conditions. These results show a novel and potentially therapeutic mechanism of EMT in hypoxia that has never before been seen in an ocular system.

Introduction

According to the World Health Organization in 2011 almost 18 million people were diagnosed with cataracts making it the second leading cause of blindness in the world [7]. To date the majority of cataracts are treated by a surgeon removing the cataractous lens and placing an artificial intraocular lens inside the capsular bag. Due to the invasiveness of this surgery the normally hypoxic lens becomes exposed to atmospheric oxygen for a brief period of time. As stated previously by Petrash et al ". . . although cataract surgery is considered a safe and effective surgical procedure, it can be conservatively estimated that up to 20% of cataract cases develop

PCO, which results in a loss of clear vision following a period of weeks to months after surgery." [11]. PCO occurs as the residual lens epithelial cells that line the inside of the lens capsule proliferate and migrate along the capsule until they reach its posterior aspects (Figure 1.3). During PCO the lens epithelial cells undergo a transformation from an epithelial phenotype to a mesenchymal stem cell phenotype in a process known as EMT [11]. As part of this transition normal epithelial cells become myofibroblast-like and express mesenchymal markers like α-SMA and fibronectin [70]. Herein we propose that EMT initiates during the brief exposure to atmospheric oxygen and continues to persist once the lens is back in hypoxia after the surgery.

The brief introduction of atmospheric oxygen during the surgery activates several signaling pathways chief among them being the transforming growth factor-β (TGF-β)/Wnt signaling pathway. Under normal physiological conditions TGF-β exists in its latent form; however, several studies in the lens detected the biologically active form of TGF-β in patients suffering from PCO; suggesting that TGF-β becomes activated during exposure to atmospheric oxygen [71-73]. Active TGF-β, via the Wnt signaling pathway leads to inactivation of GSK-3β and translocation of β-catenin to the nucleus [71-73]. Nuclear β-catenin induces the expression of mesenchymal proteins like α-SMA and fibronectin leading to EMT [71-73]. Apart from inducing EMT nuclear β-catenin is also known to induce VEGF synthesis [74]. The VEGF synthesis is likely to provide resistance against mitochondrial depolarization by maintaining the levels of the anti-apoptotic proteins pBcl-2 and Bcl-2 [69]. Previous studies in our lab have demonstrated that these two independent cellular events (Mitoprotection and EMT) are regulated by nuclear β-catenin in HLE-B3 cells under conditions of atmospheric oxygen (data not shown). Furthermore, those studies proved the inhibition of β-catenin had the dual effect of preventing EMT and causing significant mitochondrial depolarization; indicating that β-catenin is an

inadequate target to prevent EMT in atmospheric oxygen due to the cell being driven towards apoptosis.

Under conditions of atmospheric oxygen GSK-3β, and subsequently β-catenin, becomes the main protein regulating the two independent parallel pathways of EMT and mitoprotection. However, this may not be the case under hypoxic conditions due to the presence of HIF-1α and HIF-2α. Neelam et al (2013) demonstrated "that the survival of human lens epithelial cells in hypoxia depends on the uninterrupted and sustained synthesis of VEGF levels controlled by the expression of either of the hypoxia inducible factors, HIF-1α or HIF-2α . . . with the novelty of the finding being that a decrease in the manifestation of HIF-1α may be compensated for by HIF-2α accumulation and vice versa." [69]. Thus, during hypoxia the two HIF proteins can affect mitochondrial depolarization and maintain ΔΨ through their compensatory regulation of VEGF. Additionally, it has been demonstrated in the cancer literature that both HIF-1α and HIF-2α have an increased association with β-catenin in nucleus under hypoxic conditions [75, 76]. When either HIF-1α or HIF-2α associates with β-catenin in the nucleus it can cause increased transcription of a multitude of genes [75, 76]. Combined, these studies suggest a role for the HIF proteins in influencing the two independent parallel pathways of EMT and mitoprotection under hypoxic conditions.

Utilizing specific inhibitors for GSK-3β and only one of the two HIF proteins we demonstrate that the persistence of EMT in hypoxia can be blocked, as measured by the lack of the EMT marker proteins α-SMA and fibronectin. Inhibition of only one HIF protein while simultaneously inhibiting GSK-3β increased the levels of VEGF allowing the cells to maintain ΔΨ. Further, we reconfirmed our results using normal BLECs. The BLECs showed a similar result of losing EMT marker proteins in the presence of a GSK-3β inhibitor and a HIF translation

inhibitor. Collectively, the results presented herein will provide a novel mechanism for EMT, under hypoxic conditions; a concept that has not been previously established in an ocular system.

Methods

Materials: Glycogen Synthase Kinase inhibitor SB216763 was purchased from Sigma-Aldrich (St. Louis, MO). HIF-1α translation inhibitor (KC7F2) and HIF-2α translation inhibitor (CAS882268-69-1) were purchased from EMD Chemicals (Billerica, MA). Stock inhibitors were prepared by addition to DMSO as follows: 16 mM for SB216763, 100 mM for the HIF-1α translation inhibitor and 100 mM for the HIF-2α translation inhibitor. The mitochondrial dye JC-1 was obtained from Life Technologies (Grand Island, NY). All other reagents were acquired from other commercially available sources as previously reported [14].

Cell cultures: HLE-B3 cells, a human lens epithelial cell line immortalized by the SV-40 virus [46], were obtained from U. Andley (Washington University School of Medicine, Department of Ophthalmology, St. Louis, MO). Authentication of the HLE-B3 cell line was verified by STR profile analysis (American Type Culture Collection, Manassas, VA.) and confirmed that the cell was human and of female origin, as originally reported by Andley et al. [46]. A copy of the STR profile is available upon request. All studies with HLE-B3 cells were performed with pre-frozen stock cells (maintained in liquid nitrogen) between passages 14 to 17 and no experiments exceeded 5 passages beyond the initial stock cell passage. The cells were maintained in MEM containing 5.5 mM glucose supplemented with 20% fetal bovine serum (Gemini Bio-Products, Sacramento, CA), 2 mM L-glutamine, nonessential amino acids, and 0.02 g/L gentamycin solution (Sigma-Aldrich) and cultured at 37 ^{0}C and 5% CO_2 to 95% O_2 [14]. Cells were sub-cultured four to five days prior to the experiment and placed in MEM containing 20% fetal bovine serum. Twenty four hours prior to the day of the experiment, cells were

switched to serum-free MEM. Unless otherwise specified, all experiments followed a common protocol; cells were maintained in atmospheric oxygen (~21% O_2) for 90 min, and then switched to hypoxic conditions (~1% O_2) for 3 h. At the end of the hypoxic exposure the cells were either lysed, stained with JC-1, or had their supernatants collected. Each experiment was executed with cells treated as follows: control DMSO only (mock inhibitor treatment), 12μM SB216763, 12μM SB216763 + 50μM HIF-1α translation inhibitor, or 12μM SB216763 + 50μM HIF-2α translation inhibitor. The DMSO concentration per experiment never exceeded 0.05%.

Bovine eyes obtained from a local abattoir were transported on ice to the laboratory, where the lenses were removed aseptically. BLECs were isolated and cultured in MEM containing 20% fetal bovine serum. All studies with BLECs were performed on cells of passage 2.

Western blot analysis: Whole cell lysates were collected from HLE-B3 cultures using the method of hot protein extraction as described by Henrich et al. [52]. The cell cultures were rinsed at room temperature with phosphate buffered saline in final concentration: 150 mM sodium chloride, 10 mM sodium phosphate monobasic, 40 mM sodium phosphate dibasic, pH 7.4, prior to the monolayers being lysed with hot lysis buffer (~100 ^{0}C); subsequently scraped into 1.7 ml micro centrifuge tubes and immediately sonicated. The lysis buffer consists of 0.12 M Tris-HCl (pH 6.8), 4% sodium dodecyl sulfate, and 20% glycerol [14]. In some experiments cytoplasmic and nuclear lysates were collected from HLE-B3 epithelial cell cultures after inhibitor treatment using the NE-PER nuclear and cytoplasmic extraction kit (Thermo Scientific Pittsburg, PA). Part of the lysate (whole cell, cytoplasmic, or nuclear) samples were removed and used to determine the protein concentration. The protein concentration was calculated by using a DC protein assay kit from Bio-Rad (Hercules, CA). The lysate samples contained 25 μg of

protein, 1X sodium dodecyl sulfate laemmli buffer, and 1.5µl 2-Mercaptoethanol (Sigma-Aldrich). The lysate samples were then boiled for 5 minutes and the proteins resolved on 12% sodium dodecyl sulfate-polyacrylamide gels. The proteins were then transferred to a nitrocellulose membrane (Bio-Rad, Hercules, CA). The electrophoresis and Western blot apparatus were provided by Hoefer Scientific (Holliston, MA).

For Western blot analysis, nitrocellulose membranes were blocked with Tris-buffered saline containing 0.1% bovine serum albumin for 60 minutes. These membranes were probed overnight at 4 ^{0}C with primary antibodies at a 1:1000 dilution. The blots were then rinsed with Tris-buffered saline containing 0.1% bovine serum albumin and 0.02% Tween-20 for 5 min 4X and then incubated in either goat anti-rabbit horseradish peroxidase conjugate or goat anti-mouse horseradish peroxidase conjugate at a 1:10000 dilution (Santa Cruz Biotechnology, Santa Cruz, CA) for 60 minutes at room temperature. Blots were again rinsed 4X 5 min washes, and proteins were detected using a SuperSignal West Femto chemiluminescent kit from Pierce (Rockford, IL) [14]. Probed membranes were visualized on a Fluoro Chem TM 8900 imager (Alpha Innotech, San Leandro, CA). Each Western blot profile represents one preliminary run thus densitometry and statistical analysis was not performed on all blots.

Primary antibodies used in this study were rabbit anti-fibronectin (EMD Millipore, Billerica, MA), mouse anti-Actin, mouse anti-α-smooth muscle actin (Sigma-Aldrich, St. Louis, MO), rabbit anti-β-catenin, and rabbit anti-LaminA/C antibody (Cell Signaling Technology, Danvers, MA).

ELISA: ELISA was performed for the detection of VEGF in HLE-B3 cells using an Invitrogen Human VEGF ELISA kit (Grand Island, NY). HLE-B3 cells were cultured in 25 cm^2 tissue culture flasks with MEM containing 20% fetal bovine serum. The media was then

switched to serum-free MEM prior to the initiation of the experiment. Flasks were set up as four groups of triplicates. Each independent group was treated with either 0.05% DMSO, 12μM SB216763, 12μM SB216763 + 50μM HIF-1α translation inhibitor, or 12μM SB216763 + 50μM HIF-2α translation inhibitor. All the flasks were exposed to atmospheric oxygen (~21% O_2) for 90 min and then placed into hypoxic (~1% O_2) conditions for 3 hrs. At the end of the hypoxic exposure the cell-free supernatants were collected and analyzed according to manufacturer's instructions. The optical density at 450 nm was determined using a Molecular Devices Spectramax 190 (Sunnyvale, CA). For calculating the significant difference in VEGF levels, a student's t-test was performed by collecting the supernatants from three individual cell cultures stemming from an initial single cell population using the software from Graphpad Prism, version 5.00 (La Jolla, CA). Statistical significance was determined based upon a P value < 0.05. Error bars represent SEM.

JC-1 fluorescence and emission spectra analysis: HLE-B3 cells subjected to DMSO or inhibitor treatments during hypoxic exposure were stained with the cationic dye JC-1 (Life Technologies, Grand Island, NY) to determine $\Delta\Psi$. JC-1 is a membrane permeant lipophilic dye that exists as J-aggregates in the mitochondrial matrix (red fluorescence) and as monomers in the cytoplasm (green fluorescence). During mitochondrial depolarization the red J-aggregates will flow out of the mitochondria and accumulate in the cytosol as green monomers [47]. Thus, depolarization can be measured as an increasing green/red fluorescent intensity ratio.

The JC-1 assay is carried out as follows; HLE-B3 cell monolayers were maintained in serum-free MEM with or without inhibitor treatment and brought through 90 min of atmospheric oxygen (~21% O_2) into hypoxia (~1% O_2). The cell cultures were maintained in hypoxic conditions for 3 h in the presence or absence of an inhibitor. At the end of the hypoxic exposure,

the hypoxic media on cells (oxygen depleted) was poured off and fresh (oxygen rich) serum-free MEM (with or without an inhibitor) was added containing 5µg/ml JC-1 for 30 minutes in a tissue culture incubator. The stained HLE-B3 cells were then rinsed twice using serum-free MEM and fresh oxygenated serum-free MEM (with or without inhibitor, but no JC-1 dye) was added. After the addition of fresh media a random field of cells had the fluorescent emission spectra analyzed by a Cary Eclipse spectrofluorometer (Varian Inc., Belrose, Australia).

Fluorescence emission spectra were collected every 150 sec for 90 min. Measurements were performed in front-face mode using secondary cultures of HLE-B3 cells on coverslips in the presence of an inhibitor or DMSO. The JC-1 emission spectrum was measured with the excitation at 470 nm. For analysis of ratiometric changes of the JC-1 spectrum, we performed spectral deconvolution with Mathcad software (Parametric Technology Corp., Needham, MA). The deconvolution was based on experimental measurements, fluorophore reference spectra and the utilization of an algorithm for least squares minimization to produce corresponding unmixed spectra in graph form with error provided in minimal least squares values for flexibility in analysis. After deconvolution, the green/red fluorescent intensity ratios (540/595nm) were calculated to determine mitochondrial depolarization. This assay was run on two independent populations of cells for each treatment with only the average of the green/red ratio for each time point being shown.

Results

The inhibition of HIF-1α alone coupled with SB216763 treatment can decrease the levels of EMT marker proteins. Two independent populations of HLE-B3 cells were treated with either 0.05% DMSO, 12 µM SB216763, 12 µM SB216763 + 50 µM HIF-1α translation inhibitor or 12 µM SB216763 + 50 µM HIF-2α translation inhibitor to determine which HIF protein is the main

protein associating with β-catenin and subsequently influencing the levels of the EMT marker proteins. Treated and mock treated cells were placed in atmospheric oxygen (~21% O_2) for 90 min and then switched into hypoxia (~1% O_2) for 3 h. Following the hypoxic exposure total cell lysates were collected and the levels of fibronectin and α-SMA were measured utilizing immunoblotting. Mock treated DMSO controls showed a low level of EMT marker proteins while SB216763 treated cells showed a significant increase in the levels of fibronectin and α-SMA (Figure 4.1). HLE-B3 cells treated with SB216763 along with the HIF-1α translation inhibitor demonstrated a marked decrease in the levels of EMT marker proteins whereas cells treated with SB216763 and a HIF-2α translation inhibitor demonstrated no change in these proteins relative to SB216763 only treated cells (Figure 4.1).

The loss of either HIF-1α or HIF-2α during SB216763 treatment does not lower nuclear β-catenin or VEGF levels. It has previously been shown that HIF-1α and HIF-2α have compensatory roles in maintaining VEGF levels under hypoxic conditions [69]. Additionally, previous studies using SB21673 alone in atmospheric oxygen have demonstrated significantly higher levels of VEGF relative to mock treated DMSO controls (data not shown). Similar to those studies VEGF levels were measured to assess the effect of combining the SB216763 inhibitor with either a HIF-1α translation inhibitor or a HIF-2α translation inhibitor. HLE-B3 cells were treated with either 0.05% DMSO, 12 μM SB216763, 12 μM SB216763 + 50 μM HIF-1α translation inhibitor or 12 μM SB216763 + 50 μM HIF-2α translation inhibitor and then placed into atmospheric oxygen (~21% O_2) for 90 min followed by exposure to hypoxia (~1% O_2) for 3 h. Cell free supernatants were collected from three independent cell populations for each treatment at the end of the 3 h hypoxic exposure. The VEGF levels in the supernatants were analyzed by ELISA. All three treatments, SB216736, SB216763 + a HIF-1α translation inhibitor,

or SB216763 + a HIF-2α translation inhibitor, demonstrated significantly increased levels of VEGF relative to DMSO mock treated controls (Figure 4.2A).

Further studies looking at the levels of nuclear β-catenin were conducted to determine if the increases in VEGF observed previously were due to higher levels of β-catenin in the nucleus. After being treated with either 0.05% DMSO, 12 μM SB216763, 12 μM SB216763 + 50 μM HIF-1α translation inhibitor or 12 μM SB216763 + 50 μM HIF-2α translation inhibitor HLE-B3 cells were placed in atmospheric oxygen (~21% O_2) for 90 min followed by exposure to hypoxia (~1% O_2) for 3 h. Once the hypoxic exposure was finished, the cells were lysed and the nuclear and cytoplasmic fractions were collected using the manufacturers recommended protocol. Immunoblots demonstrated higher levels of β-catenin under all treatments: SB216736, SB216763 + a HIF-1α translation inhibitor or SB216763 + a HIF-2α translation inhibitor (Figure 4.2B). These blots revealed a positive correlation between higher levels of nuclear β-catenin and higher levels of VEGF. Confirming what has been shown in previous experiments conducted in atmospheric oxygen (data not shown).

SB216763 treatment in conjunction with HIF-1α inhibition does not lead to mitochondrial depolarization. In Chapter II it was previously shown that HLE-B3 cells treated with SB216763 had less mitochondrial depolarization as compared to controls under conditions of oxidative stress (Figure 2.1). A similar analysis was implemented to demonstrate that the combination of SB216763 + a HIF-1α translation inhibitor does not cause mitochondrial depolarization presumably due to inactivation of GSK-3β coupled with increased levels of VEGF. HLE-B3 cells were treated with 0.05% DMSO, 12 μM SB216763, or 12 μM SB216763 + 50 μM HIF-1α translation inhibitor and then placed in atmospheric oxygen (~21% O_2) for 90 min followed by exposure to hypoxia (~1% O_2) for 3 h. At the end of the hypoxic exposure the

media was poured off and fresh media containing DMSO, SB216763, or SB216763 + a HIF-1α translation inhibitor and the JC-1 dye was added. The cells were then placed into atmospheric oxygen for 30 min. Following the JC-1 application, the media was replaced with fresh media containing DMSO, SB216763, or SB216763 + a HIF-1α translation inhibitor. The cells were subsequently observed using emission spectroscopy every 150 sec for 90 min. The green/red intensity ratio of the DMSO treated cells slightly increased over time whereas the SB216763 and SB216763 + a HIF-1α translation inhibitor treated cells had green/red intensity ratios that were lower than the DMSO control (Figure 4.3).

With the goal of these studies being to find a sufficient way to prevent EMT without harming the mitochondria, JC-1 analysis was not performed on SB216763 + a HIF-2α translation inhibitor treated cells due to the cells demonstrating no decrease in EMT marker proteins.

Bovine lens epithelium demonstrates a similar response to the inhibition of HIF-1α and SB216763 treatment as compared to HLE-B3 cells. Recently it has been suggested that due to HLE-B3 cells being virally transformed they no longer have similar characteristics to normal lens epithelium. To prove that our results (and subsequent interpretations) have not been compromised by the viral transformation of the HLE-B3 cells, we repeated the DMSO, SB216763, SB216763 + a HIF-1α translation inhibitor or SB216763 + a HIF-2α translation inhibitor total cell lysate experiments, as described previously, with secondary cultures of normal BLECs. Both fibronectin and α-SMA were present in BLECs treated with DMSO and no significant increase of both these proteins was observed in SB216763 treated cells as compared to DMSO mock treated controls (Figure 4.4). As seen with the HLE-B3 cells (Figure 4.1), BLECs treated with a combination of SB216763 + a HIF-1α translation inhibitor demonstrated a significant loss of fibronectin relative to SB216763 alone treated cells; however, these BLEC

samples only had a slight decrease in α-SMA (Figure 4.4). The BLECs treated with SB216763 + a HIF-2α translation inhibitor had no loss in either fibronectin or α-SMA relative to SB216763 treated cells (Figure 4.4); similar to what was observed in the HLE-B3 results (Figure 4.1).

Discussion

During cataract surgery the naturally hypoxic lens is exposed to atmospheric oxygen. As discussed in the introduction this brief exposure to atmospheric oxygen can activate several signal transduction pathways including one that leads to a buildup of β-catenin in the nucleus [71-73]. It has been demonstrated previously in HLE-B3 cells that higher levels of nuclear β-catenin can affect two independent parallel pathways: one pathway leads to increases in the expression of fibronectin and α-SMA, proteins that indicate the onset of EMT, while the other pathway leads to an increase in the pro-survival protein VEGF (data not shown). Additionally, these studies showed that blocking β-catenin prevented the expression of EMT proteins while also causing the harmful effect of massive mitochondrial depolarization due to a loss of VEGF (data not shown). From these studies it was concluded that β-catenin is the sole protein responsible for influencing both the levels of EMT marker proteins and the level of VEGF under conditions of atmospheric oxygen. Two important questions arose from these studies: (1) "Is the same β-catenin driven mechanism of EMT that occurs in atmospheric oxygen being utilized by lens cells during hypoxic exposure?" And, (2) "Can the mechanisms that regulate EMT in hypoxia be manipulated in such a way as to cause a loss of EMT without potentially harming the cell via increased susceptibility to mitochondrial depolarization?"

The studies herein aimed to answer these questions by utilizing the results of the previously stated preliminary studies looking at β-catenin along with what is currently known about the HIF proteins. Working in hypoxic conditions brings in the added benefits of the HIF

proteins. As previously discussed in the introduction HIF proteins have been demonstrated to associate with β-catenin, possibly influencing the expression of EMT marker proteins, as well as have compensatory roles in maintaining VEGF, thereby maintaining ΔΨ [69, 75, 76]. Using this information we theorized that by potentially targeting either HIF-1α or HIF-2α the persistence of EMT could be stopped without the associated drop in VEGF as seen when targeting β-catenin.

To test this theory HLE-B3 cells were treated with SB2167863 to cause an increase in the production of EMT proteins by increasing nuclear β-catenin levels through the inactivation of GSK-3β (Figure 4.1). In addition to SB216763 cells were treated with either a HIF-1α translation inhibitor or a HIF-2α translation inhibitor to see if the increase in EMT proteins caused by SB216763 treatment could be decreased or blocked. In the case of inhibiting HIF-1α there was a loss of fibronectin and α-SMA; however, such a loss was not observed when HIF-2α was inhibited (Figure 4.1). This result indicates that HIF-1α is the primary HIF protein that associates with β-catenin.

To ensure the compensatory role of the HIF proteins remains in the presence of SB216763 an ELISA looking at VEGF levels was run. When GSK-3β is inactivated by SB216763 in hypoxia there is a subsequent increase in VEGF (Figure 4.2A). The increase in VEGF caused by GSK-3β inactivation was not affected when either HIF-1α or HIF-2α was inhibited (Figure 4.2A); indicating that the compensatory role of the HIF proteins in hypoxia remains even in the presence of SB216763. The reason for the increase in VEGF observed in all treated cells is due to an increase in nuclear β-catenin brought on by the inactivation of GSK-3β. The pro-survival function of VEGF in lens cells has been shown to play a major role in preventing the loss of ΔΨ [69]. Thus, the increase in VEGF of all treated cells should have the beneficial effect of increasing mitoprotection.

To determine whether the inhibition of HIF-1α has any detrimental effects on the cell, specifically causing mitochondrial depolarization, a JC-1 analysis was conducted. Inactivation of GSK-3β can cause a decrease in mitochondrial depolarization directly through the mitochondrial permeability transition pore [54] and indirectly by increasing the levels of the pro-survival protein VEGF. SB216763 treated cells were analyzed with JC-1 which demonstrated that these cells underwent less depolarization as compared to DMSO mock treated cells (Figure 4.3). This lack of mitochondrial depolarization was also observed in the SB216763 + a HIF-1α translation inhibitor treated cells; presumably due to the direct (via the mitochondrial permeability transition pore) and indirect (via VEGF) effects of inhibiting of GSK-3β (Figure 4.3). This result confirms that inhibiting HIF-1α has no detrimental effects on the cell due to the compensatory role of HIF-2α in maintaining VEGF expression; and, due to the increased mitoprotection afforded by GSK-3β inactivation.

HLE-B3 cells are a virally transfected cell that have had their cell cycle mechanisms manipulated in such a way as to allow for continuous replication. Recently, it has been suggested by our peers that this manipulation of the cell cycle has fundamentally altered HLE-B3 cells into something that no longer resembles a human lens epithelial cell. As stated previously, our older passages of cells have been shown to have no difference from the originally reported cell. To further prove that the viral transformation of HLE-B3 cells does not skew our results normal BLECs were treated with DMSO, SB216763, SB216763 + a HIF-1α translation inhibitor or SB216763 + a HIF-2α translation inhibitor. Similar to HLE-B3 cells, fibronectin and α-SMA were present in normal BLECs treated with SB216763 whereas the levels of these EMT marker proteins decreased when HIF-1α was inhibited in the presence of SB216763 (Figure 4.4). Like the HLE-B3 cells inhibition of HIF-2α in the presence of SB216763 had no effect on the levels

of fibronectin and α-SMA as compared to the SB216763 treated cells (Figure 4.4). From the BLECs studies we conclude that HIF-1α, not HIF-2α, can influence EMT; presumably through its association with β-catenin. This association combined with the compensatory role of HIF-2α suggests HIF-1α as a potential target to prevent EMT without driving the mitochondria towards depolarization.

In conclusion, the last part of this project demonstrated that HIF-1α plays a pivotal role in EMT in lens epithelial cells that are under hypoxic cell culture conditions. Furthermore, it has been proven that this pivotal role can be manipulated to prevent EMT from persisting in such a way as to not harm either diseased or non-diseased cells by maintaining $\Delta\Psi$.

Figures

Figure 4.1

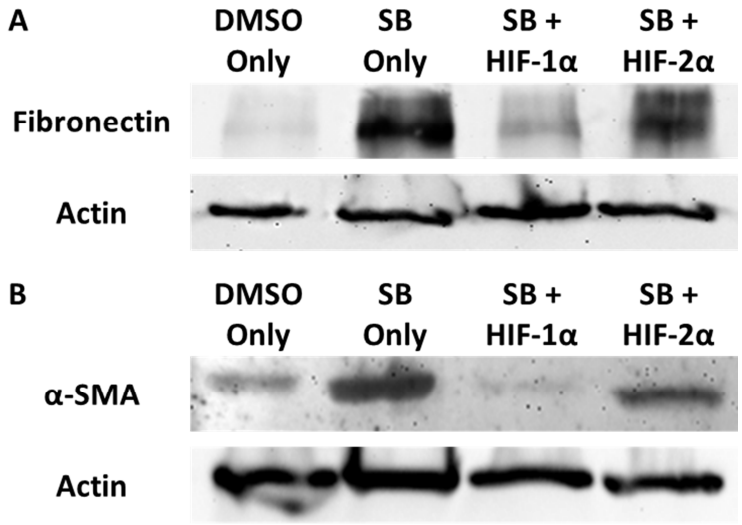

Figure 4.1. Western blot analysis of fibronectin and α-SMA in HLE-B3 cells treated with DMSO, SB216763, SB216763 + a HIF-1α translation inhibitor, or SB216763 + a HIF-2α translation inhibitor. (**A** & **B**) Total cell lysates were collected from >85% confluent HLE-B3 cell cultures that were incubated for 90 min in serum-free MEM, under conditions of atmospheric oxygen (~21% O_2), containing either 0.05% DMSO vehicle,12 μM SB216763, 12μM SB216763 + 50 μM HIF-1α translation inhibitor or 12 μM SB216763 + 50 μM HIF-2α translation inhibitor. Cells were then exposed to hypoxia (~1% O_2) for 3 h. Cultures were collected at the end of the hypoxic incubation period. Total cell lysates were analyzed with immunoblots using 25 μg of protein per lane. Anti-actin was used to normalize the bands to ensure equivalent lane loading. Low levels of fibronectin and α-SMA was evident in DMSO mock treated cells. High levels of fibronectin and α-SMA were observed in the cells treated with SB216763 or SB216763 + a HIF-2α translation inhibitor while significant inhibition of these two EMT marker proteins was noted in cells treated with SB216763 + a HIF-1α translation inhibitor.

Figure 4.2

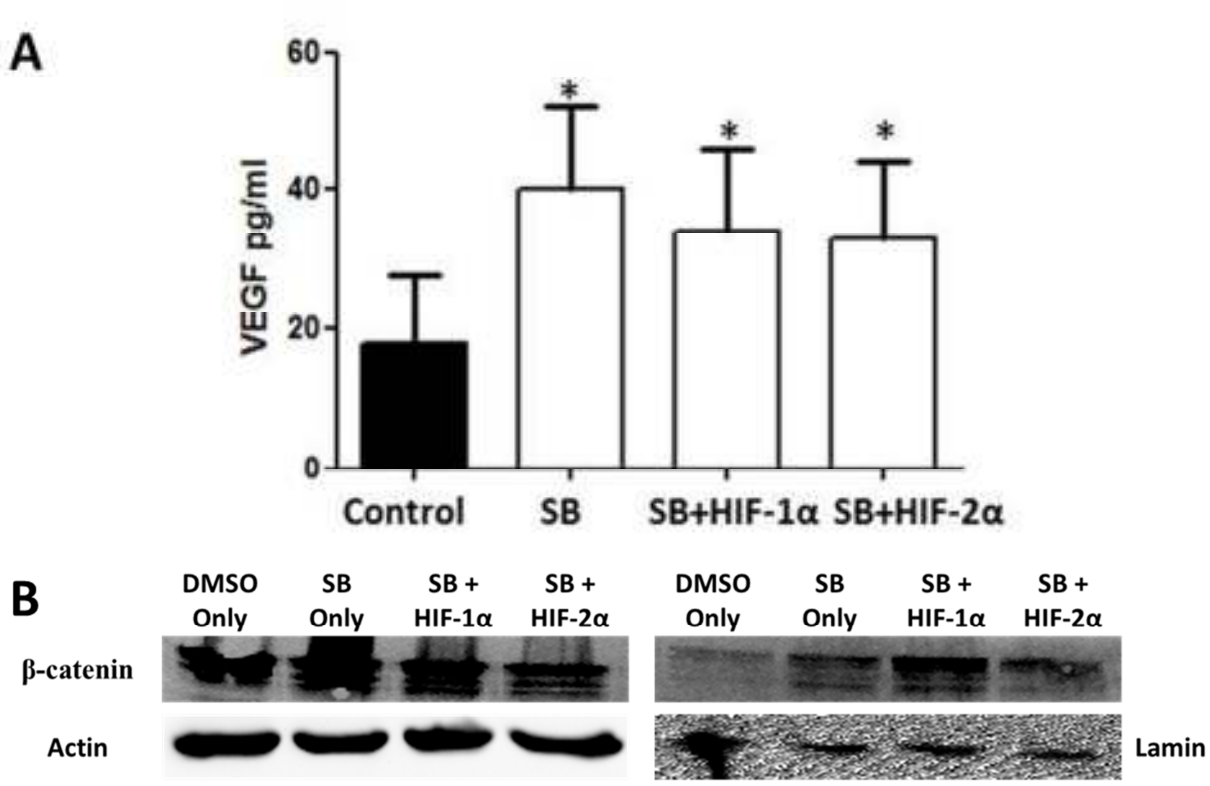

Figure 4.2. A: Detection of VEGF levels in HLE-B3 cells treated with DMSO, SB216763, SB216763 + a HIF-1α translation inhibitor, or SB216763 + a HIF-2α translation inhibitor. HLE-B3 cells were cultured in 25 cm^2 flasks containg MEM with 20% fetal bovine serum that was later switched to serum-free MEM on the day of the experiment. Cells were treated with 0.05% DMSO vehicle, 12 μM SB216763, 12 μM SB216763 + 50 μM HIF-1α translation inhibitor or 12 μM SB216763 + 50 μM HIF-2α translation inhibitor and then placed in atmospheric oxygen (~21% O_2) for 90 min. After the 90 min incubation the cells were exposed to hypoxic conditions (~1% O_2) for 3 h. At the end of the hypoxic exposure cell-free supernatants were collected in triplicates from all the cells. The VEGF levels were measured for all supernatants by ELISA. Samples were derived from three independent cell populations. A student *t* test was performed and significantly higher levels of VEGF were detected in cells

treated with either SB216763, SB216763 + a HIF-1α translation inhibitor, or SB216763 + a HIF-2α translation inhibitor as compared to the DMSO mock treated control. Error bars represent standard error. The asterisks (*) indicate $p<0.05$. **B: Detection of nuclear β-catenin levels in cells treated with DMSO, SB216763, SB216763 + a HIF-1α translation inhibitor, or SB216763 + a HIF-2α translation inhibitor.** The cells were treated with either 0.05% DMSO vehicle, 12 μM SB216763, 12 μM SB216763 + 50 μM HIF-1α translation inhibitor or 12 μM SB216763 + 50 μM HIF-2α translation inhibitor for 90 min un atmospheric oxygen (~21% O_2) followed by 3 h of hypoxia (~1% O_2). At the end of the 3 h hypoxic exposure, the cells' cytoplasmic and nuclear lysates were collected. To normalize the lysates, actin was used for a loading control for the cytoplasmic fraction while lamin was used as a loading control for the nuclear fraction. The levels of β-catenin in the cytoplasmic extracts were unchanged, whereas; there was an increase in the β-catenin levels in the SB216763, SB216763 + HIF-1α translation inhibitor and SB216763 + HIF-2α translation inhibitor treated cells relative to controls.

Figure 4.3

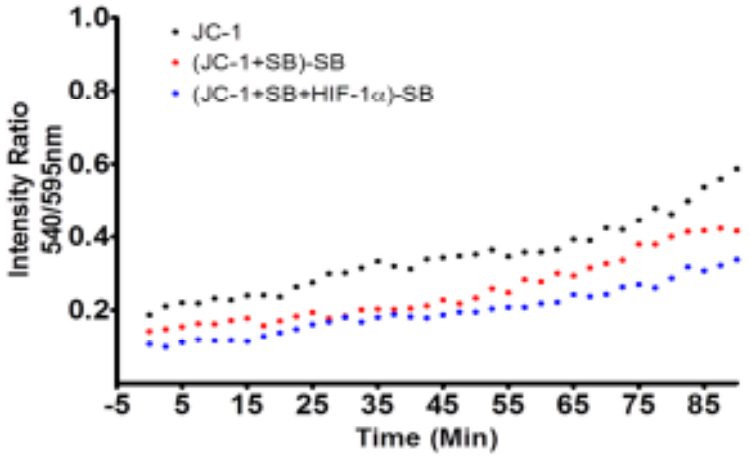

Figure 4.3 Emission spectrum analysis of mitochondrial depolarization in HLE-B3 cells treated with DMSO, SB216763, SB216763 + a HIF-1α translation inhibitor, or SB216763 + a HIF-2α translation inhibitor. HLE-B3 cells were incubated for 90 min with serum-free MEM, under atmospheric conditions (~21% O_2), containing 0.05% DMSO vehicle,12 µM SB216763, 12µM SB216763 + 50 µM HIF-1α translation inhibitor or 12 µM SB216763 + 50 µM HIF-2α translation inhibitor. Cells were switched to hypoxia (~1% O_2) for 3 h. At the end of the hypoxic exposure, the cells had their media removed, and fresh, oxygenated serum-free MEM containing 5 µg/ml JC-1 and either DMSO, SB216763, SB216763 + a HIF-1α translation inhibitor or SB216763 + a HIF-2α translation inhibitor added for 30 min in atmospheric oxygen. At the end of the 30 min incubation period, the media was again switched with fresh serum-free MEM containing DMSO in the absence of the JC-1 dye. The same field of cells had its emission spectrum scanned every 150 sec for 90 min. Serial scans of the emission spectrum of HLE-B3 DMSO + JC-1 control cells (black dots) demonstrated a slight increase in the green emission (540nm) to red emission (595nm) ratio. The trend of increasing green to red ratio in the SB216763 treated (red dots) and the SB216763 + HIF-1α translation inhibitor treated (blue dots)

cells was noted. These trends however were overall less than DMSO mock treated cells. This assay was run on two independent populations of cells for each treatment with only the average of the green/red ratio for each time point being shown.

Figure 4.4

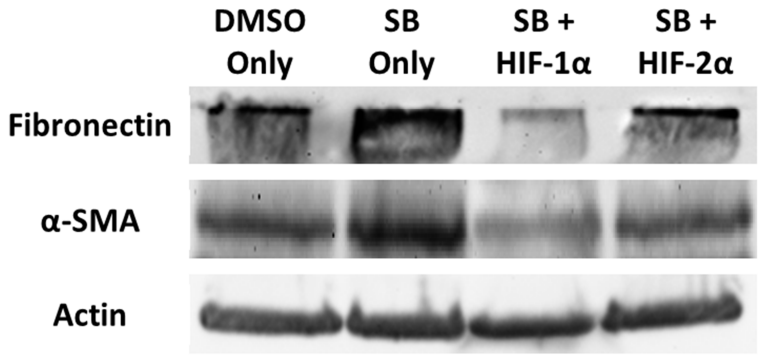

Figure 4.4. Western blot analysis of fibronectin and α-SMA in secondary cultures of normal BLECs treated with DMSO, SB216763, SB216763 + a HIF-1α translation inhibitor, or SB216763 + a HIF-2α translation inhibitor. BLECs were incubated for 90 min in serum-free MEM, under conditions of atmospheric oxygen (~21% O_2), containing either 0.05% DMSO vehicle,12 μM SB216763, 12 μM SB216763 + 50 μM HIF-1α translation inhibitor or 12 μM SB216763 + 50 μM HIF-2α translation inhibitor. Cells were then exposed to hypoxia (~1% O_2) for 3 h and then collected. Total cell lysates were analyzed with immunoblots using 25 μg of protein per lane. Anti-actin was used to normalize the bands to ensure equivalent lane loading. Both the SB216763 treated and SB216763 + HIF-2α translation inhibitor treated cells had levels of fibronectin and α-SMA that were unchanged relative to DMSO mock treated control cells. However, SB216763 + HIF-1α translation inhibitor treated cells had markedly lower levels of fibronectin and only slightly lower levels of α-SMA. This experiment with secondary cultures of normal BLECs affirms that the results observed with the HLE-B3 cells (Figure 4.1) was not influenced by viral transformation.

CHAPTER V

General Discussion

Summation & Conclusions

GSK-3β is a crucial enzyme involved in several cellular functions [32-34]. The studies herein initially focused on understanding the connection between GSK-3β activity and its effect on mitoprotection. To that end, the inhibitor SB216763 was chosen to inhibit the activity of GSK-3β. While utilizing this drug two novel discoveries were made. The first discovery was that the drug SB216763 auto-fluoresces and provides a broad contribution to any fluorescence being measured making any analysis of fluorescence inconclusive. Fortunately the auto-fluorescent contribution of the SB216763 drug can be suppressed using a novel technique involved with measuring the emission spectrum of SB216763. Utilizing this novel technique in conjunction with JC-1 staining our studies were able to demonstrate that mitoprotection can be increased and mitochondrial depolarization prevented when HLE-B3 cells are treated with SB216763 (Figures 2.1 & 4.3).

The second discovery made by our studies was that the drug SB216763 does not prevent the auto-phosphorylation of GSK-3β relative to control cells but rather blocks the enzymes' ability to phosphorylate its downstream substrates (in our studies GS), indicating that the catalytic site of GSK-3β was inactivated (Figure 3.2). The phosphorylation of GSK-3β occurs in the presence of SB216763 because this drug does not prevent the auto-phosphorylation site from becoming phosphorylated but rather blocks the catalytic site of this enzyme from becoming active. We concluded from the SB216763 studies that it is the catalytic site of GSK-3β that confers prevention of mitochondrial depolarization; not the auto-phosphorylation site. This

mitoprotective role for GSK-3β was further confirmed by the lack of mitochondrial depolarization that was observed in HLE-B3 cells treated with SB216763 (Figures 2.1 & 4.3).

In order to further define the mitoprotective mechanisms implemented by HLE-B3 cells our studies looked at the effects of inhibiting ERK1/2; a protein that can regulate the activity of GSK-3β. HLE-B3 cells treated with UO126 demonstrated a similar western blot profile to those treated with SB216763; i.e. unchanged levels of pGSK-3β but a loss of pGS (Figures 3.2 & 3.3). This similarity suggests that cells treated with UO126 should have increased mitoprotection which would be shown by a relatively unchanged green/red ratio during JC-1 analysis. Instead of observing decreased mitochondrial depolarization, JC-1 analysis of UO126 treated cells revealed an ever increasing green/red ratio indicating that massive depolarization was occurring over time (Figure 3.3 bottom panels). With the completion of the JC-1 analysis and immunoblots for SB216763 or UO126 treated HLE-B3 cells Specific Aim #1 was finished (Figure 5.1). However, a second aim developed out of these studies because it became incumbent upon us to study why the UO126 treated cells depolarized even though GSK-3β was inactivated.

Speceific Aim #2 (Figure 5.1) set out to determine why the Western blot profiles for SB216763 or UO126 treated cells were the same while the JC-1 profiles were drastically different (Figures 2.1, 3.2, & 3.3). Previous studies in our lab have demonstrated that JNK can become inactivated when HLE-B3 cells are treated with UO126 (unpublished observation). Furthermore, studies in various cell types have shown that both ERK1/2 and JNK can independently influence apoptosis through their ability to phosphorylate pBcl-2 [58-63]. The phosphorylation of Bcl-2 can subsequently control the translocation of BAX to the mitochondria which in turn influences the induction of apoptosis [63-67]. Thus, one possible explanation for

the discrepancy in JC-1 profiles between SB216763 treated and UO126 treated cells is that the UO126 treated cells are being driven towards apoptosis.

Further Western blot analysis of UO126 treated cells revealed a decrease in phspho-c-Jun (a measure of JNK activity) and a decrease in pBcl-2 while BAX levels remained unchanged relative to controls (Figure 3.4). These immunoblots suggest that the loss of either ERK1/2 or JNK activity can lead to a loss of pBcl-2. To investigate whether ERK1/2 or JNK inactivation was responsible for the loss of pBcl-2 two different inhibitors of JNK activity (SP600125 & AS601245) were utilized. Both inhibitors demonstrated that JNK inactivation had no effect on the levels of pBcl-2 (Figure 3.5). From these results we concluded that the loss of JNK inactivity was completely artifactual and had no influence over pBcl-2 or mitochondrial depolarization.

Once it was definitively proven that the loss of ERK1/2 activity not the loss of JNK activity caused a loss of pBcl-2 which subsequently drove the UO126 treated cells towards apoptosis, Specific Aim #2 was accomplished (Figure 5.1). This drive towards apoptosis is what causes the cells to be more susceptible to mitochondrial depolarization upon treatment with UO126. Although, to clarify, the studies used in Specific Aim #2 demonstrated that UO126 cells are trending towards apoptosis but these cells are not apoptotic as indicated by the lack of caspase-3 activity (Figure 3.7). Furthermore, it has been suggested by our peers that the results we are observing could be caused by the viral transfection that HLE-B3 cells undergo to become an immortalized cell line. To determine if the viral transfection caused any misinterpretation of our results, normalized BLECs were treated with UO126 under conditions identical to those utilized in the experiments with the HLE-B3 cells. These studies proved that similar to HLE-B3 cells, BLECs lose pBcl-2 and undergo massive depolarization when treated with UO126 (Figure 3.8 & 3.9); further validating our conclusions.

With the mechanism of UO126 induced depolarization (Figure 5.1) fairly understood our studies began to take what was gleaned from the GSK-3β studies and move towards more clinically relevant applications. As discussed previously, studies in our lab have demonstrated a pivotal role for GSK-3β in the initiation of EMT due to GSK-3β's ability to regulate the levels of nuclear β-catenin. Those studies concluded that in atmospheric oxygen nuclear β-catenin controls two parallel independent pathways. One pathway influences the expression of the EMT marker proteins, fibronectin and α-SMA, while the other pathway influences VEGF expression and subsequently mitoprotection (Figure 5.2). Those previous studies focused on preventing the initiation of EMT by causing a drop in nuclear β-catenin. Losing the nuclear β-catenin decreased the production of EMT marker proteins but also had the harmful effect of causing massive mitochondrial depolarization. Thus, it was concluded that targeting β-catenin for preventing EMT was not a viable option due to the potentially harmful effects it may have on non-diseased cells (i.e. those cells that are not undergoing EMT and still have their epithelial phenotype). This conclusion prompted the creation of Specific Aim #3 which would focus on targeting enzymes that could block EMT but not affect the $\Delta\Psi$ under hypoxic conditions.

Similar to atmospheric oxygen conditions, β-catenin plays a major role in EMT marker protein expression and VEGF expression under hypoxic conditions. However, one major difference between atmospheric oxygen and hypoxia is the presence of HIF proteins that can only occur in hypoxia. As discussed in Chapter IV the HIF proteins (specifically HIF-1α and HIF-2α) are known transcription factors of VEGF and share a compensatory role for one another in maintaining VEGF expression during hypoxia [69]. Additionally, it has been indicated in the cancer literature that these proteins can associate with β-catenin to influence the production of EMT marker proteins such as fibronectin and α-SMA [75, 76]. These studies suggest that the

HIF proteins could be a potential target for blocking EMT without any adverse effects to the mitochondria.

The last portion of this project set out to determine whether blocking HIF-1α or HIF-2α in EMT induced cells (via SB21673) could prevent the expression of EMT marker proteins but maintain ΔΨ through continuous VEGF expression during hypoxia. When cells were exposed to SB216763 + a HIF-1α inhibitor there was a loss of fibronectin and α-SMA whereas those cells treated with SB216763 + a HIF-2α inhibitor showed no decrease in these proteins (Figure 4.1) a result that was similarly seen in normal BLECs (Figure 4.4). Further experiments revealed that blocking HIF-1α in the presence of SB216763 had no effect on VEGF expression (Figure 4.2) or mitoprotection (Figure 4.3). These results allow us to conclude that HIF-1α is the most viable target for preventing EMT without effecting ΔΨ. Specific Aim #3 (Figure 5.3) was completed after identifying HIF-1α as a potential target for treating EMT without harming non-diseased cells. With the novel discovery of the link between HIF-1α and preventing EMT this project has come to a natural conclusion.

Overall, the project described herein has far reaching implications in developing novel therapies to combat EMT; or, at the very least the conclusions of this project "should compel researchers to widen their outlook and appreciate that each study represents only a pebble in the mountain of human knowledge that sits upon an entire continent of unknown." (Dr. Jerel Adam Fields, PhD)

Implications

As stated previously in the introduction, the main implications of our work pertain to ocular systems, specifically EMT and how it can lead to PCO in the lens. It is our goal to provide understanding of the mechanisms that drive EMT in lens cells. We believe the mechanisms

described herein have just begun to provide that understanding and will eventually lead to the development of new therapies to prevent PCO. Already preliminary results indicate that it is possible to prevent EMT from persisting without harming non-diseased cells by inhibiting HIF-1α. These results suggest that HIF-1α could potentially be targeted post cataract surgery as a means to block the onset of PCO; subsequently preventing patients from going blind. If the HIF-1α/EMT connection holds true in normal human lens tissue, a whole new avenue of research could be opened not only in the field of PCO but other fields of study as well.

In addition to PCO, EMT has recently become the focus of many cancer studies. This increased focus is due enlarge part to the theory that EMT is the main mechanism by which cancer cells become more metastatic [77, 78]. These studies are determined to find new ways to prevent cancer from metastasizing by blocking EMT. The data presented herein has contributed to this field of research by providing HIF-1α as a potential target for preventing invasive cancers from spreading. Should the results from Chapter IV hold true in cancer cells then great strides could be made in treating highly metastatic cancers that utilize EMT to spread throughout the body. For example, our research could possibly lay the ground work for being able to prevent stage 4 metastatic cancers which would have the potential to be paradigm shifting in the way we view the treatment of highly invasive cancers.

In addition to EMT the findings presented in this project could be beneficial to a smaller area of research. The main focus of research in metastatic cancer has been on understanding the mechanisms involved with EMT while the field of mesenchymal to epithelial transition (MET) has been relatively untouched. Only within the last few years have preliminary studies been conducted to examine MET in various cancer cell types while virtually no studies have been conducted in an ocular system. It is possible that the same proteins that drive EMT could be

manipulated or targeted to drive the reverse reaction of MET, potentially turning diseased cells back into normal non-diseased cells. Thus the studies herein may provide insights into the fundamental mechanisms of EMT that will one day be the keys to unlocking our understanding of MET. While this scenario is highly idealized it provides a glimpse into the far reaching effects of understanding the mechanisms that drive EMT and how that understanding can be applied to similar cellular events. However, before any strides can be made into applying the mechanisms of EMT to MET a few more studies should be implemented to provide a more detailed understanding of the mechanism that drives EMT under hypoxic conditions.

Future Directions

The last portion of this project has done well in defining the mechanisms that drive EMT under hypoxic conditions; which provided a natural stopping point. However, to potentially add a more detailed understanding of EMT mechanisms future studies should look at the effects of blocking β-catenin translocation to the nucleus in hypoxia. Studies on HLE-B3 cells in atmospheric oxygen have previously shown that β-catenin is the sole protein regulating the production of EMT marker proteins. These studies demonstrated used XAV-939, a small molecule inhibitor known to selectively degrade β-catenin by stabilizing the AXIN protein in the β-catenin destruction complex [79]. However, these studies proved that XAV-939 successfully inhibits β-catenin's transcriptional function by preventing β-catenin from entering the nucleus not by increasing the degradation of β-catenin.

Similar studies utilizing XAV-939 under hypoxic conditions could be implemented. The focus of these studies would be to determine the necessity of β-catenin in the expression of both EMT marker proteins and VEGF when HIF proteins are present in the cell due to hypoxic exposure. Should the loss of β-catenin cause a drop in VEGF levels it would indicate that VEGF

expression would require the presence of β-catenin and either HIF-1α or HIF-2α. However, if the VEGF levels do not change in the absence of nuclear β-catenin then this would suggest the HIF proteins are the main proteins regulating VEGF production. The latter result would be very fascinating because it would demonstrate a strong difference in the mechanisms of EMT in atmospheric oxygen vs hypoxia; in that β-catenin could potentially be targeted in hypoxia to prevent EMT without disrupting ΔΨ. In terms of the EMT marker proteins, a loss of β-catenin should lead to a loss of fibronectin and α-SMA. Should the loss of fibronectin and α-SMA not occur in the presence of XAV-939 under hypoxic conditions it would suggest that some other protein(s) (possibly HIF proteins) is controlling the persistence of EMT in hypoxia.

It has been suggested in the cancer literature that HIF proteins could be directly influencing the levels of EMT marker proteins without needing to associate with β-catenin. According to this mechanism the HIF proteins bind to a protein known as Twist1 and from there influence the transcription of EMT proteins [80]. Twist1 focused research is so new that there are no known inhibitors of this protein prompting pharmaceutical and chemical companies to work as fast as possible to make inhibitors for this protein. The only technique currently available to inhibit Twist1 is the use of siRNA to knock down the expression of this potentially crucial protein. Thus, one potential future study is to knockdown Twist1 in hypoxia to see if EMT can be prevented. This is an important future study, because once the HIF/Twist1/EMT signaling mechanism has been elucidated in full, pharmaceutical companies will have more incentive to create candidate compounds that target Twist1. These compounds which are currently being researched may one day provide novel treatments against not only pathological conditions in the intraocular lens but also aggressively metastatic forms of cancer.

Figures

Figure 5.1

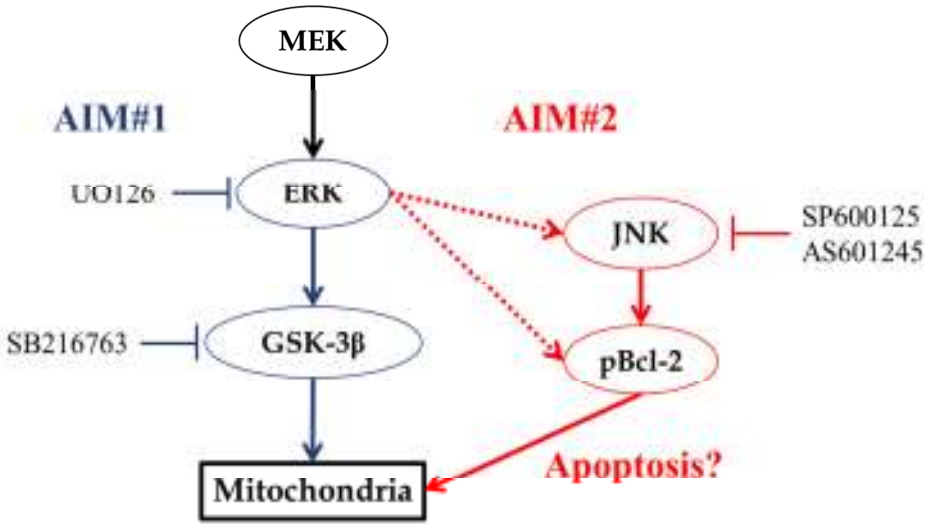

Figure 5.1 Diagram of Specific Aims 1 and 2. Aim#1 set forth to determine if GSK-3β is a crucial enzyme in the regulation of mitoprotection; and, determine whether its activity can be influenced by inactivating one of its upstream regulators (ERK1/2). Aim#2 focused on determining how the regulatory protein ERK1/2 regulates mitoprotection by influencing the levels of apoptotic proteins.

Figure 5.2

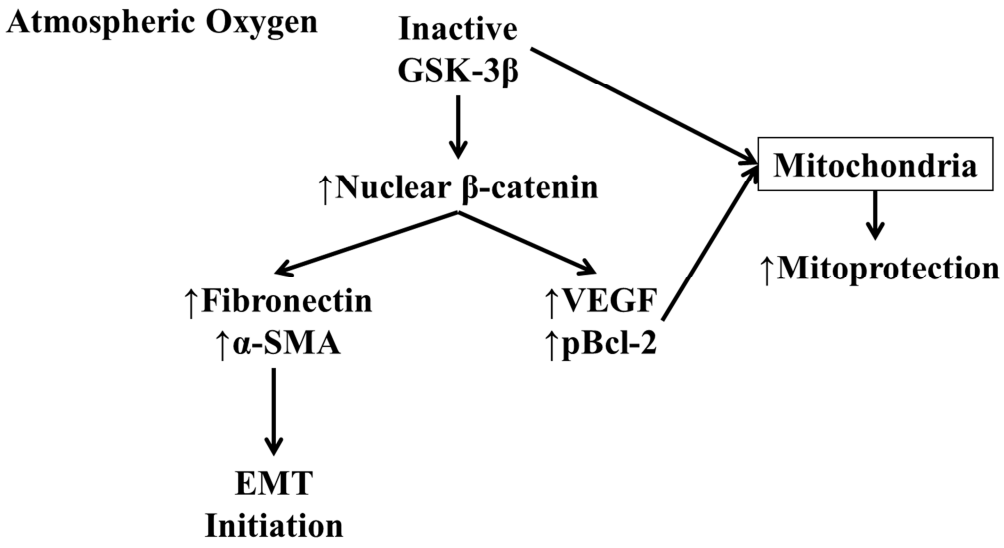

Figure 5.2 Schematic of the proposed mechanism that drives the initiation of EMT in atmospheric oxygen. According to previous studies this mechanism relies heavily on β-catenin and suggests it to be the main protein regulating fibronectin, α-SMA, and VEGF production.

Figure 5.3

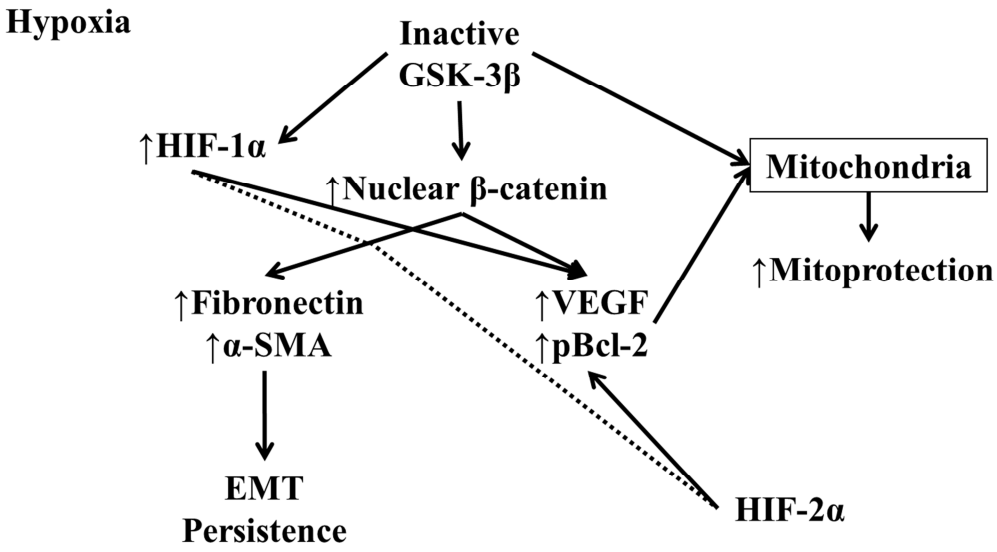

Figure 5.3 Schematic of the proposed mechanism that drives the persistence of EMT in hypoxia. According to the data presented herein (Chapter IV), in addition to β-catenin, the HIF proteins (mainly HIF-1α) play a prominent role in the expression of fibronectin, α-SMA, and VEGF.

LIST OF PUBLICATIONS

Paxton WF, **Brooks MM**, Howell M, Tolk N, Kang WP, & Davidson JL. Role of Deuterium Desorption Kinetics on the Thermionic Emission Properties from Polycrystalline Diamond Films with Respect to Kinetic Isotope Effects. *Journal of Applied Physics*. 2014; 115: 234904.

Brooks MM, Neelam S, & Cammarata PR. Lenticular Mitoprotection. Part B: GSK-3β and regulation of mitochondrial permeability transition for lens epithelial cells in atmospheric oxygen. *Molecular Vision*. 2013; 19: 2457-67.

Brooks MM, Neelam S, Fudala R, Gryczynski I, & Cammarata PR. Lenticular Mitoprotection. Part A: Monitoring mitochondrial depolarization with JC-1 and artifactual fluorescence by the GSK-3β inhibitor, SB216763. *Molecular Vision*. 2013; 19: 1406-12.

Neelam S, **Brooks MM**, & Cammarata PR. Lenticular Cytoprotection. Part 1: The role of hypoxia inducible factors -1α and -2α and vascular endothelial growth factor in lens epithelial cell survival in hypoxia. *Molecular Vision*. 2013; 19: 1-15.

ACKNOWLEDGEMENTS

I would like to acknowledge my mentor Dr. Patrick Cammarata and my lab mate Sudha Neelam for the unwavering support of this project over these last five years. Additionaly, I would like to acknowledge my collaborators Dr. Ignacy Gryczynski and Dr. Rafal Fudala for their help in developing the emission spectroscopy technique. Without their help this project would have been dead from the start. It was only after the development of this technique that great strides were made in this project. Last but certainly not least I would like to acknowledge Dr. I-Fen Chang and Dr. Larry Oakford for their help in the capture and analysis of the JC-1 data.

Also I would like to give special thanks to my committee members; whose valuable input on this project helped me become the scientist I am today. In addition to my committee I would like to give special thanks to the Department of Cell Biology, Anatomy, and Immunology faculty and staff. Their continued support throughout this project is highly appreciated and it should be noted that without their support this project would have never made the strides it did. Finally, I would like to give special thanks to Kathleen Borgmann, who was our lab neighbor for a little over four years. Her willingness to always lend a helping hand and provide countless favors for our lab is greatly appreciated and had a substantial influence in moving this project forward.

REFERENCES

1. Kuszak JR, Zoltoski RK, Sivertson C. Fibre cell organization in crystalline lenses. Exp Eye Res 2004; 78(3):673-87.
2. Berthoud VM, Minogue PJ, Osmolak P, Snabb JI, Beyer EC. Roles and regulation of lens epithelial cell connexins. FEBS Lett 2014; 588(8):1297-303.
3. Kuszak JR, Zoltoski RK, Tiedemann CE. Development of lens sutures. Int J Dev Biol 2004; 48(8-9):889-902.
4. Trokel S. The physical basis for transparency of the crystalline lens. Invest Ophthalmol 1962; 1:493-501.
5. Wride MA. Lens fibre cell differentiation and organelle loss: many paths lead to clarity. Philos Trans R Soc Lond B Biol Sci 2011; 366(1568):1219-33.
6. Sivak JG, Kreuzer RO. Spherical aberration of the crystalline lens. Vision Res 1983; 23(1):59-70.
7. Rao GN, Khanna R, Payal A. The global burden of cataract. Curr Opin Ophthalmol 2011; 22(1):4-9.
8. Huang B, He W. Molecular characteristics of inherited congenital cataracts. Eur J Med Genet 2010; 53(6):347-57.
9. Horwitz J. Alpha-crystallin can function as a molecular chaperone. Proc Natl Acad Sci U S A 1992; 89(21):10449-53.
10. Takemoto L, Boyle D. The possible role of alpha-crystallins in human senile cataractogenesis. Int J Biol Macromol 1998; 22(3-4):331-7.
11. Petrash JM. Aging and age-related diseases of the ocular lens and vitreous body. Invest Ophthalmol Vis Sci 2013; 54(14):ORSF54-9.

12. Wormstone IM. Posterior capsule opacification: a cell biological perspective. Exp Eye Res 2002; 74(3):337-47.

13. Huang L, Tang D, Yappert MC, Borchman D. Oxidation-induced changes in human lens epithelial cells 2. Mitochondria and the generation of reactive oxygen species. Free Radic Biol Med 2006; 41(6):926-36.

14. Flynn JM, Lannigan DA, Clark DE, Garner MH, Cammarata PR. RNA suppression of ERK2 leads to collapse of mitochondrial membrane potential with acute oxidative stress in human lens epithelial cells. Am J Physiol Endocrinol Metab 2008; 294(3):E589-99.

15. Farber JL KM, Coleman JB Mechanisms of cell injury by activated oxygen species. Lab Invest 1990; 62:670-9.

16. Shabalina IG, Nedergaard J. Mitochondrial ('mild') uncoupling and ROS production: physiologically relevant or not? Biochem Soc Trans 2011; 39(5):1305-9.

17. Pan Y. Mitochondria, reactive oxygen species, and chronological aging: a message from yeast. Exp Gerontol 2011; 46(11):847-52.

18. Adrain C, Martin SJ. The mitochondrial apoptosome: a killer unleashed by the cytochrome seas. Trends Biochem Sci 2001; 26(6):390-7.

19. Jacobson MD, Weil M, Raff MC. Programmed cell death in animal development. Cell 1997; 88(3):347-54.

20. Savill J, Fadok V. Corpse clearance defines the meaning of cell death. Nature 2000; 407(6805):784-8.

21. Baines CP. The molecular composition of the mitochondrial permeability transition pore. J Mol Cell Cardiol 2009; 46(6):850-7.

22. Crow MT, Mani K, Nam YJ, Kitsis RN. The mitochondrial death pathway and cardiac myocyte apoptosis. Circ Res 2004; 95(10):957-70.

23. Halestrap A. Biochemistry: a pore way to die. Nature 2005; 434(7033):578-9.

24. Rasola A, Bernardi P. The mitochondrial permeability transition pore and its involvement in cell death and in disease pathogenesis. Apoptosis 2007; 12(5):815-33.

25. Juhaszova M, Wang S, Zorov DB, Nuss HB, Gleichmann M, Mattson MP, Sollott SJ. The identity and regulation of the mitochondrial permeability transition pore: where the known meets the unknown. Ann N Y Acad Sci 2008; 1123:197-212.

26. Zhai P, Sadoshima J. Overcoming an energy crisis?: an adaptive role of glycogen synthase kinase-3 inhibition in ischemia/reperfusion. Circ Res 2008; 103(9):910-3.

27. Bijur GN, Jope RS. Glycogen synthase kinase-3 beta is highly activated in nuclei and mitochondria. Neuroreport 2003; 14(18):2415-9.

28. Nishihara M, Miura T, Miki T, Tanno M, Yano T, Naitoh K, Ohori K, Hotta H, Terashima Y, Shimamoto K. Modulation of the mitochondrial permeability transition pore complex in GSK-3beta-mediated myocardial protection. J Mol Cell Cardiol 2007; 43(5):564-70.

29. Juhaszova M, Zorov DB, Kim SH, Pepe S, Fu Q, Fishbein KW, Ziman BD, Wang S, Ytrehus K, Antos CL, Olson EN, Sollott SJ. Glycogen synthase kinase-3beta mediates convergence of protection signaling to inhibit the mitochondrial permeability transition pore. J Clin Invest 2004; 113(11):1535-49.

30. Juhaszova M, Zorov DB, Yaniv Y, Nuss HB, Wang S, Sollott SJ. Role of glycogen synthase kinase-3beta in cardioprotection. Circ Res 2009; 104(11):1240-52.

31. Li Q, Michaud M, Canosa S, Kuo A, Madri JA. GSK-3beta: a signaling pathway node modulating neural stem cell and endothelial cell interactions. Angiogenesis 2011; 14(2):173-85.

32. Doble BW, Woodgett JR. GSK-3: tricks of the trade for a multi-tasking kinase. J Cell Sci 2003; 116(Pt 7):1175-86.

33. Grimes CA, Jope RS. The multifaceted roles of glycogen synthase kinase 3beta in cellular signaling. Prog Neurobiol 2001; 65(4):391-426.

34. Kim WY, Wang X, Wu Y, Doble BW, Patel S, Woodgett JR, Snider WD. GSK-3 is a master regulator of neural progenitor homeostasis. Nat Neurosci 2009; 12(11):1390-7.

35. Cohen P, Frame S. The renaissance of GSK3. Nat Rev Mol Cell Biol 2001; 2(10):769-76.

36. Gomez L, Paillard M, Thibault H, Derumeaux G, Ovize M. Inhibition of GSK3beta by postconditioning is required to prevent opening of the mitochondrial permeability transition pore during reperfusion. Circulation 2008; 117(21):2761-8.

37. Forster K, Richter H, Alexeyev MF, Rosskopf D, Felix SB, Krieg T. Inhibition of glycogen synthase kinase 3beta prevents peroxide-induced collapse of mitochondrial membrane potential in rat ventricular myocytes. Clin Exp Pharmacol Physiol 2010; 37(7):684-8.

38. Di Lisa F, Canton M, Menabo R, Kaludercic N, Bernardi P. Mitochondria and cardioprotection. Heart Fail Rev 2007; 12(3-4):249-60.

39. Murphy E, Steenbergen C. Mechanisms underlying acute protection from cardiac ischemia-reperfusion injury. Physiol Rev 2008; 88(2):581-609.

40. Rasola A, Sciacovelli M, Chiara F, Pantic B, Brusilow WS, Bernardi P. Activation of mitochondrial ERK protects cancer cells from death through inhibition of the permeability transition. Proc Natl Acad Sci U S A 2010; 107(2):726-31.

41. Gerhardt D, Bertola G, Dietrich F, Figueiro F, Zanotto-Filho A, Moreira Fonseca JC, Morrone FB, Barrios CH, Battastini AM, Salbego CG. Boldine induces cell cycle arrest and apoptosis in T24 human bladder cancer cell line via regulation of ERK, AKT, and GSK-3beta. Urol Oncol 2014; 32(1):36 e1-9.

42. Ramos JW. The regulation of extracellular signal-regulated kinase (ERK) in mammalian cells. Int J Biochem Cell Biol 2008; 40(12):2707-19.

43. McCubrey JA, Steelman LS, Chappell WH, Abrams SL, Wong EW, Chang F, Lehmann B, Terrian DM, Milella M, Tafuri A, Stivala F, Libra M, Basecke J, Evangelisti C, Martelli AM, Franklin RA. Roles of the Raf/MEK/ERK pathway in cell growth, malignant transformation and drug resistance. Biochim Biophys Acta 2007; 1773(8):1263-84.

44. Ding Q, Xia W, Liu JC, Yang JY, Lee DF, Xia J, Bartholomeusz G, Li Y, Pan Y, Li Z, Bargou RC, Qin J, Lai CC, Tsai FJ, Tsai CH, Hung MC. Erk associates with and primes GSK-3beta for its inactivation resulting in upregulation of beta-catenin. Mol Cell 2005; 19(2):159-70.

45. Shi Y, Barton K, De Maria A, Petrash JM, Shiels A, Bassnett S. The stratified syncytium of the vertebrate lens. J Cell Sci 2009; 122(Pt 10):1607-15.

46. Andley UP, Rhim JS, Chylack LT, Jr., Fleming TP. Propagation and immortalization of human lens epithelial cells in culture. Invest Ophthalmol Vis Sci 1994; 35(7):3094-102.

47. Salvioli S, Ardizzoni A, Franceschi C, Cossarizza A. JC-1, but not DiOC6(3) or rhodamine 123, is a reliable fluorescent probe to assess delta psi changes in intact cells: implications for studies on mitochondrial functionality during apoptosis. FEBS Lett 1997; 411(1):77-82.

48. Flynn JM, Cammarata PR. Estradiol attenuates mitochondrial depolarization in polyol-stressed lens epithelial cells. Mol Vis 2006; 12:271-82.

49. Coghlan MP, Culbert AA, Cross DA, Corcoran SL, Yates JW, Pearce NJ, Rausch OL, Murphy GJ, Carter PS, Roxbee Cox L, Mills D, Brown MJ, Haigh D, Ward RW, Smith DG, Murray KJ, Reith AD, Holder JC. Selective small molecule inhibitors of glycogen synthase kinase-3 modulate glycogen metabolism and gene transcription. Chem Biol 2000; 7(10):793-803.

50. Thotala DK, Geng L, Dickey AK, Hallahan DE, Yazlovitskaya EM. A new class of molecular targeted radioprotectors: GSK-3beta inhibitors. Int J Radiat Oncol Biol Phys 2010; 76(2):557-65.

51. Brooks MM, Neelam S, Cammarata PR. Lenticular mitoprotection. Part B: GSK-3beta and regulation of mitochondrial permeability transition for lens epithelial cells in atmospheric oxygen. Mol Vis 2013; 19:2451-67.

52. Henrich LM, Smith JA, Kitt D, Errington TM, Nguyen B, Traish AM, Lannigan DA. Extracellular signal-regulated kinase 7, a regulator of hormone-dependent estrogen receptor destruction. Mol Cell Biol 2003; 23(17):5979-88.

53. Cole A, Frame S, Cohen P. Further evidence that the tyrosine phosphorylation of glycogen synthase kinase-3 (GSK3) in mammalian cells is an autophosphorylation event. Biochem J 2004; 377(Pt 1):249-55.

54. Brooks MM, Neelam S, Fudala R, Gryczynski I, Cammarata PR. Lenticular mitoprotection. Part A: Monitoring mitochondrial depolarization with JC-1 and artifactual fluorescence by the glycogen synthase kinase-3beta inhibitor, SB216763. Mol Vis 2013; 19:1406-12.

55. Bennett BL, Sasaki DT, Murray BW, O'Leary EC, Sakata ST, Xu W, Leisten JC, Motiwala A, Pierce S, Satoh Y, Bhagwat SS, Manning AM, Anderson DW. SP600125, an

anthrapyrazolone inhibitor of Jun N-terminal kinase. Proc Natl Acad Sci U S A 2001; 98(24):13681-6.

56. Carboni S, Hiver A, Szyndralewiez C, Gaillard P, Gotteland JP, Vitte PA. AS601245 (1,3-benzothiazol-2-yl (2-[[2-(3-pyridinyl) ethyl] amino]-4 pyrimidinyl) acetonitrile): a c-Jun NH2-terminal protein kinase inhibitor with neuroprotective properties. J Pharmacol Exp Ther 2004; 310(1):25-32.

57. Jarpe MB, Widmann C, Knall C, Schlesinger TK, Gibson S, Yujiri T, Fanger GR, Gelfand EW, Johnson GL. Anti-apoptotic versus pro-apoptotic signal transduction: checkpoints and stop signs along the road to death. Oncogene 1998; 17(11 Reviews):1475-82.

58. Lei K, Nimnual A, Zong WX, Kennedy NJ, Flavell RA, Thompson CB, Bar-Sagi D, Davis RJ. The Bax subfamily of Bcl2-related proteins is essential for apoptotic signal transduction by c-Jun NH(2)-terminal kinase. Mol Cell Biol 2002; 22(13):4929-42.

59. Fan M, Goodwin M, Vu T, Brantley-Finley C, Gaarde WA, Chambers TC. Vinblastine-induced phosphorylation of Bcl-2 and Bcl-XL is mediated by JNK and occurs in parallel with inactivation of the Raf-1/MEK/ERK cascade. J Biol Chem 2000; 275(39):29980-5.

60. Kharbanda S, Saxena S, Yoshida K, Pandey P, Kaneki M, Wang Q, Cheng K, Chen YN, Campbell A, Sudha T, Yuan ZM, Narula J, Weichselbaum R, Nalin C, Kufe D. Translocation of SAPK/JNK to mitochondria and interaction with Bcl-x(L) in response to DNA damage. J Biol Chem 2000; 275(1):322-7.

61. Maundrell K, Antonsson B, Magnenat E, Camps M, Muda M, Chabert C, Gillieron C, Boschert U, Vial-Knecht E, Martinou JC, Arkinstall S. Bcl-2 undergoes phosphorylation by c-Jun N-terminal kinase/stress-activated protein kinases in the presence of the constitutively active GTP-binding protein Rac1. J Biol Chem 1997; 272(40):25238-42.

62. Yamamoto K, Ichijo H, Korsmeyer SJ. BCL-2 is phosphorylated and inactivated by an ASK1/Jun N-terminal protein kinase pathway normally activated at G(2)/M. Mol Cell Biol 1999; 19(12):8469-78.

63. Deng X, Xiao L, Lang W, Gao F, Ruvolo P, May WS, Jr. Novel role for JNK as a stress-activated Bcl2 kinase. J Biol Chem 2001; 276(26):23681-8.

64. Ito T, Deng X, Carr B, May WS. Bcl-2 phosphorylation required for anti-apoptosis function. J Biol Chem 1997; 272(18):11671-3.

65. Ruvolo PP, Deng X, May WS. Phosphorylation of Bcl2 and regulation of apoptosis. Leukemia 2001; 15(4):515-22.

66. Murphy KM, Ranganathan V, Farnsworth ML, Kavallaris M, Lock RB. Bcl-2 inhibits Bax translocation from cytosol to mitochondria during drug-induced apoptosis of human tumor cells. Cell Death Differ 2000; 7(1):102-11.

67. Nomura M, Shimizu S, Ito T, Narita M, Matsuda H, Tsujimoto Y. Apoptotic cytosol facilitates Bax translocation to mitochondria that involves cytosolic factor regulated by Bcl-2. Cancer Res 1999; 59(21):5542-8.

68. Smiley ST, Reers M, Mottola-Hartshorn C, Lin M, Chen A, Smith TW, Steele GD, Jr., Chen LB. Intracellular heterogeneity in mitochondrial membrane potentials revealed by a J-aggregate-forming lipophilic cation JC-1. Proc Natl Acad Sci U S A 1991; 88(9):3671-5.

69. Neelam S, Brooks MM, Cammarata PR. Lenticular cytoprotection. Part 1: The role of hypoxia inducible factors-1alpha and -2alpha and vascular endothelial growth factor in lens epithelial cell survival in hypoxia. Mol Vis 2013; 19:1-15.

70. Marcantonio JM, Vrensen GF. Cell biology of posterior capsular opacification. Eye (Lond) 1999; 13 (Pt 3b):484-8.

71. Saika S, Miyamoto T, Ishida I, Shirai K, Ohnishi Y, Ooshima A, McAvoy JW. TGFbeta-Smad signalling in postoperative human lens epithelial cells. Br J Ophthalmol 2002; 86(12):1428-33.

72. de Iongh RU, Wederell E, Lovicu FJ, McAvoy JW. Transforming growth factor-beta-induced epithelial-mesenchymal transition in the lens: a model for cataract formation. Cells Tissues Organs 2005; 179(1-2):43-55.

73. Skurk C, Maatz H, Rocnik E, Bialik A, Force T, Walsh K. Glycogen-Synthase Kinase3beta/beta-catenin axis promotes angiogenesis through activation of vascular endothelial growth factor signaling in endothelial cells. Circ Res 2005; 96(3):308-18.

74. Easwaran V, Lee SH, Inge L, Guo L, Goldbeck C, Garrett E, Wiesmann M, Garcia PD, Fuller JH, Chan V, Randazzo F, Gundel R, Warren RS, Escobedo J, Aukerman SL, Taylor RN, Fantl WJ. beta-Catenin regulates vascular endothelial growth factor expression in colon cancer. Cancer Res 2003; 63(12):3145-53.

75. Choi H, Chun YS, Kim TY, Park JW. HIF-2alpha enhances beta-catenin/TCF-driven transcription by interacting with beta-catenin. Cancer Res 2010; 70(24):10101-11.

76. Jiang YG, Luo Y, He DL, Li X, Zhang LL, Peng T, Li MC, Lin YH. Role of Wnt/beta-catenin signaling pathway in epithelial-mesenchymal transition of human prostate cancer induced by hypoxia-inducible factor-1alpha. Int J Urol 2007; 14(11):1034-9.

77. Gonzalez DM, Medici D. Signaling mechanisms of the epithelial-mesenchymal transition. Sci Signal 2014; 7(344):re8.

78. Thiery JP. Epithelial-mesenchymal transitions in tumour progression. Nat Rev Cancer 2002; 2(6):442-54.

79. Huang SM, Mishina YM, Liu S, Cheung A, Stegmeier F, Michaud GA, Charlat O, Wiellette E, Zhang Y, Wiessner S, Hild M, Shi X, Wilson CJ, Mickanin C, Myer V, Fazal A, Tomlinson R, Serluca F, Shao W, Cheng H, Shultz M, Rau C, Schirle M, Schlegl J, Ghidelli S, Fawell S, Lu C, Curtis D, Kirschner MW, Lengauer C, Finan PM, Tallarico JA, Bouwmeester T, Porter JA, Bauer A, Cong F. Tankyrase inhibition stabilizes axin and antagonizes Wnt signalling. Nature 2009; 461(7264):614-20.

80. Liu Y, Liu Y, Yan X, Xu Y, Luo F, Ye J, Yan H, Yang X, Huang X, Zhang J, Ji G. HIFs enhance the migratory and neoplastic capacities of hepatocellular carcinoma cells by promoting EMT. Tumour Biol 2014; 35(8):8103-14.